GENERATION OF SUPERHYDROPHOBIC SURFACES BY ELECTROSPINNING PROCESS

by
KAZIM ACATAY

Submitted to the Graduate School of Engineering and Natural Sciences
in partial fulfillment of
the requirements for the degree of
Doctor of Philosophy

Sabancı University
Spring 2004

GENERATION OF SUPERHYDROPHOBIC SURFACES
BY ELECTROSPINNING PROCESS

APPROVED BY:

Assoc. Prof. Dr. Yusuf Z. Menceloğlu (Dissertation Supervisor)	………………………
Prof. Dr. Ali Rana Atılgan	………………………
Assoc. Prof. Dr. Canan Baysal	………………………
Assoc. Prof. Dr. A. Levent Demirel	………………………
Asst. Prof. Dr. Alpay Taralp	………………………

DATE OF APPROVAL: …………………………

ABSTRACT

A surface having water contact angle (WCA) higher than 150^o is named as superhydrophobic surface. To exhibit superhydrophobic feature, a surface should have micron scale roughness on an inherently hydrophobic material. This extreme water-repellency feature has found many applications both in industry and in daily-life. Current production processes of superhydrophobic surfaces are either time consuming or expensive. A cost-effective, widely applicable and practical way of production is necessary.

In this study, superhydrophobic surfaces were generated by utilization of electrospinning process, which is a continuous nanofiber production process from a polymeric solution under an electrical field. By this method, a straightforward and inexpensive way to fabricate very stable superhydrophobic surfaces with an advantage of tunable WCA and low sliding angle were discovered.

Poly-(acrylonitrile-co-dimethyl meta-isopropenyl benzyl isocyanate) polymer was synthesized, and electrospun after the addition of a fluorinated hydroxyl-ended oligomer. The effects of viscosity of electrospinning solution, fluorine content and molecular weight of the copolymer to surface morphology and WCA of the electrospun film were investigated by using scanning electron microscope, goniometer, atomic force microscope and nuclear magnetic resonance instruments.

Experiments proved that deliberate incorporation of the beads into the film resulted in extreme water-repellency. It was found that, as the viscosity of the solution was decreased, the density of the polymeric beads, so the film roughness in three dimensions, was increased to more than 150^o WCA values for the electrospun films. In the molecular weight of copolymer study, electrospinning of lower molecular weight copolymer was generated solely bead morphology, which resulted the highest WCA of 166.7±2.2^o with the lowest water sliding angle of 4.3±0.8^o.

In addition to these studies, the films were subjected to droplet pressing between identical superhydrophobic surfaces to determine the stability of their superhydrophobicity. And this study showed that our electrospun films have the most stable superhydrophobic state in the literature.

ÖZET

Su damlasının, üzerinde 150°’den fazla açı yaptığı yüzeyler süperhidrofobik yüzeyler olarak adlandırılırlar. Bir yüzeyin süperhidrofobik özellik gösterebilmesi için hem üzerinde mikrometre mertebesinde pürüzlülük, hem de doğal olarak hidrofobik olan malzemeden imal edilmiş olması gerekir. Bu ileri seviyedeki su iticilik özelliği, sanayide ve günlük hayatta bir çok uygulama bulmaktadır. Süperhidrofobik yüzeylerin mevcut üretim işlemleri ya çok uzun süren, ya da pahalı işlemlerdir. Düşük maliyetli, geniş uygulama alanı olan ve elverişli bir üretim işleminin geliştirilmesi gereklidir.

Bu çalışmada, süperhidrofobik yüzeyler, polimer çözeltilerinden elektrik alan altında nanometre çaplı fiber üretme yöntemi olan, elektrodokuma ile üretilmiştir. Çok kararlı süperhidrofobik yüzeylerin, kontrol edilebilir temas açılı ve düşük su kayma açılı halde, elektrodokuma yöntemi ile üretimi bulunmuştur.

Poli-(akrilonitril-ko-dimetil meta-izopropenil benzil izosiyanat) kopolimeri sentezlenmiş, ve hidroksil-sonlu, florlu bir oligomer ilavesinin ardından elektrodokuması gerçekleştirilmiştir. Vizkositenin, flor miktarının ve kopolimer moleküler ağırlığının, elektrodokunmuş filmlerin yüzey yapısına ve su ile yaptığı temas açısına etkisi araştırılmıştır. Çalışma esnasında taramalı elektron mikroskobu, goniometre, atomik güç mikroskobu ve nükleer manyetik rezonans cihazları kullanılmıştır.

Deneyler göstermiştir ki, elektrodokunmuş yüzeylere, kasti olarak boncukların eklenmesi had safhada su iticiliğe sebep olmaktadır. Çözeltinin vizkositesi azaldıkça, polimerik boncukların yoğunluğu ve dolayısıyla filmin pürüzlülüğü artmaktadır. Bu da su ile temas açısının 150°’nin üzerine çıkmasını sağlamaktadır. Kopolimer moleküler ağırlığının yapıya etkisi çalışmasında ise, düşük moleküler ağırlıklı kopolimerin elektrodokunması tamamen boncuktan oluşan bir yapı vermiştir. Bu yüzey üzerinde 166.7±2.2° su temas açısı ve 4.3±0.8° su kayma açısı ölçülmüştür.

Bu çalışmalara ek olarak, filmlerin süperhidrofobik kararlılıklarının test edilmesi amacıyla, aynı tip iki film arasına bir su damlası yerleştirilerek preslenmiştir. Bu çalışma göstermiştir ki, elektrodokunmuş yüzeylerimiz mevcut literatürdeki en kararlı süperhidrofobik yüzeylerdir.

Aileme,

özellikle de minik Eda'ya ...

ACKNOWLEDGMENTS

During my PhD study in Sabancı University, many colleagues have helped, supported and encouraged me. First of all, I would like to state my thanks to Dr. Yusuf Z. Menceloğlu. Without his academic insight and patience, such a study could never be present. I would like to give sincere gratitude to Dr. Canan Baysal, Dr. Alpay Taralp, Dr. Cleva Ow-Yang, Dr. Mehmet Ali Gülgün and Dr. Ali Rana Atılgan for their critical thinking and endless desire to share their ideas on the subject.

I also would like to acknowledge Eren Şimşek for his helps and genius questions throughout the tedious experimental work and Karahan Bulut for his aids on the drawings of this thesis.

Finally, I would like to express my gratitude and infinite thanks to: My parents, Gülser and Turhan Acatay, who have brought me this opportunity and endlessly supported throughout my life, and my wife, Ebru, my daughter, Eda, and my mother-in-law, Nilgül Özyurt, for their patience and infinite support until the first day of my PhD years. If they are not available in my life, publishing this thesis will not be as pleasurable as it is now.

TABLE OF CONTENTS

Page

LIST OF FIGURES

LIST OF TABLES

LIST OF ABBREVIATIONS

AFM	Atomic Force Microscope
AIBN	Azobisisobutyronitrile
AN	Acrylonitrile
CA	Contact Angle
CAH	Contact Angle Hysteresis
CVD	Chemical Vapor Deposition
DC	Direct Current
DMF	Dimethylformamide
DSC	Differential Scanning Calorimeter
FT-IR	Fourier Transform Infrared
HMW	Higher Molecular Weight
LMW	Lower Molecular Weight
MWNT	Multi-Walled Nanotube
NMR	Nuclear Magnetic Resonance
PAN	Polyacrylonitrile
PEG	Polyethyleneglycol
PEO	Polyethyleneoxide
PMMA	Polymethymethacrylate
PTFE	Polytetrafluoroethylene
PVA	Polyvinylalcohol
QAC	Quaternary Ammonium Compound
SEM	Scanning Electron Microscope
T2EH	Tin (II) ethyl hexanoate
TMI	α,α-Dimethyl meta-isopropenyl benzyl isocyanate
WCA	Water Contact Angle
XPS	X-Ray Photoelectron Spectroscopy

GENERATION OF SUPERHYDROPHOBIC SURFACES BY ELECTROSPINNING PROCESS

by
KAZIM ACATAY

Submitted to the Graduate School of Engineering and Natural Sciences
in partial fulfillment of
the requirements for the degree of
Doctor of Philosophy

Sabancı University
Spring 2004

GENERATION OF SUPERHYDROPHOBIC SURFACES BY ELECTROSPINNING PROCESS

APPROVED BY:

Assoc. Prof. Dr. Yusuf Z. Menceloğlu (Dissertation Supervisor)	………………………
Prof. Dr. Ali Rana Atılgan	………………………
Assoc. Prof. Dr. Canan Baysal	………………………
Assoc. Prof. Dr. A. Levent Demirel	………………………
Asst. Prof. Dr. Alpay Taralp	………………………

DATE OF APPROVAL: …………………………

ABSTRACT

A surface having water contact angle (WCA) higher than 150^o is named as superhydrophobic surface. To exhibit superhydrophobic feature, a surface should have micron scale roughness on an inherently hydrophobic material. This extreme water-repellency feature has found many applications both in industry and in daily-life. Current production processes of superhydrophobic surfaces are either time consuming or expensive. A cost-effective, widely applicable and practical way of production is necessary.

In this study, superhydrophobic surfaces were generated by utilization of electrospinning process, which is a continuous nanofiber production process from a polymeric solution under an electrical field. By this method, a straightforward and inexpensive way to fabricate very stable superhydrophobic surfaces with an advantage of tunable WCA and low sliding angle were discovered.

Poly-(acrylonitrile-co-dimethyl meta-isopropenyl benzyl isocyanate) polymer was synthesized, and electrospun after the addition of a fluorinated hydroxyl-ended oligomer. The effects of viscosity of electrospinning solution, fluorine content and molecular weight of the copolymer to surface morphology and WCA of the electrospun film were investigated by using scanning electron microscope, goniometer, atomic force microscope and nuclear magnetic resonance instruments.

Experiments proved that deliberate incorporation of the beads into the film resulted in extreme water-repellency. It was found that, as the viscosity of the solution was decreased, the density of the polymeric beads, so the film roughness in three dimensions, was increased to more than 150^o WCA values for the electrospun films. In the molecular weight of copolymer study, electrospinning of lower molecular weight copolymer was generated solely bead morphology, which resulted the highest WCA of 166.7±2.2^o with the lowest water sliding angle of 4.3±0.8^o.

In addition to these studies, the films were subjected to droplet pressing between identical superhydrophobic surfaces to determine the stability of their superhydrophobicity. And this study showed that our electrospun films have the most stable superhydrophobic state in the literature.

ÖZET

Su damlasının, üzerinde 150^{o}'den fazla açı yaptığı yüzeyler süperhidrofobik yüzeyler olarak adlandırılırlar. Bir yüzeyin süperhidrofobik özellik gösterebilmesi için hem üzerinde mikrometre mertebesinde pürüzlülük, hem de doğal olarak hidrofobik olan malzemeden imal edilmiş olması gerekir. Bu ileri seviyedeki su iticilik özelliği, sanayide ve günlük hayatta bir çok uygulama bulmaktadır. Süperhidrofobik yüzeylerin mevcut üretim işlemleri ya çok uzun süren, ya da pahalı işlemlerdir. Düşük maliyetli, geniş uygulama alanı olan ve elverişli bir üretim işleminin geliştirilmesi gereklidir.

Bu çalışmada, süperhidrofobik yüzeyler, polimer çözeltilerinden elektrik alan altında nanometre çaplı fiber üretme yöntemi olan, elektrodokuma ile üretilmiştir. Çok kararlı süperhidrofobik yüzeylerin, kontrol edilebilir temas açılı ve düşük su kayma açılı halde, elektrodokuma yöntemi ile üretimi bulunmuştur.

Poli-(akrilonitril-ko-dimetil meta-izopropenil benzil izosiyanat) kopolimeri sentezlenmiş, ve hidroksil-sonlu, florlu bir oligomer ilavesinin ardından elektrodokuması gerçekleştirilmiştir. Vizkositenin, flor miktarının ve kopolimer moleküler ağırlığının, elektrodokunmuş filmlerin yüzey yapısına ve su ile yaptığı temas açısına etkisi araştırılmıştır. Çalışma esnasında taramalı elektron mikroskobu, goniometre, atomik güç mikroskobu ve nükleer manyetik rezonans cihazları kullanılmıştır.

Deneyler göstermiştir ki, elektrodokunmuş yüzeylere, kasti olarak boncukların eklenmesi had safhada su iticiliğe sebep olmaktadır. Çözeltinin vizkositesi azaldıkça, polimerik boncukların yoğunluğu ve dolayısıyla filmin pürüzlülüğü artmaktadır. Bu da su ile temas açısının 150^{o}'nin üzerine çıkmasını sağlamaktadır. Kopolimer moleküler ağırlığının yapıya etkisi çalışmasında ise, düşük moleküler ağırlıklı kopolimerin elektrodokunması tamamen boncuktan oluşan bir yapı vermiştir. Bu yüzey üzerinde 166.7 ± 2.2^{o} su temas açısı ve 4.3 ± 0.8^{o} su kayma açısı ölçülmüştür.

Bu çalışmalara ek olarak, filmlerin süperhidrofobik kararlılıklarının test edilmesi amacıyla, aynı tip iki film arasına bir su damlası yerleştirilerek preslenmiştir. Bu çalışma göstermiştir ki, elektrodokunmuş yüzeylerimiz mevcut literatürdeki en kararlı süperhidrofobik yüzeylerdir.

Aileme,

özellikle de minik Eda'ya ...

ACKNOWLEDGMENTS

During my PhD study in Sabancı University, many colleagues have helped, supported and encouraged me. First of all, I would like to state my thanks to Dr. Yusuf Z. Menceloğlu. Without his academic insight and patience, such a study could never be present. I would like to give sincere gratitude to Dr. Canan Baysal, Dr. Alpay Taralp, Dr. Cleva Ow-Yang, Dr. Mehmet Ali Gülgün and Dr. Ali Rana Atılgan for their critical thinking and endless desire to share their ideas on the subject.

I also would like to acknowledge Eren Şimşek for his helps and genius questions throughout the tedious experimental work and Karahan Bulut for his aids on the drawings of this thesis.

Finally, I would like to express my gratitude and infinite thanks to: My parents, Gülser and Turhan Acatay, who have brought me this opportunity and endlessly supported throughout my life, and my wife, Ebru, my daughter, Eda, and my mother-in-law, Nilgül Özyurt, for their patience and infinite support until the first day of my PhD years. If they are not available in my life, publishing this thesis will not be as pleasurable as it is now.

TABLE OF CONTENTS

Page

LIST OF FIGURES

LIST OF TABLES

Page

LIST OF ABBREVIATIONS

AFM	Atomic Force Microscope
AIBN	Azobisisobutyronitrile
AN	Acrylonitrile
CA	Contact Angle
CAH	Contact Angle Hysteresis
CVD	Chemical Vapor Deposition
DC	Direct Current
DMF	Dimethylformamide
DSC	Differential Scanning Calorimeter
FT-IR	Fourier Transform Infrared
HMW	Higher Molecular Weight
LMW	Lower Molecular Weight
MWNT	Multi-Walled Nanotube
NMR	Nuclear Magnetic Resonance
PAN	Polyacrylonitrile
PEG	Polyethyleneglycol
PEO	Polyethyleneoxide
PMMA	Polymethymethacrylate
PTFE	Polytetrafluoroethylene
PVA	Polyvinylalcohol
QAC	Quaternary Ammonium Compound
SEM	Scanning Electron Microscope
T2EH	Tin (II) ethyl hexanoate
TMI	α,α-Dimethyl meta-isopropenyl benzyl isocyanate
WCA	Water Contact Angle
XPS	X-Ray Photoelectron Spectroscopy

CHAPTER 1

INTRODUCTION

Since the ancient times, human being wants to own or control the excellent features and systems of nature. In the beginning, s/he preferred to adore the forces of nature. As the reasons of the features were discovered, respect to this excellence had raised, and initiated an obsession to mimic them. The main driving force of many recent scientific studies are identical; to mimic nature. The inspiration behind this dissertation is similar. It was originated from the leaves of Lotus, which may be the most frequently invoked plant in the world. The reason lies under its ever-clean appearance resembling an unblemished purity. In numerous parts of the world it has been a symbol of fertility, beauty, birth and sunlight.[1] However, paradoxically, the lotus grows in muddy waters, emerging from them unblemished and untouched by pollution.[1] So, why does mud adhere to other plants, but not to the lotus? What makes this plant different? How does it work?

In 90's, Wilhelm Barthlott, a botanist of the University of Bonn in Germany, and his student Christoph Neinhus published their 20-year of scanning electron microscope (SEM) studies on numerous plants with a chief observation showing that the ever-clean leaves of the lotus are rough.[2,3] Each leaf surface is covered with tiny bumps, 5-10 μm in height and about 10-15 μm apart each other (Figure 1.1). In addition to this, the uneven surface itself is covered with waxy, hydrophobic, water repellent, crystals, measuring around 1 nm in diameter.[4] If we think today's industrial efforts on creating smooth surfaces, this fact may stun. Thus, surface cleanliness and surface roughness appeared to be exactly backward. So, the botanists patented this discovery and coined it with the term "lotus effect".

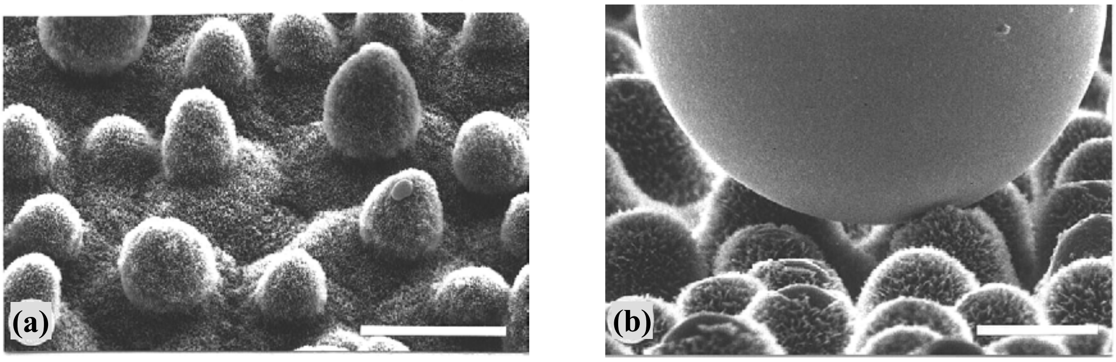

Figure 1.1 The SEM images of lotus (nelumbo nucifera) leaf: (a) Lotus leaf surface, scale bar 20 μm, (b) a mercury droplet on the leaf surface, bar 50 μm.[2]

Actually, the underlying mechanism of the mystery is simple. Imagine a flat surface covered with nails each pointing upward. If you gently place a ragged piece of paper on this nail forest, the strength of adhesion between the paper and the surface depends on the contact area. Due to the nails, the contact area is decreased, so removal of the paper becomes easier when compared to a smooth surface. Here, the surface covered with nails represents the surface of the lotus leaf, and the ragged paper represents dirt. Therefore, the removal of mud, dust etc. is easier on lotus leaf due to its weak interaction with the surface, and can easily be removed, carried away, by a rolling water droplet or wind. So, the surface seems to be forever clean due to its self-cleaning capability.

Previously, we mentioned the hydrophobic, water repellent nature of the wax crystals present on the lotus leaf. On hydrophobic surfaces, when a water droplet ia placed on to the surface, the droplet tends to bead or shrink away from the solid surface, instead of spreading on the surface as it is on hydrophilic surfaces (Fig. 1.2). The level of hydrophobicity and hydrophilicity is compared by their contact angle values, which is a measurement of the angle formed between the surface of a solid and the line tangent to the droplet radius from point of contact with the solid (Fig. 1.2). A water contact angle (WCA) of zero results in wetting, while an angle between 0^{o} and 90^{o} in spreading of the liquid drop (hydrophilicity). Angles greater than 90^{o} indicate a hydrophobic surface. The maximum WCA achieved by smooth surfaces is slightly more than 120^{o}.[5] However, Barthlott and Neinhuis measured 162^{o} on lotus leaf.[3] The WCA on lotus leaf is 40^{o} more than the maximum attainable angle by the smooth surfaces. This indicates a huge enhancement on the WCA due to increased surface roughness, and such surfaces with WCA higher than 150° are called superhydrophobic.

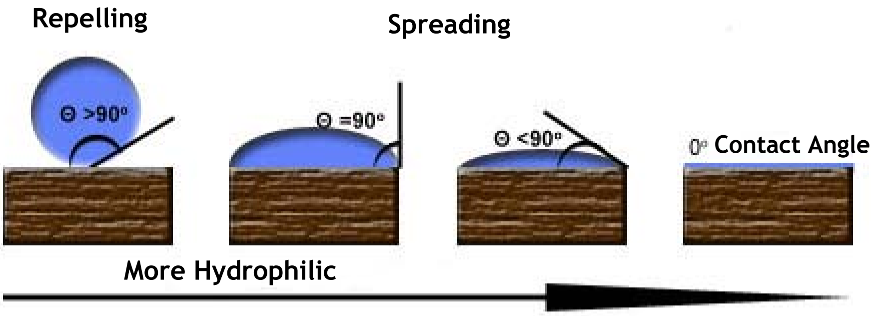

Figure 1.2 Water droplets on different wettability characteristic solid surfaces.

Interestingly, enhancement of WCA with surface roughness had been pointed 60 years before the discovery of self-cleaning mechanism of lotus leaf.[6,7] However, nobody could combined this with self-cleaning phenomena and could explained the lotus purity until Barthlott and Neinhus.

Water repellency has a great industrial and practical importance. Their potential and current applications are forever clean buildings and skyscrapers windows, prevention of adhesion of snow to antennas, self-cleaning traffic indicators, the reduction of frictional drag on ship hulls, stain-resistant textiles[8], anti-oxidation[9], minimization of contamination in biotechnological applications and lowering the resistance to flow in microfluidic applications[10]. Each of these high value added fields are following new developments in water repellent surfaces.

Due to this broad range of benefits, many attempts to understand and manufacture superhydrophobic surfaces have been spent. Several produce super water-repellent surfaces via addition of fillers (like silica particles), templating, machining, controlled crystallization, lithography, chemical vapor deposition, phase separation, and plasma etching. However, each of the processes possess one or more disadvantages, such as being time-consuming, expensive or material specific. Nowadays, almost all new articles in the field are on new methods for the production of superhydrophobic surfaces.

In this dissertation, the results of polymeric superhydrophobic surfaces created via a novel nanofiber manufacturing process, electrospinning, were presented. This research is unique, because until now electrospinning process has not been applied to generate superhydrophobic surfaces, and its hydrophobic nature has not been reported. This production process has offered the advantage of generation of superhydrophobic surfaces by a simple, inexpensive and material independent processing method. When these are combined with high potential of electrospinning of being easily incorporated to mass production processes, the value of this original work can be realized better.

After this introductory section, a chapter for the background of this research is available. In Chapter 2, more detail on processes, their histories and current studies are explained for both superhydrophobic surfaces and electrospinning process. The background chapter is followed by Chapter 3, which deals on the experimental methods and materials used in this research. In Chapter 4, the results are presented and discussed, and in Chapter 5 additional studies on electrospinning of various polymeric materials are presented. In the final chapter, Chapter 6, conclusions are reviewed, and potential future works on this study are presented.

CHAPTER 2

BACKGROUND

2.1 Water-Solid Interaction

2.1.1 Wetting

On the subject of wetting, dewetting and spreading, one can find extensive amount of theoretical and experimental articles.[11] Even though these subjects are extensively studied, they are still attracting many researchers attention especially for industrial expectations.[12]

When we place a liquid droplet onto a solid substrate, because there are three phases in contact (liquid-solid-air), there will be three surface tensions that have to be considered. Two hundred years ago, Young formulized this phenomenon with a simple mechanical balance, named Young's equation:[13]

$$\cos\theta = \frac{(\gamma_{SV} - \gamma_{SL})}{\gamma_{LV}} \tag{2.1}$$

where θ is the contact angle of liquid with solid, and γ_{SV}, γ_{SL}, γ_{LV} are the surface tensions at the interface of solid-vapor, solid-liquid and liquid-vapor, respectively (Figure 2.1). The unit of surface tension is $mJ.m^{-2}$ or $mN.m^{-1}$, and typical surface tensions are between 20 and 1000 $mJ.m^{-2}$.

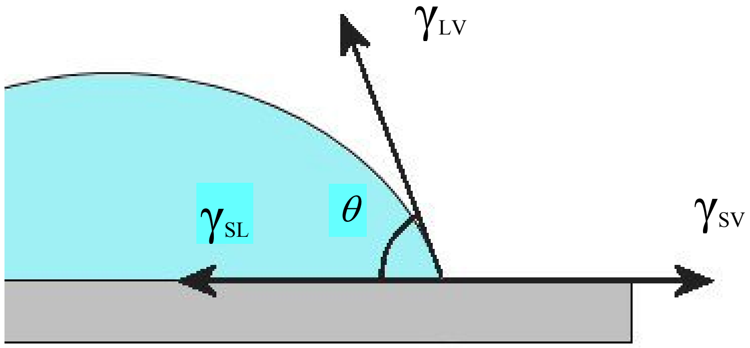

Figure 2.1 Surface tension vectors on a liquid droplet sitting over a solid substrate.

When a liquid is placed in contact with the solid, capillary forces drive the interface spontaneously towards equilibrium. As the drop spreads, the contact angle relaxes from its initial maximum value of 180° at the moment of contact to its equilibrium angle θ in the case of partial wetting or 0°, if the liquid wets the solid completely.[14]

When we take a closer look to the Young's equation:

> "…if ($\gamma_{SV} - \gamma_{SL}$) is larger than γ_{LV}, the drop tends to spread completely ($\theta = 0^o$) and wet the solid. Such as, silicone oil on most solids. Conversely, a liquid film coating a solid will be stable if the same condition is satisfied. This explains why low surface tension liquids wet most surfaces. For this reason, surfactants, which lower the liquid/vapor surface tension, will be often added to a paint to make it wetting. … In the second case, if ($\gamma_{SL} - \gamma_{SV}$) is larger than γ_{LV}, the drop should be in a pure drying situation, sitting on the solid like a marble ($\theta = 180^o$). But there is no physical system which realizes this complete drying situation."[13]

2.1.2 Definition of Commonly Used Terms in Hydrophobicity Literature

Incomplete presentations of the experimental results on superhydrophobic surfaces, which may lead to misleading understanding, are reported.[15,16] In this respect, the meaning of the terms should be clarified.

The contact angle measurements are mainly divided into two, as static contact angle and dynamic contact angle measurements.

In the static contact angle measurement, a drop of liquid with a diameter 2-6 mm is gently deposited on a flat film and its contact angle is measured. It is also termed as stationary "advancing" contact angle.[15]

The dynamic contact angle describes the happenings at the liquid-solid boundary during the wetting and dewetting processes.[17] Dynamic contact angle can be measured either by moving the deposited liquid or the solid with a speed as constant as possible. A 2 mm diameter drop of liquid is deposited on the solid surface, and the drop is slowly enlarged, or advanced, by addition of more liquid. The contact angle initially increases, than the drop front starts to move as the drop advances. This is the maximum angle that can be achieved, and this measurement is called the "advancing contact angle" measurement. By continuously wetting fresh surfaces, the advancing angle represents the contact angle which is formed directly on the contact of liquid and solid. Than, this large droplet is drawn back into the syringe and the liquid front starts to recede. The contact angle measured during this event is termed as "receding contact angle". The receding contact angle allows to make a statement about the macroscopic roughness of the solid.[17] The difference between these two angles is called contact angle hysteresis (CAH), and gives a measure on the heterogeneity of the surface.

Another dynamic contact angle measurement method is moving the solid surface. In this method, the surface is tilted as much as possible and, just before sliding of the drop, the contact angle at the front and at the rear of the droplet are calculated. This method is very similar to the advancing and receding WCA measurement method.

An alternative dynamic contact angle measurement method is by slowly tilting the surface and measure the angle of inclined surface at which the drop starts to roll (slide). So, this result is published as "the sliding (tilt) angle" data.[18] One important point in this method is its droplet weight dependence.[19]

A superhydrophobic surface must possess both high static WCA and low CAH, or sliding angle, together. Only in this way it can be named as superhydrophobic.

In addition to these, McCarthy's group preferred to make an additional classification and coined ultrahydrophobicity and ultralyophobicity.[15,16] To be ultrahydrophobic, the solid surface must present both a WCA higher than 150^o and low CAH, like in superhydrophobicity. And to be an ultralyophobic surface, independent of the WCA, water droplet should not pin on the surface. So, a material may exhibit low WCA as well as low CAH. Chen et al. reported surfaces with 105^o advancing and 104^o receding WCAs, which represents 1^o of CAH.

2.1.3 Chemistry Driven Hydrophobicity

Chemical hydrophobicity is produced by employing hydrocarbon, fluorine or siloxane rich materials in the chemistry of the surface. A well known hydrophobic material is polytetrafluoroethylene (PTFE), which has trade name of Teflon. It has high water and oil resistance in addition to its organic solvents resistance. Here, because fluorine has a small atomic radius and the highest electronegativity in the periodic table, it forms a stable covalent bond with carbon, so significantly lowers surface free energy.[5] Water contact angles and surface energies of several plastics are listed in Table 2.1.

Table 2.1 WCA and surface energies of common plastics.

Material	Surface Energy (mJ m^{-2})	WCA (^{o})
Polyacrylonitrile (PAN)	40	73
Polymethylmethacrylate (PMMA)	41	74
Nylon 6,6	38	79
Polyethylene	33	96
Polypropylene	26	108
Paraffin	19	110
Teflon	18	112

Zisman et al. reported that in the case of hydrocarbon surface, the surface energy decreases in the following order: $–CH_2–$ (bulk polyethylene); a mixture of $–CH_2–$ and $–CH_3$ groups (thin films of hexadecane); $–CH_3$ groups in a monolayer (octadecylamine monolayer); $–CH_3$ groups in a crystal plane (hexatriacontane cleavage surface). A similar ordering is observed for fluorocarbon surfaces (just replace the hydrogen with the fluorine atom)[20]. Tsibouklis and Nevell has indicated similar ordering as $–CH_2$ (36 mJ m^{-2})> $–CH_3$ (30 mJ m^{-2})> $–CF_2$ (23 mJ m^{-2})>$–CF_2H$>$–CF_3$ (15 mJ m^{-2}).[21] These indicate that the lowest surface energy can be obtained by closely packed $–CF_3$s. Nishino et al. generated the closest hexagonal packed $–CF_3$ groups with epitaxially grown n-perfluoroeicosane, $C_{20}F_{42}$ and measured 122^o advancing and 116^o receding WCA, and a surface energy of 6.7 mJ m^{-2}.[5] The maximum surface roughness was measured as 8 Å on this surface.

Tsibouklis et al. had reported and experimentally proved several rule of thumbs of low surface energy surfaces especially for antifouling applications.[21-24] They suggested that "amorphous, comb-like polymers possessing a flexible linear backbone onto which side chains with low intermolecular interactions are attached will exhibit low values of surface energy". The wetting behavior can be summarized by four structural features of the macromolecule: i) nature of the pendant chain; ii) length of the pendant chain; iii) nature of the linking moiety; and iv) nature of the polymer backbone. Their data showed that nature of the pendant chain did the most remarkable effect on surface energy. Such as, substitution of fluorinated groups as pendant chains yielded much lower surface energies than their alkyl-substituted counterparts. The length of the pendant perfluorinated moiety is also very crucial. As the length of the pendant moiety increases, the surface tension of the film decreases. However, roughness of the film increases as well. They published surface energy as low as 5.5 mJ m^{-2}, but the surface had the roughness of 8.25 nm, with 125^o WCA and 30^o CAH.[21]

2.1.4 Theory of Superhydrophobicity

As we stated in the introductory section, superhydrophobic surfaces can only be produced by generating sub-micron or micron level roughness on the inherently hydrophobic surfaces. The foundations of roughness induced hydrophobicity were developed by the articles of Robert N. Wenzel[6,25] and Cassie-Baxter[7,26].

Wenzel, in his 1936 article, stated that not only the balance between the interfacial tensions of water-liquid-air was a direct measure of the contact angle, but also the physical condition of the surface to be wetted was important. He pointed that as the roughness of the solid surface had been increased, and if the water followed the protrusion and cavities of the surface, the actual surface available was more than the smooth area. Hence, a greater intensity of surface energy acted to the liquid drop, so classical Young's equation should be modified. In this respect, he defined the term "roughness factor, r" for this homogeneous wetting case:

$$r = \frac{\text{actual surface}}{\text{geometric projected surface}} \qquad (2.2)$$

$$\cos\theta' = r\,\frac{(\gamma_{SV} - \gamma_{SL})}{\gamma_{LV}} = r.\cos\theta \qquad (2.3)$$

Since r is always larger than unity, introducing r into Young's equation enhances both the hydrophobicity of hydrophobic surfaces, and the hydrophilicity of hydrophilic surfaces. In either case, the roughness magnifies the wetting properties of the solid (Figure 2.2).

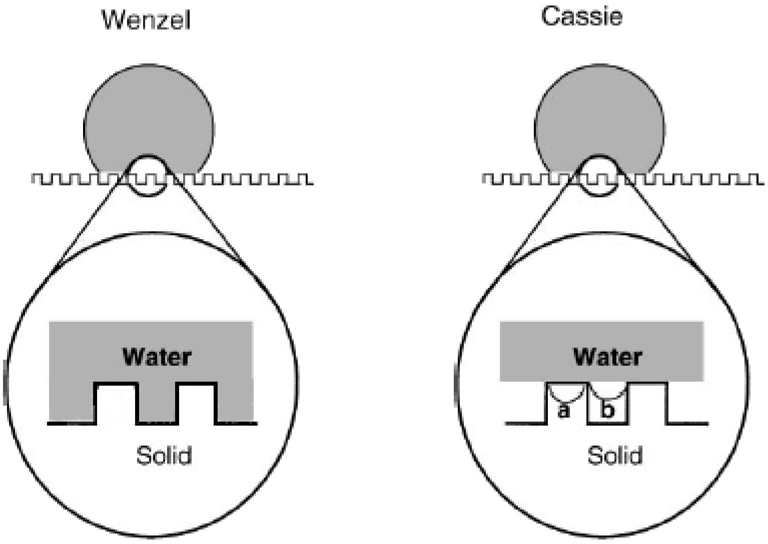

Figure 2.2 Schematic representations of Wenzel and Cassie-Baxter states.

Cassie and Baxter stated that a rough surface can be considered as a kind of porous medium where the penetration of the liquid is not favorable. Thus, air remains trapped below the liquid, which sits above a patchwork of solid and air. So, this heterogeneous surface consists of two materials, solid and air. If we take the fraction of liquid surface in contact with solid as φ_s, and in contact with air as $(1 - \varphi_s)$, new contact angle of this composite surface can be expressed as:

$$\cos \theta' = \varphi_s \cos \theta + (1 - \varphi_s) \cos 180^o = -1 + \varphi_s (\cos \theta + 1) \qquad (2.4)$$

In this regime, the hydrophobicity of a rough surface is emphasized by the decrease of the solid-liquid contact area.

In summary, Wenzel regime enhances WCA by pinning of the liquid to the surface, whereas Cassie-Baxter regime enhances WCA by minimum contact with the solid surface. This difference strongly affects CAH of the regimes as for Cassie regime CAH is lower than in Wenzel mode. So, sliding angle is lower and self-cleaning property is better.

A question may arise: when does a homogeneous wetting (Wenzel) turn to the heterogeneous (Cassie-Baxter) wetting, what is its limit? This has been first simulated by Johnson and Dettre on sinusoidal surfaces[27]. They showed that as the surface roughness factor increased, both WCA and CAH enhanced. However, after a certain limit (~ 1.7), as the WCA continued to increase, CAH started to decrease. This decrease in CAH is a consequence of the switching of the dominant hydrophobicity mode from Wenzel to Cassie-Baxter due to the increase of the air fraction at the interface between the solid and water.

2.1.5 Reviews of Recent Studies

In this section, the recent publications on the field of superhydrophobicity were briefly reviewed, and their chief results were presented. The recent papers were selected, because, previous review articles on the field reviewed the preliminary studies in details, and we preferred to deliver information on the current trends and studies.

Otten and Herminghaus have studied two superhydrophobic plant surface with totally different surfaces morphologies in their article.[28] One is Indian Cress, which has a surface like Lotus leaf, with a surface decorated with three different length scales of micrometric roughness (First length scale is a few tens of microns by the epidermal cells, second, ~1 μm wax crystals on top of the cell surface, and the last was the distance of the wax crystal bundles, ~5 μm). Other is Lady's Mantle, which has a hairy water-repellent surface. Both let water droplets run off easily over their surfaces. Also, a model system composed of a patterned substrate which was made up of carbon nanotube bundles with 10 μm high. In these bundles, each nanotube had a few nanometers diameter. First, they studied the Indian Cress surface. When a water droplet placed onto the rough surface of Indian Cress, ~180^o WCA was measured. However, when micron-scale water droplets were grown by cooling the solid surface, ~140^o WCA was measured. The reason of this WCA loss is; when droplet is placed onto the surface it traps air underneath the water between roughness, but when a droplet was slowly grown by condensing water on the surface, the condensed water fills the cavities during growing, thus no air pockets was generated and lower WCA was observed. Same was observed for the carbon nanotube bundles decorated surface. Thus, the water repellence of micro-rough plant leaves is due to a specific surface comprising a hierarchy of length scales. The material of which the structure was made of must possess a contact angle >90^o, and air is entrapped below the water droplet resulting very high WCA. However, the hairs of Lady's Mantle exhibited WCA well below than 90^o both for advancing and receding WCA measurements. During the condensing of water droplet on the surface, first the droplets started to nucleate on the cuticula surface below the hairs, then after a certain volume suddenly the drop was lifted from the cuticula into the brush, and no decrease in WCA was measured between the condensed and normal water droplet cases. The lift of the droplet was explained energetically favorable situation of hydrophilic hairs than the hydrophobic cuticula. The water droplet prefers to pass to hydrophilic hairs. Their studies on the reason of high WCA has shown that when a water droplet was left or condensed on the surface, the hairs, which are underneath the droplet, prefer to create bundles, thus mechanically resists to the entrance of water droplet. This results a superhydrophobic surface. For hairy situation, the important parameters are the distance between the hairs (their density) and the hair's elastic modulus. So, a different approach by nature to superhydrophobicity was presented and underlying mechanism was first presented.

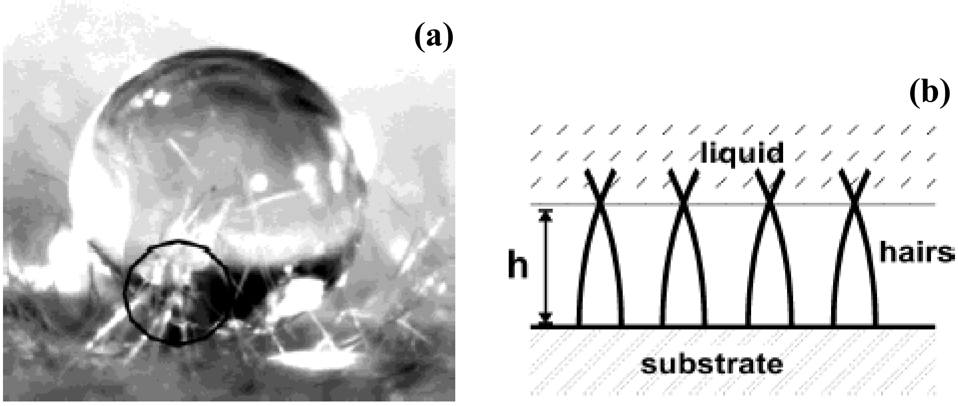

Figure 2.3 (a) 1 mm diameter water droplet on an Indian Cress leaf, (b) Sketch of the elastic deformation of the hairs due to bundle formation at the interface.[28]

Gu *et al* had studied superhydrophobicity from a different point by combining it with structural color.[29] They were inspired from the wings of butterfly which exhibits both lotus effect and fancy colors. They used inverse opal which is a solid material that consists of a three-dimensional network. It has ordered monodisperse air spheres that is resulting an optical stop band. Thus, by naked eye, various colors can be seen according to the spacing between the roughnesses. The inverse opal films were fabricated by dipping and slowly withdrawing a glass slide into a suspension, consisting of mixture of a few hundred nanometer diameter polystyrene and 6 nm diameter silica nanoparticles. During very slow withdrawing, the polystyrene beads generated a well-ordered structure, whereas the nanoparticles of silica were filled the gaps between the beads. Than, the films were calcined at 450^{o}C to remove the polymer and to solidify the silica particles. Finally, they were coated with fluoroalkylsilane by thermal chemical vapor deposition. Finally, a rough surface composed of well-ordered meshes was obtained. SEM images exhibited a hexagonal arrangement of the air spheres encircled by the silica networks. The resultant films showed different colors from blue to red according to the diameter of the holes. The WCA of the film with 275 nm center-to-center between the neighboring air spheres were measured as 155^{o}. In conclusion, by fabricating uniform inverse opal films the group had generated surfaces with both structural color and superhydrophobicity, which may be useful for decorative applications.

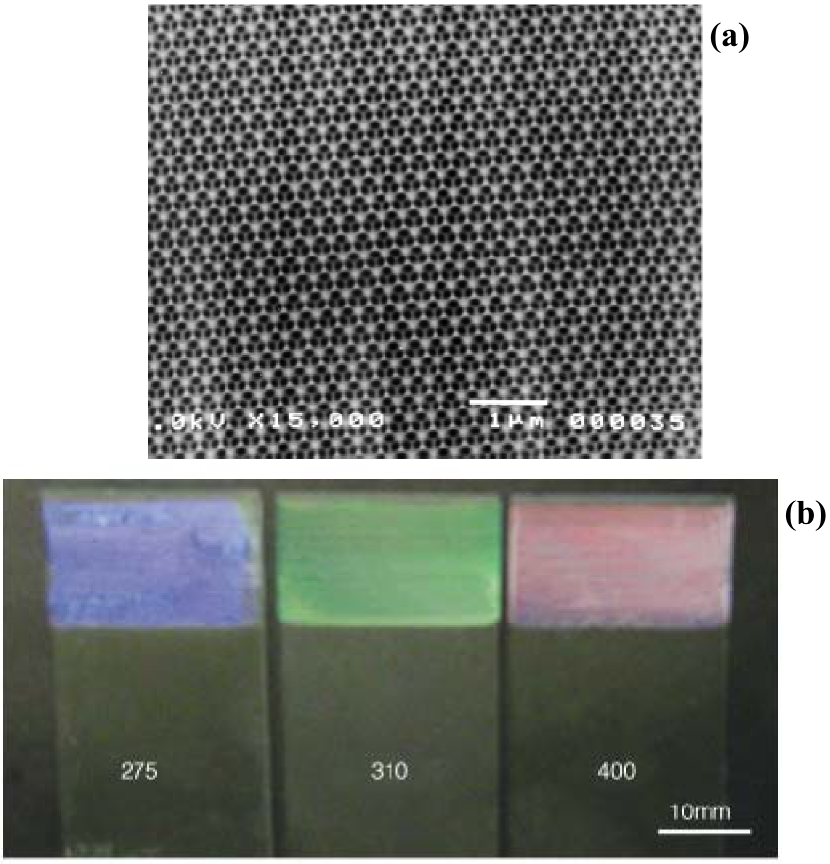

Figure 2.4 (a) SEM image of an inverse opal film with a center-to-center distance between neighboring holes of 275 nm, and (b) Three different colors from the inverse opal.[29]

A superhydrophobic surface via generating a vertically aligned multi-walled nanotube (MWNT) forest were created and coated with a nonwetting coating, PTFE. To deposite vertically aligned nanotubes, Lau *et al* used a plasma enhanced chemical vapor deposition (PECVD) technique.[30] First, nickel (Ni) catalyst islands were formed on an oxidized (20 nm) silicon substrate through the sintering of a thin (5 nm) Ni film at 650^{o}C. Second, nanotubes were grown from these islands of catalyst in a DC plasma discharge of acetylene and ammonia. The height of nanotubes was controlled by the plasma deposition time, where typical nanotube growth rate was 330 nm/min. A height of 2 µm nanotube forests with 10 MWNTs per µm^2 could be wetted by water easily. And when the samples were examined after drying, it was observed that the nanotubes forced into bundles under the surface tension effect of evaporating water. If taller (10-15 µm) nanotube forests were generated, WCA of 161^{o} angle was observed for a short period of time. However, the droplets were not stable and with in a few minutes they swept into the forest voids. Than, the group coated the nanotubes in the forest with the

PTFE, through a hot filament chemical vapor deposition (HFCVD) process. In this respect, hexafluoropropylene oxide (HFPO) gas was thermally decomposed at 500^{o}C to form difluorocarbene (CF_2) radicals, and radicals polymerized into PTFE with the aid of initiator. The advancing and receding WCA of PTFE coated nanotubes were found as 170o and 160o, respectively. In addition to static measurements, dynamic measurements were also performed. The bouncing of a water droplet on the forest surface was imaged by a high speed camera. Also, condensations of micrometer diameter droplets were investigated with ESEM and no wetting was observed. When the φ_s in Cassie-Baxter equation was calculated, it was found as 11% for 60 nm (coated) average radius 10 nanotubes per μm^2 surfaces. This φ_s value results 170^{o} and 158^{o}, respectively, which was in good agreement with the measured values. Finally, the group measured the advancing and receding WCA of the coated nanotube forests at different heights (0.2 to 1.1 μm). It was observed that as the tube height increased, advancing did not change too much, but receding angles were increased, so CAH was decreased.

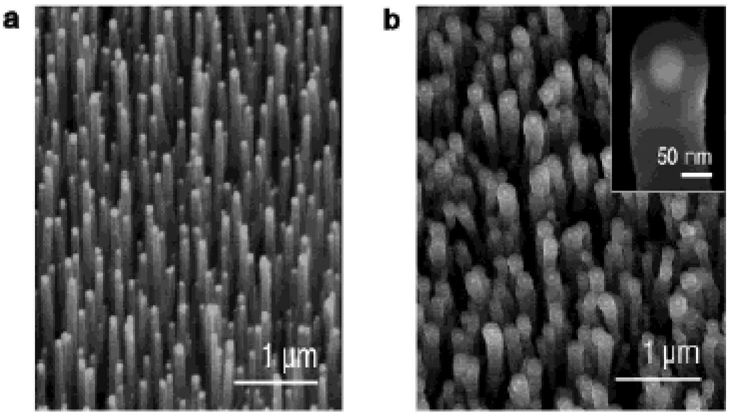

Figure 2.5 SEM images of carbon nanotube forests. (a) Not coated, (b) after PTFE coating.[30]

Superhydrophobicity can also be generated by patterning large-area periodic nanosphere arrays. In this respect, Shiu *et al* had spin-coated the monodisperse polystyrene beads (440 nm in diameter) solution, and achieved a self-organized close-packed nanostructures.[31] Single- and double-layer polystyrene arrays could be created by adjusting the speed of the coater and concentration of surfactants in the polystyrene solution. Than, the surfaces were exposed to varying periods of time of oxygen plasma etching, which reduced the diameter of the beads while keeping their separation distance constant. After etching, monolayers of beads with varying diameters from 440 nm to 190 nm were obtained. In addition to this, the etched surfaces were modified by octadecanethiol (ODT), after covering with 20-nm-thick gold film. When the gold coating and ODT modification was performed onto a flat substrate, the resultant WCA was measured as 114°. However, the etched surfaces resulted 135° for 400 nm diameter up to 168° for 190 nm. For double-layer polystyrene bead morphology, the measured WCA was around 170°, which was higher than the maximum in single layered surface. SEM studies on double-layer bead morphology had shown that around 10 % of defects were available on the surface, so a third-level of roughness were introduced to the system. In addition to experimental studies, the group performed a simple theoretical study on the monolayer bead morphology by using Wenzel and Cassie-Baxter equations, and concluded that the situation can be properly explained by Cassie-Baxter equation. If the contact area is taken as the upper part of the beads, and the Cassie's modified equation for hemispherical case was used, the equation fitted to the experimental results very well. Finally, the advancing and receding angle studies were performed, and the hysteresis were found as 20-30°, which was not a low hysteresis value. And they concluded as: "…the dynamic contact angle measurement indicates that well-ordered two-dimensional nanostructured systems have relatively large water contact angle hysteresis."

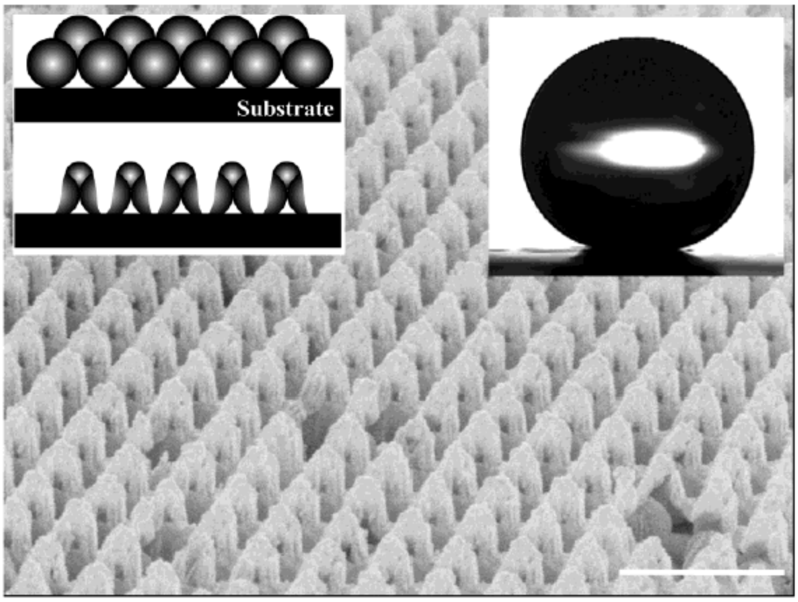

Figure 2.6 SEM image of a 440-nm-diameter double layer polystyrene surface after 120 sec of oxygen plasma treatment. Bar is 1 μm.[31]

An interesting study is on the coating of mesh screen with a superhydrophobic and superoleophilic film.[32] This can be used for the continuous separation of diesel oil and water or to generate corrosive liquid (acids and alkalis) resistant meshes. In this respect, a homogeneous emulsion was prepared by mixing polytetrafluoroethylene (PTFE, 30 wt %), adhesive (polyvinylacetate, 10 wt %), dispersant (PVA, 8 wt %), surfactant (sodium dodecyl benzene sulfonate, 2 wt %) and distilled water (the rest). The emulsion was than sprayed evenly on several stainless steel mesh screens, and subsequently placed into 350°C oven for 30 minutes. The resultant was a mesh screen mainly covered with low-surface energy PTFE. Smooth film of PTFE had about 121.6±1.8° contact angle with water and 11.2±1.6° contact angle with diesel oil. Thus, it is intrinsically hydrophobic and oleophilic. However, when roughness was introduced, due to Wenzel case, both hydrophobicity and oleophilicity was enhanced. This resulted a film having 156.2±2.8° WCA with "about 4° sliding angle" and 0±1.3° contact angle with diesel oil. When a mixture of water and diesel oil was poured onto this PTFE coated mesh screen, the diesel oil easily passed the screen whereas the water part was collected on the top of the mesh screen. During the contact angle measurements on different mesh sizes the optimum pore diameter of the film was found as 50-200 μm. Below or above these limits, the WCA was decreased, and diesel oil contact angle was increased. In summary, a simple liquid filter was generated to easily separate water and oil mixtures.

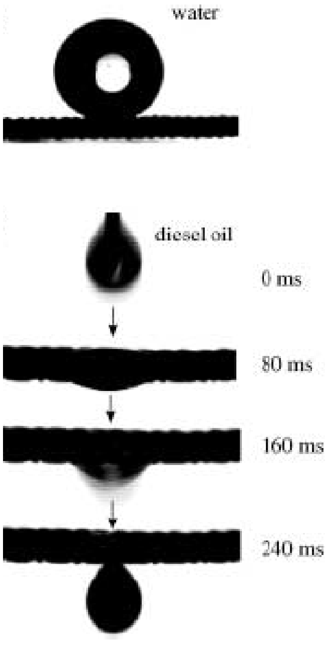

Figure 2.7 The test with water and diesel oil on the prepared coating mesh film.[32]

Superhydrophobic surfaces are generated via producing rough surfaces from inherently hydrophobic materials. However, Feng *et al* generated superhydrophobic surface from polyvinylalcohol (PVA) which has a 72.1±1.1° WCA.[33] The group generated vertically aligned PVA nanofibers by using the templates of anodic aluminum oxide membranes. The average fiber diameter of PVA nanofibers were measured as 72.1 nm at the tip with an average interfiber distance of, approximately, 361.8 nm. The nanofiber density was, approximately, 7.07×10^8 nanofibers per square centimeter, and the average length of the fibers were 14.3 μm. The WCA of this PVA nanofiber surface was measured as 171.2±1.6°. In several previous studies[34-36], it has been proposed that when the precursor of the PVA solution is compressed into the nanometer-scale pores of the template, due to strong orientation of the PVA molecules intermolecular hydrogen bonds are created. In addition to this, most of the hydrophobic groups may be at the surface, which would minimize the free energy of the system, thus makes the nanofiber upper-most surface hydrophobic. In this respect, to see the orientation of the hydrophobic $-CH_2-$ groups to the interface, XPS studies were performed, and it was seen that the exterior surface of the nanofibers were mainly composed of $-CH_2-$ groups. Whereas the cast film sample of the PVA showed same $-CH_2-$ composition both on the surface and the interior. Thus, by the aid of alignment of hydrophobic surfaces to the surface and high level of roughness on the surface, a superhydrophobic surface can be generated from an inherently hydrophilic material.

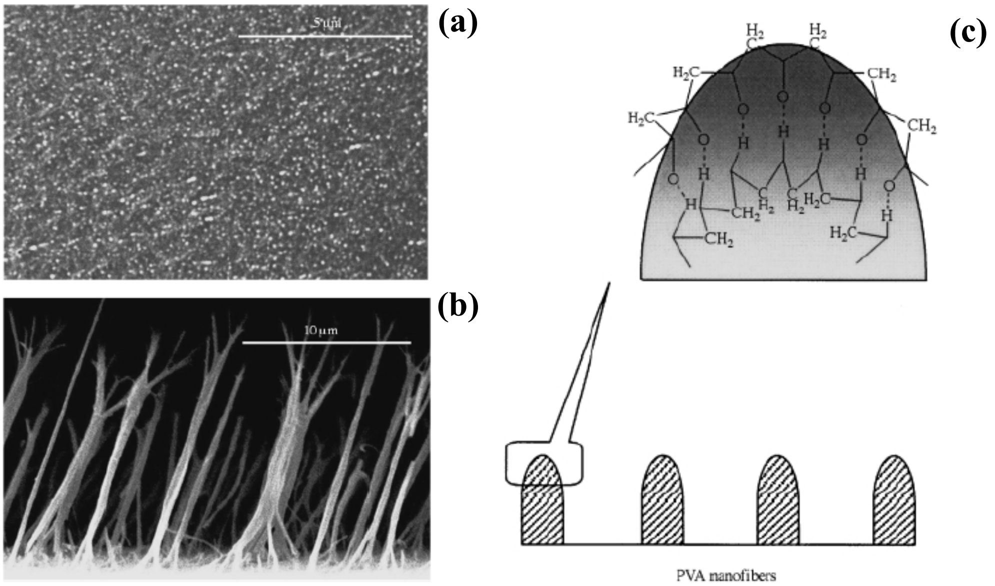

Figure 2.8 SEM images of the PVA nanofibers (a) from top, and (b) cross-sectional. (c) Possible conformation modes of the PVA molecules at air/solid interface.[33]

Zhang et al had prepared ZnO columnar films on $SnO_2:F_2$ substrate by cathodic electrodeposition in a three-electrode reactor at 70°C.[37] ZnO nanocolums with 125 nm average diameter had grown to ~1 μm in height within 60 minutes. Their density was about 24 columns/μm^2, and hexagonal phase of ZnO was measured by X-ray diffraction. Than, the ZnO films were treated by the refluxing vapor of heptafluorodecyltrimethoxysilane (FAS) in anhydrous toluene for 2 hours. In addition to this, single crystal flat ZnO films were also prepared and covered with FAS. The flat films exhibited 112°/82° advancing/receding WCA. However, the ZnO nanocolumnar surfaces exhibited a superhydrophobic surface behavior with 167.0±0.7° advancing and 159.0±0.8° receding contact angles, thus yielding 8° of WCA hysteresis. After the ZnO nanocolumnar surface covered with FAS, when it was exposed to 150 mW/cm^2 ultraviolet light for 20 minutes, the contact angle was reduced from 167° to <5°. Thus, a superhydrophilic surface was resulted. X-Ray Photoelectron (XPS) studies had shown that after irradiation, alkyl chain of FAS had been decomposed to generated some active oxygen species ($HO^{\cdot}$, O_2^{-}, and H_2O_2). By the cleavage of hydrophobic FAS chain, it turned to hydrophilic silica structure, thus lower than 5° WCA was measured on previously superhydrophobic ZnO nanocolumnar films.

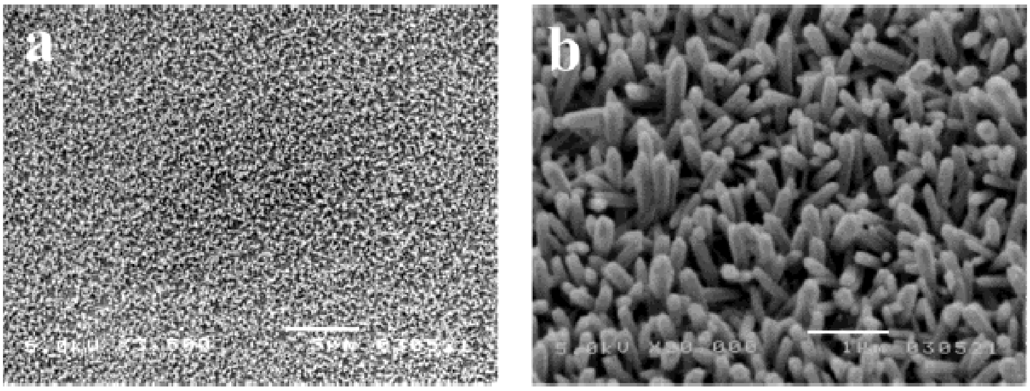

Figure 2.9 SEM images of ZnO nanocolumns. The bar in a is 5 μm, and in b is 1μm. b was taken at 30° tilt angle.[37]

Liu *et al* synthesized a superhydrophobic surface, which could reversibly turn to superhydrophilic when exposed to UV illumination.[38] The superhydrophobic surface was synthesized by Au-catalyzed chemical vapor deposition of ZnO. Equal amount of carbon powder and ZnO powder were placed into a quartz boat which was placed into a furnace with Au-coated substrates. After heated to 600-650°C at a rate of 1 °C/sec and kept for 60 minute at that temperature under Argon gas flow, the substrate were covered with ZnO. In the SEM images it was seen that, the surface was covered with many block-shaped protuberances with 320-560 nm which were decorated with many ZnO nanopapillae with a size from 21.6 to 41 nm. The AFM roughness was found within the range of 600-1191 nm. On this surface, water droplets made 164.3^{o} contact angle. When the surface was subjected to UV illumination, within 1000 minutes, the WCA were decreased $<5^{o}$. If this illuminated surface was placed in the dark or was heated, within several days, superhydropilic surface was reconverted to superhydrophobic. The reason of this reversible change was explained as: "…the electron and hole generated by ZnO under band gap illumination will move to the surface to react with the lattice metal ions Zn^{+2} to form Zn^{+} defective sites and the lattice oxygen to form the surface oxygen vacancies, respectively. … When it was placed in the dark or was heated, oxygen atoms that result from the recovery of its initial state can replace these oxygen vacancies gradually", so the wettability is reconverted.

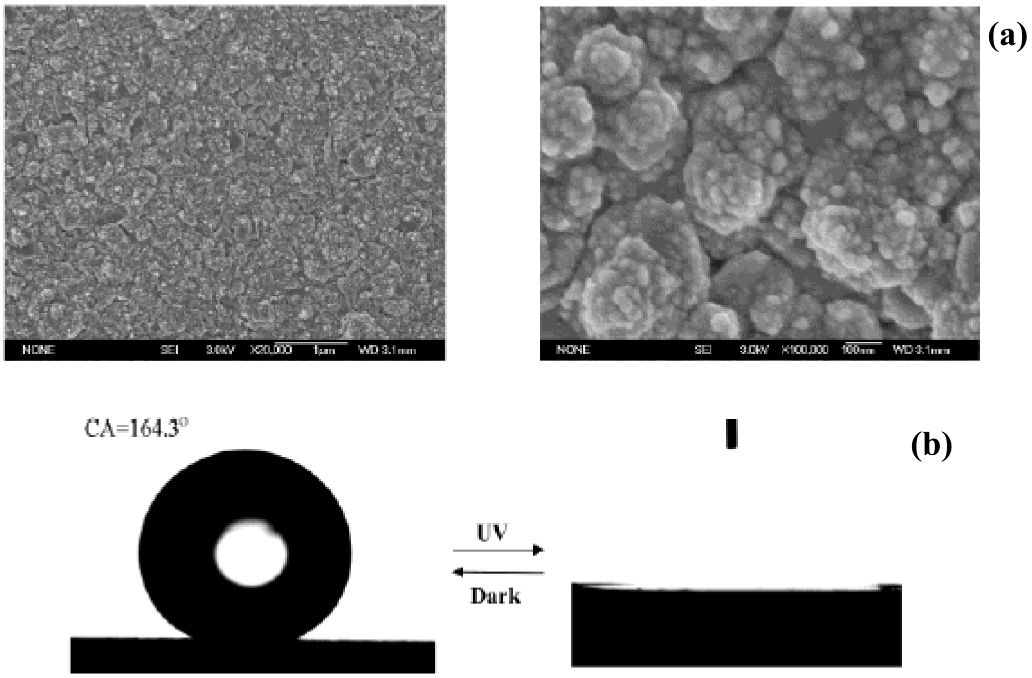

Figure 2.10 (a) SEM images of Au catalyzed ZnO thin film, (b) Water droplet on the superhydrophobic and superhydrophilic surface of ZnO.[38]

Krupenkin *et al* has induced sharp transition between wetting states on a nanoscale rough surface from superhydrophobic to nearly complete wetting by electrowetting effect.[39] In electrowetting, low voltage of electricity is applied between the liquid droplet and the substrate, thus the effective energy of the solid-liquid interface can be dynamically adjusted, and the wetting state can be successfully varied. In this respect, group prepared silicon wafers which were decorated with 350 nm in diameter and 7 μm in height cylindrical posts with pitches varying between 1 to 4 μm. Than, to electrically isolate the posts 50 nm of thermal oxide was grown, and to create a hydrophobic surface an additional fluorocarbon layer of 20 nm thick was deposited by plasma assisted chemical vapor deposition using C_4F_8. To measure the effect of electrowetting on the wetting of decorated surfaces, high-surface-tension liquids (water and molten salt) and low-surface-energy liquids (cyclopentanol and octanol) were used after a small amount of salt was added to them for electrical conductivity. After deposition of the liquid droplets, a Pt-wire was inserted into the droplets for the application of electricity. For molten salt case, a mobile and ~180^o CA exerting droplet at no voltage applied situation were underwent a sharp transition to the immobile and low CA situation after application of 22 V electricity. Similar was observed for cyclopentanol application at 50 V. To understand the nature of these transitions, a UV-curable resin was employed, and the penetration of liquid in the nanostructured layer by application of the electricity was demonstrated. So, the widest possible tunability range, from superhydrophobicity to complete wetting (irreversibly), was achieved by using electrowetting.

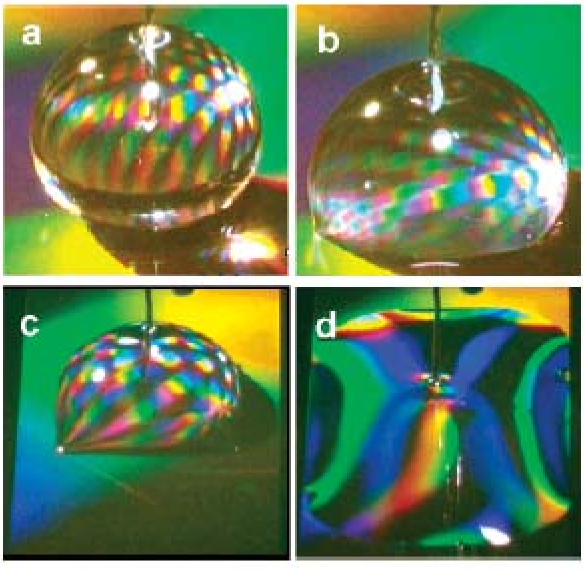

Figure 2.11 Photographs of: (a) Molten salt droplet with no voltage application, (b) after voltage application, (c) cyclopentanol droplet with no voltage application, and (d) after voltage application.[39]

A novel pattern for controlling the surface wettability is by adjusting the anisotropic structure of surface generated by aligned carbon nanotube (ACNT) films.[40]

ACNTs can be grown normal to the substrate by chemical vapor deposition (CVD) method. The nanotubes are dense and at the same length. By using ACNTs, Sun et al proposed a method to control the wettability of surfaces. They, first, manufactured patterned silicon templates with the square pillars of 30 μm in height, and 10 μm in width. As the spacing between pillars 6, 10, 13, 15 and 20 μm were selected. After this, by CVD, ACNTs were produced on the surface of silicon template. At the horizontal sections of the template the ACNTs were grown vertically, whereas at the vertical regions (side-walls of pillars) the ACNTs were grown horizontally. The ACNTs diameters were ranging between 25 to 50 nm, and their length was around 10 μm. Thus, especially for the 6 and 10 μm spacing cases, the ACNTs on neighboring pillars touched each other and curled. Than, the ACNTs wettability was modified by vinyltrimethoxysilane (VTMS) and (2-(perfluorooctyl)ethyl)trimethoxysilane (FETMS). The smooth films of VTMS and FETMS were yielded 78.1 ± 1.8^o and 111.9 ± 2.1^o, respectively. When the virgin silicon templates were covered with VTMS, the WCA was measured as 158 ± 1.5^o. For VTMS modified ACNT covered surfaces, the WCA was measured for 20, 15, 13, 10 and 6 μm spacing samples as 21.2 ± 1.5^o, 153.3 ± 3.3^o, 154.9 ± 1.5^o, 27.2 ± 1.8^o and 20.8 ± 2.3^o, respectively. While the wetting in 6 and 10 μm cases happened immediately, for 20 μm case, first, the droplet made a high contact angle, but it lowers within the time, and after about 10 seconds, it immediately spreaded. The reason of wetting at 6 and 10 μm were explained by the curling of ACNTs, and they facilitated the reach of water droplet to the horizontal ACNTs. Thus, the water droplet was spreaded in the horizontal segments due to the capillary effect. Because the ACNTs were not hydrophobic. In 13, 15 and 20 μm cases, there were less or no curling, so the vertical ACNTs restricted the reach of water to the horizontal sections. However, because the number of vertical ACNTs were lower in 20 μm spacing case, after a certain period the water could reach the horizontal segments and immediately spreads. In FETMS treated case, the WCAs were all measured higher than 150^o. Because the ACNTs were intrinsically hydrophobic, when the water droplet reached to the horizontal sections, wetting did not occur. These results showed that anisotropic microstructures can bring a better control over the surface wettability. By simply varying the spacing between the micropillars or coating of ACNTs, the transition between superhydrophobicity and high hydrophilicity can be induced.

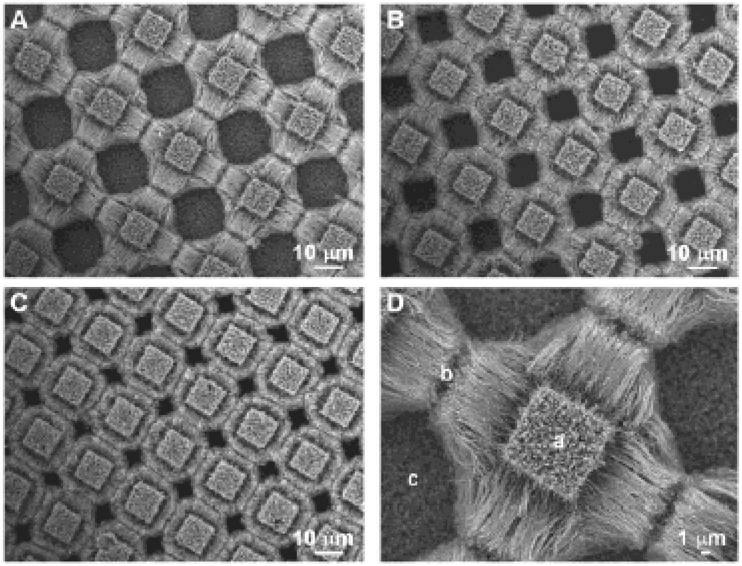

Figure 2.12 SEM images of anisotropic ACNT microstructures. (A, B and C) Periodic ACNT arrays with pillar height of 20, 15 and 10 μm, respectively. In the figure D, the ACNT array at A was magnified, and a, b, c represents vertical ACNT arrays on the top of pillars, horizontal ACNT array on the side walls of pillars, and ACNTs grown from the bottom of the templates, respectively.[40]

2.1.6 Stability of Superhydrophobicity or Water Droplet Pressing

At the designing stage of the superhydrophobic surface, by using Cassie-Baxter and Wenzel formulas we can calculate the apparent WCA on our surfaces. However, previous studies in the literature are not conclusive regarding which formula to use and when. Recently, there is a discussion on the determination of governing state on a superhydrophobic surface.[41-46]

Pioneering studies showed that in addition to Cassie-Baxter and Wenzel states, there is also a metastable Cassie-Baxter state at the WCA range of Wenzel state. This metastability starts after a critical WCA, θ_c, at the border of Wenzel and Cassie-Baxter states (Figure 2.13). The reason is the trapped air below the water droplet cannot exit and continue to stay below the droplet. However, if a surface is at metastable state even with a small force application to the droplet, the replacement of air with water and transformation of a metastable Cassie-Baxter to Wenzel state is resulted. If the droplet is sitting on a stable Cassie-Baxter state governing surface, the pressure application should not change the post-pressing WCA.

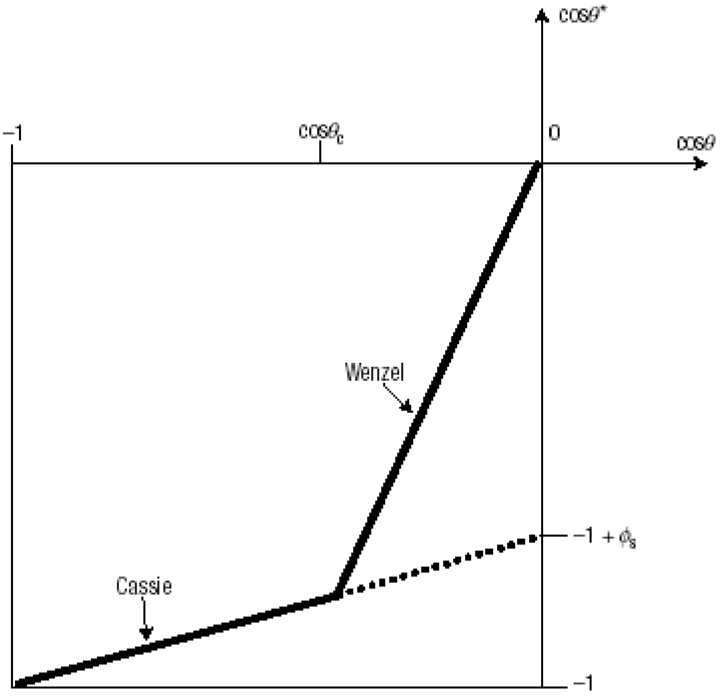

Figure 2.13 Cassie-Baxter and Wenzel states. Dotted line indicates metastable Cassie-Baxter state.

This discussion has both theoretical and industrial significance. It is important due to the relation between degree of hydrophobicity and self-cleaning. As we indicated in previous section, on the microtextured surfaces, if the regime turned from Cassie-Baxter to Wenzel the CAH and sliding angle of the water droplet dramatically increased, because the water is pinned by the water entered into the surface cavities. So, self-cleaning property has been deteriorated. Designing and knowing the level of stability of the micro-textured surfaces help us to use the surfaces at their proper application fields. Thus, if our surface is not at metastable Cassie-Baxter state, it serves durable and resists to higher pressures without loosing its highWCA.

As we know, this occurrence was first mentioned by Bico et al.[45]. On their lithographically micro-textured surfaces, they measured 170^o WCA. When they applied load to the droplet, the WCA dramatically decreased to 130^o±5^o (they did not note the magnitude of pressing). For their surface (r = 1.3 and $\theta = 118^o$), WCA calculated by Wenzel was 128^o. Thus, they pointed out that, because low contact angle is thermodynamically favorable, existence of two contact angles on a surface resembles the metastability of the high contact angle one. They concluded by indicating "the resistance of Cassie state was finite".

Later, Lafuma and Quéré proposed a series of experiment on lithographically micro-textured and perfluoroacrylate covered surfaces. Their surface had a WCA of 164 ± 3^o with "extremely low" CAH of 5^o. First, they measured WCA by condensing tiny droplets of water on textured surface. While the drop is slowly enhancing from very little volume to larger volumes, air cannot be trapped below the drop. By this method, they obtained 141 ± 3^o, with a huge CAH of $100\text{-}105^o$. This confirms the true Wenzel state formation. Secondly, they placed a water droplet between two plates covered with the same superhydrophobic material and uniaxially pressed the drop between plates. The applied pressure was calculated by Laplace equation ($\Delta P = 2\gamma|\cos\theta^*|/x$, where γ was the surface tension of water, θ^* was the contact angle while pressing, and x was the gap between the two plates). Higher than 200 Pa pressures were applied, the droplets splitted into two, one half at the top plate other at the bottom, after the load was removed (post-pressing). The reason is the increased adhesion of water droplet to both plates as a result of pressure. Lower than 200 Pa pressures, no change at post-pressing WCA was observed, so the cavities were not invaded by water. The invasion can occur through the vapor phase (condensation of a dew), or by an external pressure. They wrapped up their discussion by indicating how a superhydrophobic surface must be designed:

> "… θ_c must be as small as possible … Because of phenomenological nature of parameter φ_s, this condition is not so easy to create … It was often noticed that superhydrophobic plants indeed exhibit a large r (ratio of actual area to apparent area), due to having two levels of texture. Such a hierarchical structure does not only enhance the hydrophobicity, it also stabilizes the Cassie regime, and thus favors water repellency."

In a recent study, Marmur has modeled a rough surface with parabolic protrusions, similar to lotus plant, and theoretically studied the protrusions steepness and distance[44]. In addition to contact angle, the sliding angle was inserted to this model. Marmur theoretically proved that the Cassie-Baxter contact angle is insensitive to the protrusion distance and mildly sensitive to the steepness. This brings to nature, real life, an ease of creating randomly placed protrusions and “avoids the need for high steepness protrusions that may be more prone to erosion and breakage. And, the metastable superhydrophobicity of the lotus leaf is relatively insensitive to mild variations in the surface roughness design.

2.2 Electrospinning

Electrospinning is nowadays attention drawing method for polymer nanofiber production. By the aid of electrical force, it produces sub-micron and nanometer scale diametered, continuous, non-woven and randomly laid polymeric fibers from polymer solutions. A simple search in Web of Science database with “electrospinning or electrospun” keyword has shown that the open literature has at least doubled every year since 2000 (Figure 2.14). It should be noted that the figure just covers the articles, however as much as articles there are patents in the field[47]. The reason of growing interest to electrospinning is originated from unique properties of nanofibers, such as very large surface area to volume ratio (for instance nanofibers with a diameter of 100 nm has approximately 100 m^2/g surface area), flexibility in surface functionality, and superior mechanical performance compared with any other known form of the material[47,48]. Even there are other nanofiber production processes than electrospinning, such as drawing, template synthesis, phase separation, self-assembly, electrospinning seems to be the only method for mass-production of one-by-one continuous nanofibers from various polymers.

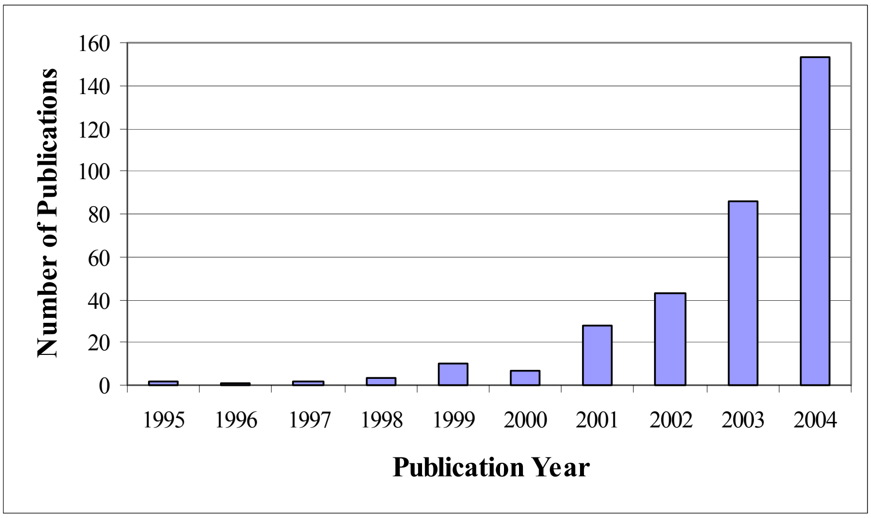

Figure 2.14 Number of publications according to the years. Web of Science database was used, and the data for 2004 is for the first seven months.

Electrospinning, or electrostatic spinning, of solutions of macromolecules fundamental idea dates back more than 70 years earlier. From 1934 to 1944, Formhals issued a series of US patents for making polymer fibers by using electrostatic force. Fibers were formed from a solution of cellulose acetate[49]. In 1966, Simons patented an apparatus for the production of non-woven fabrics of ultra-thin and light weight with electrical spinning. He also found that the fibers from low viscosity solutions tended to be shorter and finer whereas from more viscous solutions were relatively continuous. In 1971, Baumgarden had electrospun acrylic polymers from dimethylformamide solution. He generated fibers with diameters less than 1 micron, and studied relations between governing parameters of electrospinning. In 1981, Manley and Larrondo reported that continuous fibers of polyethylene and polypropylene could be electrospun from melt, without mechanical forces. They characterized the fibers via X-ray diffraction and mechanical testing.[49]

Since 1990s and especially in recent years, the electrospinning process has regained attention probably due to an increased interest to nanotechnology, and submicron or nanometer scale fabrication needs.

2.2.1 Electrospinning Process

Most of the electrospinning systems consist of three basic components: a high voltage supplier, a syringe with a needle of small diameter and a metal collecting screen. In addition to these, a syringe pump may be incorporated to the system to manage the flow rate of the fluid. After filling the syringe with the fluid, one electrode of the high voltage supplier is immersed to the fluid. The collecting screen serves as the other electrode, and for simplicity it is grounded. When high voltage supplier is activated, the fluid emerging from the tip of the syringe needle is carried from the needle to the collecting screen in the form of charged thin fiber. During this transportation in air, solvent in the fiber has been evaporated, and dry, non-woven, continuous solid fibers have collected on the grounded screen.

Even the process seems very simple; electrospinning process involves polymer science, applied physics, fluid mechanics, electrical, chemical, mechanical, material engineering and rheology.[49] This results the unmanageable nature of electrospinning.

Fong and Reneker described the electrospinning process in three stages: "(1) jet initiation and the extension of the jet along a straight line; (2) the growth of a bending instability and the further elongation of the jet, which allows the jet to become very long and thin while it follows a looping and spiraling path; (3) solidification of the jet into nanofibers." Figure 2.15 is showing the initiation of a jet of fiber from the pendent drop at the tip of the needle. At time zero, the liquid is kept in together by the aid of surface tension. When an electrical difference between the needle and grounded plate applied, the electrical forces at the surface overcame the forces associated with surface tension. A liquid jet emerged from a conical protrusion (called Taylor cone) that formed on the surface of the pendant droplet. The jet was electrically charged. The jet carried away the ions from the needle to the grounded screen. Jet diameters near the droplet were in the range of 20 to 100 μm.

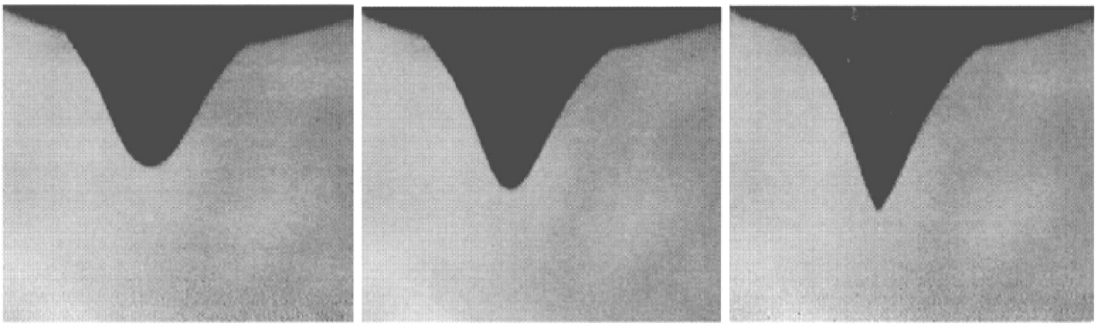

0 millisecond 20 millisecond 26 millisecond

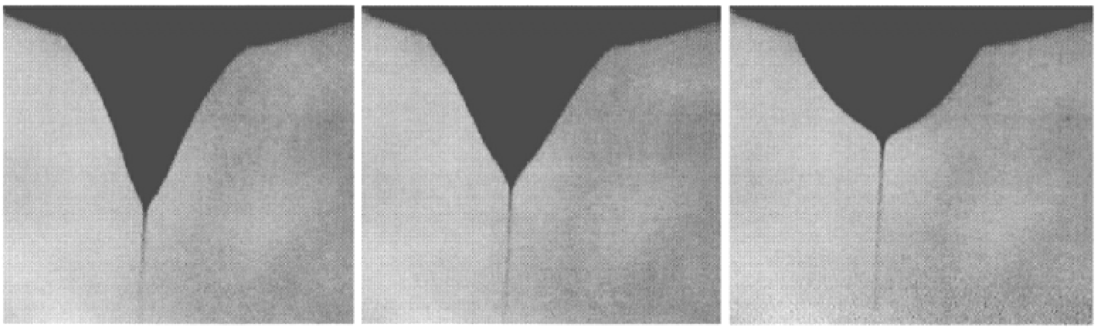

28 millisecond 34 millisecond 50 millisecond

Figure 2.15 Photographs of the pendent drop and jet, near the time the jet was ejected. Photographs were taken with 500 frames per second and 2 ms shutter speed instrument. The length of horizontal edge of each of the images was 1 mm.[49]

After initiation, generally, the jet has followed a straight path for a certain distance. Then, an electrically driven bending instability grew at the bottom end of the straight segment. The bending allowed a large elongation to occur in a small region of space. During bending, first, a smooth segment that was straight or slightly curved suddenly developed an array of bends. As the segment of the jet in each bend elongated, the linear array of bends became a series of spiraling loops with growing diameters (Figure 2.16). As the perimeter of each loop increased, the cross-sectional diameter of the jet forming the loop grew smaller. The continuous elongation each segment was most strongly influenced by the repulsion between the charges carried by adjacent segments of the jet. The elongation and the thinning of the jet continued as long as the charge on the jet supplied enough force to overcome the surface tension and viscoelastic forces. Meanwhile, the viscosity of the jet increased due to evaporation and eventually elongation stopped.[49]

Generally, the elongation of the jet during the bending instability is considered as the cause of thinning of the jet; however in some cases splitting and splaying of the jet are seen with other materials.

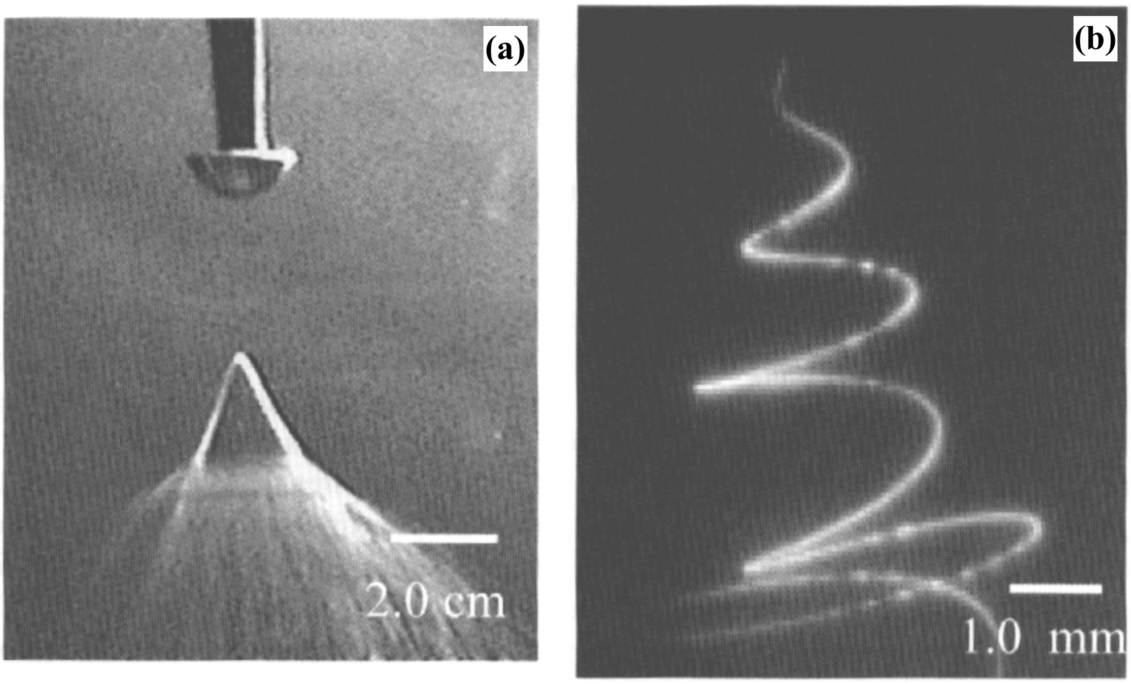

Figure 2.16 Images of the electrospinning jet with different exposure times: (a) shutter speed was 16.7 ms, (b) shutter speed was 1.0 ms.[49]

Some researchers had made changes on basic electrospinning setup such as using horizontal syringe placement instead of vertical, using rotating mandrels as grounded collector for fiber collection, or incorporation of additional electrical fields to align deposited fibers.

In addition to dissolved polymers, molten polymers at high temperature can also be made into nanofibers by electrospinning.[47,50] The electrospinning of polymer melts was carried in vacuum. The advantage of vacuum is higher electric field strength over large distances and higher temperature can be used than in air.[48] It should be noted that much less polymer have been tried to electrospun in molten form.

2.2.2 Electrospinning Processing Variables

Many parameters can influence the transformation of polymer solutions to nanofibers by electrospinning. These can be classified as: (i) the solution properties such as viscosity, elasticity, conductivity, molecular weight and structure (linear or branched) of polymer, and surface tension, (ii) governing variables such as flow rate of polymeric solution, high voltage applied, and gap between the needle and the collecting screen, (iii) ambient parameters such as solution temperature, humidity, and air velocity in the chamber.[51] As long as a polymer can be electrospun, researchers aim to achieve: (1) to control the diameters of the electrospun fibers, (2) create defect-free or defect-controllable fiber surface, and (3) collectable continuous single nanofiber filaments. However, all three are hard to achieve targets, and still many theoretical and practical efforts are spent for understanding and control of nanofibers.

The control of fiber diameter is one of the most important target in electrospinning. The fiber diameter mostly depends on the jet sizes and polymer content in them. During the travel of jet to the collector, the jet may [52,53] or may not [54,55]split into multiple jets. If the jet splits, wide range of fiber distribution is obtained; if not relatively narrow distribution is obtained. In the case of no splitting, one of the most important parameter affecting fiber diameter is the solution viscosity. There is low and high limits of the solution viscosity to create stable fibers. Out of these polymer and solvent specific ranges beads are generated, in addition to fibers. According to Doshi for the spinning of polyethylenoxide (PEO) in water, the viscosity should be in the range of 100-20000x10^{-3} Pa-s[51]. Deitzel et al. reported that the fiber diameter increased with increasing polymer concentration, so the viscosity, according to a power law relationship.[52] Demir et al. found that the fiber diameter was proportional to the cube of the polymer concentration.[56] Also, applied electrical voltage affects the fiber diameter. In general, a higher applied voltage ejects more fluid in a jet, resulting in a larger fiber diameter. In spite of all efforts to create uniform fiber diameter, they are seldom uniform.

Like viscosity, electrospinning voltage has a low limit. Below this minimum, electrical force cannot overcome the surface tension of the liquid and a jet cannot be created. A linear relation is observed between the applied voltage and the solution flow rate.[57] As the concentration of the solution increases, a greater force is required to form a jet. However, during surface tension manipulations one should keep in mind that, generally surface tension is negligibly dependent on polymer concentration. The solvent properties are more dominant. However, low surface tension does not necessarily mean defect-free fibers.[47] Also, Fong and Reneker experimentally showed that as the solution surface tension increases, mass flow rate decreases.

Fong and Reneker also reported that for PEO solution in water as the spinning voltage increases both the current and solution flow rate increase.[49] The electrical current carried by the jet increased with the square of the voltage and typical currents are at a few microampere level. “The flow rate of the solution was determined from the mass of the nanofiber collected, the concentration of the solution and the collecting time. A typical jet had a flow rate in the range from a few milligrams per minute to hundreds milligrams.”[49]

Recently, Theron et al. has extensively studied the governing parameters in electrospinning and generated empirical equations for many parameters.[58] One is the relation between tip to ground distance (gap) and electrical current. They found an exponential relation between electrical current and gap, as the gap increases the current decreases.

Another interesting issue is addition of salt into the polymer solution. Demir et al. reported a dramatic increase in mass flow with the addition of triethylbenzylammonium chloride[56]. 2 wt% of salt doubled the mass flow. Zong et al. add 1 wt% of salt during the electrospinning of biodegradable PLGA polymer for bead-free fiber production.[59] They stated that the addition of salts resulted in a higher charge density on the surface of the solution jet during electrospinning, bringing more electric charges to the jet. So, higher elongation forces were imposed to the jet under the electrical field resulting bead-free fibers.

Another concern in electrospinning is bead formation during electrospinning. The beads and bead-like structures are generally appreciated as defects [47] or by-products[60], and the solutions to eliminate them or to decrease bead density are recommended.[48,49] An electrically driven jet of a low molecular weight liquid would form droplets, as in electrospraying. There the formation of droplets is due to the capillary breakup of the the jet by surface tension. However, for polymeric solutions, the mechanism is changed and instead of breaking completely, the beads connected to each other with nanofibers.

In 1999, Fong and Reneker carried the first systematic study on the beads in electrospinning. They studied water solution of PEO, and published the first rule of thumbs on the matter. These are: (i) beads and beaded fiber are less likely to be formed for the more viscous solutions. The diameter of the beads become smaller, the average distance between beads on the fibers longer and the shape of the beads gradually changes from spherical to spindle-like as the viscosity increases. (ii) By addition of salt, net charge density is increased, and as the net charge density increases the beads become smaller and more spindle-like, while the diameter of fibers became smaller. (iii) Decreasing the surface tension by addition of alcohol to the solution reduced the size and number of beads.[60] Also, the decrease of bead density (regardless of concentration) by increasing the distance or decreasing the electrical field is reported.[48] Deitzel et al. found that, spinning voltage measurements can be used to signal the onset of the voltage at which the bead defects density substantially increases.[52] On the beads and beaded fibers issue, one of the smallest nanofiber ever made had been reported.[61] The electrospinning of styrene-butadiene-styrene (SBS) showed that the fibers between the beads had diameters as small as 3 nm.

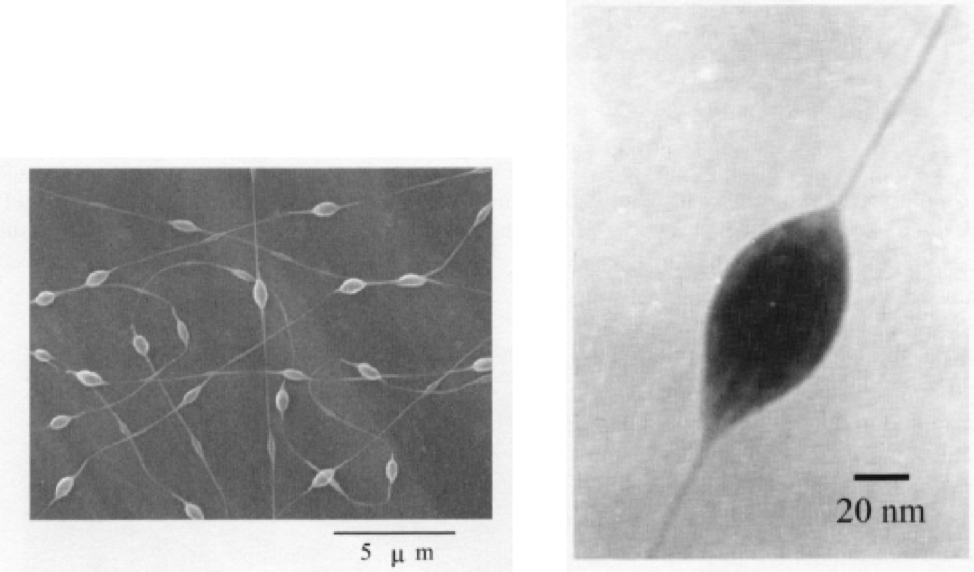

Figure 2.17 SEM image of a beaded fiber (beads on a string).[49]

Jaeger et al. studied the surface of PEO beads formed during electrospinning by atomic force microscopy (AFM) and concluded that at the molecular level, the beads possessed a highly ordered surface.

The effect of molecular weight of polymer to bead formation is studied by Koski et al., and they found that, in polyvinylalcohol (PVA)-water case, for each molecular weight, fibrous structure was stabilized above a minimum concentration of PVA.[62] This stabilization concentration was higher for low molecular weight polymers than for higher molecular weight ones.

2.2.3 Applications

Nanofibers have many practical and potential application fields and they are listed in Figure 2.18. Most of the applications are still premature and needs improvements, however many patents are taken on their applications. More than 50 % of the US patents are taken on medical prosthesis field, and followed by filtration, composite, tissue template and liquid crystal devices.[47] In this section, several applications are highlighted briefly, to show the importance and potential of electrospinning process.

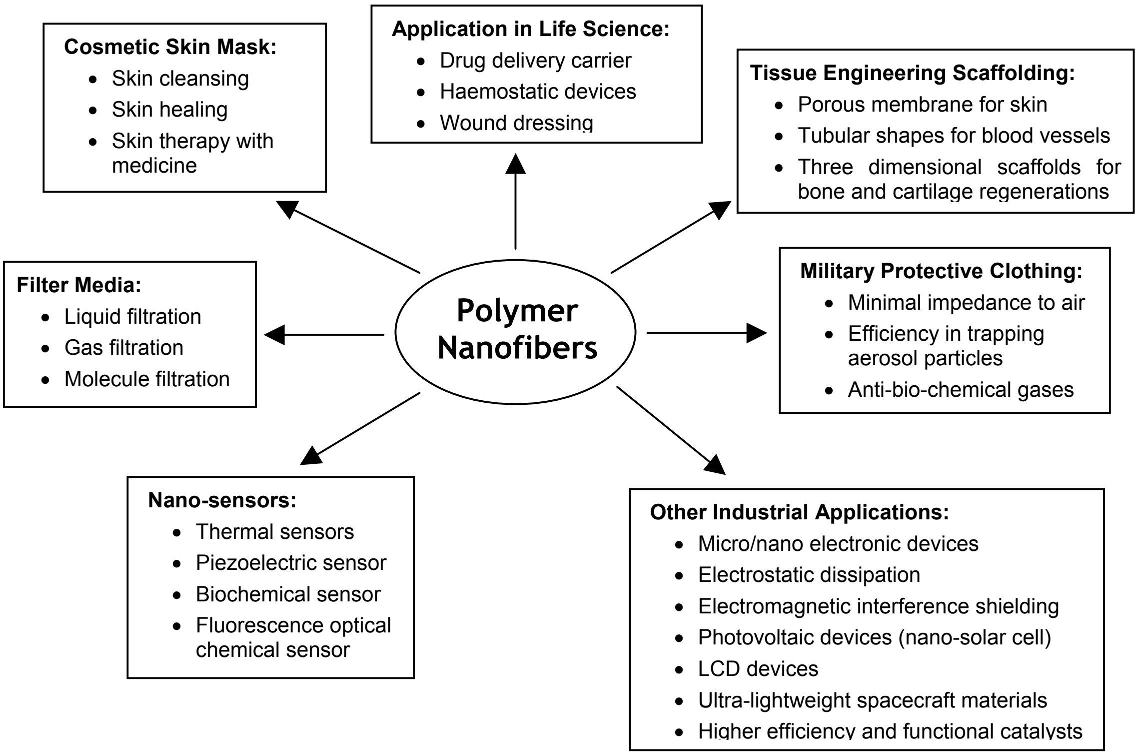

Figure 2.18 Potential applications of electrospun polymer nanofibers.[47]

One of the most important applications of micro-size fibers is composite applications. In the near future the same may be valid for nano-size fibers. Comparison of impregnating piled nanofiber sheets into epoxy matrix and virgin epoxy yielded significant increase in fracture energy whereas the fracture toughness increased marginally. For rubber matrix, the Young's modulus enhanced by ten times and the tear strength was increased twice. However, the main problem is the collection of unidirectional aligned fibers. Second obstacle is the limited publications on the nanofiber composites even many studies are held both in industry and universities. One more interesting anecdote on composite applications is efforts on the fabrication of transparent composites. Because the nanofiber diameters are smaller than the wavelength of visible light, their usage is proposed and partially studied on the reinforcement of plastic shields used by police departments and army.

Another important application, due to its great market potential, is the filtration industry.[63] Efficiency of the filtration is closely related with the fiber fineness, and it is the most important concern for filtration.[64] Electrospun mats had been tested and their efficiency on filtering of submicron size aerosols had been proven. In addition to this, nanofibers can be used for particle capturing with low pressure drop by electrostatically charging them.

Almost all of the human tissues and organs are deposited in nanofibrous forms or structures. Bone, dentin, collagen, cartilage and skin are some examples. All of them are characterized by well organized hierarchical fibrous structures realigning in nanometer scale. Some applications are for soft tissue prostheses applications, such as blood vessel; tissue template for artificial organ generation; wound dressing due to its small enough pore sizes which penetrates air but not bacteria and drug delivery because of its high surface area. In addition to all these, US army is studying on the usage of electrospun films for protective clothing application for NBC (nuclear, biological and chemical) warfare.

In the electronic field, conductive nanofibers are synthesized and they may be used for tiny electronic devices for Schottky junctions, sensors and actuators.

Commercialization of synthetic fibers with diameters in the range of nanometers has not been significantly developed, however one shared opinion in literature is the promising future of the electrospinning process.

CHAPTER 3

EXPERIMENTAL

3.1 Materials

Acrylonitrile (AN) used through out the study was kindly supplied by Aksa Akrilik Kimya Sanayi A.Ş (Yalova). It was purified first by washing with dilute H_2SO_4 (Riedel-de-Haen), than dilute Na_2CO_3 (Fluka), and distilled water. These followed by drying with anhydrous Na_2SO_4 (Merck), and finally fractional distillation over CaH_2 (Merck) under nitrogen atmosphere.[65] The purified AN was kept at 2°C in refrigerator, and consumed within 2 weeks period after purification. Second monomer of the poly-(AN-co-TMI) copolymer, unsaturated aliphatic isocyanate, α,α-dimethyl meta-isopropenyl benzyl isocyanate (TMI), was generously supplied by Cytec, and used as received (Figure 3.1).

The perfluorinated linear diol, Fluorolink-D, which was added for fluorination and crosslinking reactions was donated by Ausimont, and used as received. It is a 1000 gr/mol molecular weight, dihydroxylated linear alcohol (Figure 3.1). In addition to Fluorolink-D, ethylene glycol (Aldrich) and polyethyleneglycol (200 and 1500 gr/mol) was also used as crosslinker for hydrocarbon films.

HPLC-grade N,N-dimethylformamide (DMF, Aldrich) and tetrahydrofuran (THF, Aldrich) were used as solvent during the reactions and electrospinnings. Azobisisobutyronitrile (AIBN, Fluka) was used as addition polymerization initiator after crystallization in acetone. Tin (II) ethyl hexanoate (T2EH, ChemPur) was used without treatment as condensation reaction catalyst.

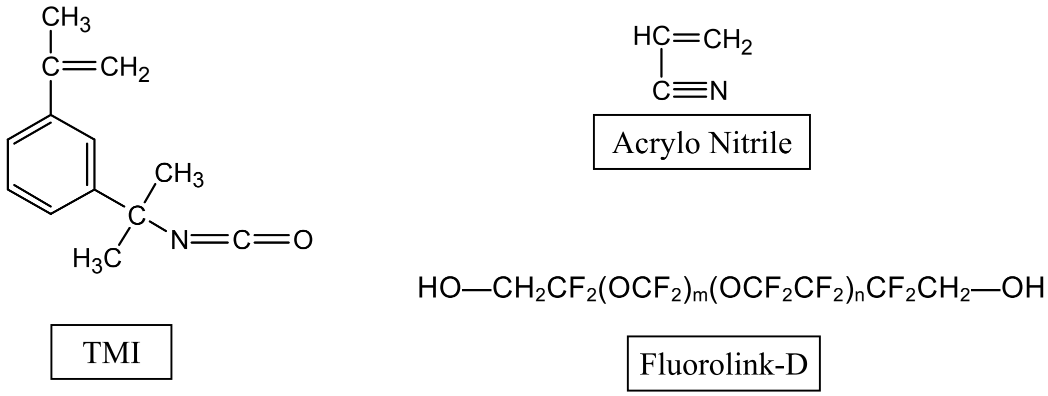

Figure 3.1 Molecular structures of TMI, Acrylo Nitrile and Fluorolink-D.

3.2 Instrumental

Molecular weights (viscosity average) of copolymers were determined by using Cannon Ubbelohde Viscometer (Size 1B). During calculations, the constants of polyacrylonitrile (PAN) in DMF at 25°C ($K = 39.2 \times 10^{-5}$ and $a = 0.75$) were used in Mark-Houwink equation.[66]

Prior to each electrospinning, the viscosity of the solution was measured by a viscometer. For that purpose, a DV-III Rheometer (Brookfield) coupled with a Wells-Brookfield Cone/Plate capable of measuring 20-200,000x10^{-3} Pa-s viscosity range was used. Wells-Brookfield Cone/Plate attachment enable us to perform viscosity measurements with only 0.5 ml of solution.

The TMI content of poly-(AN-co-TMI) copolymers was determined by proton nuclear magnetic resonance (^{1}H-NMR) study in Varian 500 MHz NMR with deuterated-DMF of Aldrich.

The electrospinning of solutions were carried by using a high voltage DC supply (CPS Model No 2594, 50 kV), a syringe with 16-gauge stainless steel tip, a syringe pump (Univentor 801) and a grounded collection screen covered with household aluminum foil. A drawing of the set-up was presented in Figure 3.2.

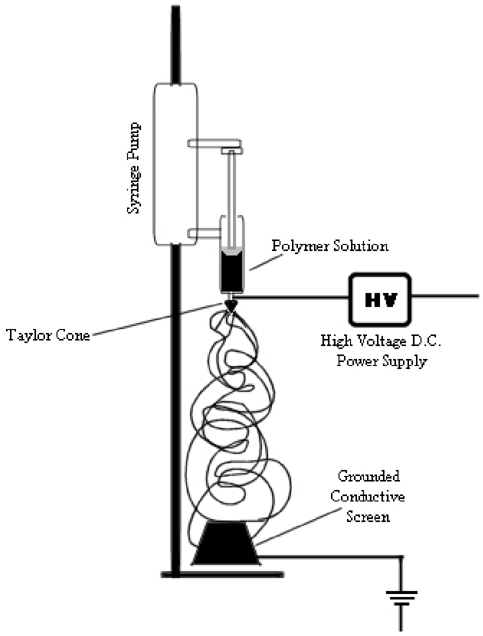

Figure 3.2 The electrospinning set-up.

Information about the surface topography of electrospun films were gathered by scanning electron microscope (SEM) and atomic force microscope (AFM) studies on the micro-textured surfaces. SEM of electrospun films was performed by using a LEO Supra VP35 FE-SEM, after depositing a conductive coating of gold onto the micro-textured films with an Emitech K950X sputter coater. Generally, imaging was performed at low accelerating voltages (0.8-2 kV) with 4-7 cm working distance. AFM studies were done with Digital Instruments Nanoscope IIIa. Because the surface roughness of electrospun films is higher than the vertical limits of AFM, only mechanically pressed samples were investigated. During AFM studies, tapping mode measurements were performed with Si tips at 0.42 N m^{-1} spring constant cantilevers.

Studies on the thermal properties of copolymers and electrospun films were carried out using a Netszch Phoenix DSC 204 differential scanning microscope (DSC) with aluminum sample pans. 10 K/min heating rate and nitrogen atmosphere were used for DSC analysis. The DSC instrument was coupled with CC 200L, liquid nitrogen cooling system for below the room temperature measurements.

Fourier Transform Infrared (FT-IR) studies were carried by using Bruker Equinox 55 instrument with Attenuated Total Reflectance (ATR) attachment.

Prior to electrospinning, the mixtures of the polymeric solution were mixed well with Vortex mixer (Velp Scientifica, $2x^3$) or Ultrasonicator of Bioblock Scientific.

3.3 Goniometry

Contact angle measurement of the electrospun films were performed using a Krüss GmbH DSA 10 Mk 2 goniometer with DSA 1 software. The aluminum foils coated with electrospun film were placed onto microscope slides by the aid of double-sided adhesive tape. The water drop commonly used for the measurements was weighing 5 mg, and the contact angles were measured at least at 10 different points for each electrospun film by using the Laplace-Young fitting method of the software. Their averages and standard deviations are presented. During the contact angle measurements, fresh distilled ultra-pure water (Millipore, Milli-Q) was used.

Sliding angle measurements were performed by placing the electrospun sample onto a long-flat surface and inclining the surface very slowly. 10 mg of ultra-pure water droplets were used for each measurement, and at least 10 measurements were performed for each film. To increase the accuracy, the length of the flat surface was varied according to the angle which sliding occurred, i.e. for low sliding angle, a long surface, and for high sliding angle, a short one.

CHAPTER 4

RESULTS AND DISCUSSION

4.1 Synthesis and Electrospinning

Poly-(AN-co-TMI) copolymer was synthesized by solution polymerization of AN with TMI in DMF solvent (Figure 4.1). 2.5, 5 and 10 mole % TMI containing reactions were run. However, the electrospun films were generated from 5 mole% TMI loaded polymerization product. AIBN was used as addition polymerization initiator at a concentration of 0.04 % relative to AN.

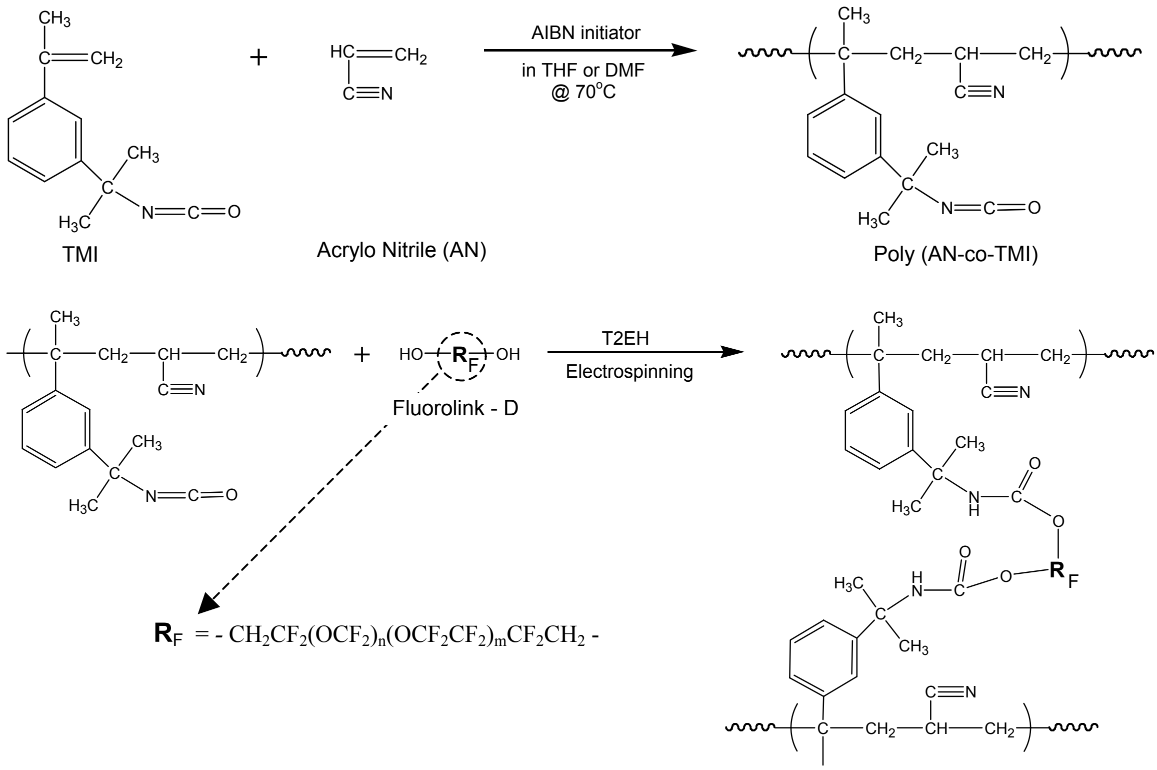

Figure 4.1 Reaction scheme for superhydrophobic surface generation by co-electrospinning of poly (AN-co-TMI) and Fluorolink-D.

The reactions were run 25 hours at 70°C, and yielded a yellowish, 30-40x10^{-3} Pa-s viscosity and 0.9 µS/cm conductivity polymeric solutions. The viscosity average molecular weight of poly-(AN-co-TMI) was determined as ~20000 gr/mol, and throughout the text this copolymer was named as higher molecular weight (HMW) copolymer.[67] After the reaction, the solution was kept at -20°C, until it was electrospun. The NMR, DSC and FT-IR characterization of the 5 mole% copolymer was presented in Figure 4.2 and Figure 4.3.

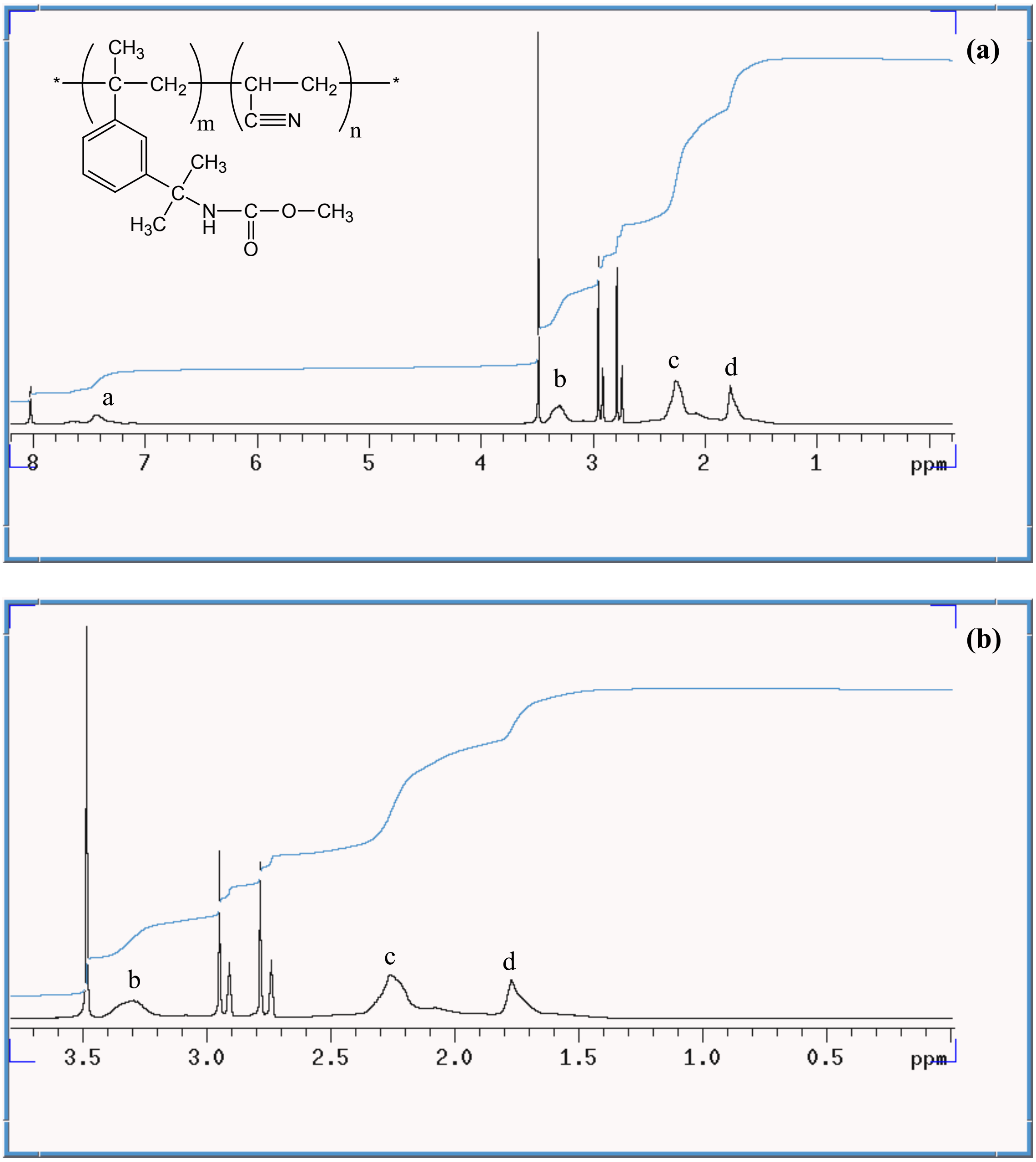

Figure 4.2 NMR spectra of poly-(AN-co-TMI) with 5 mole% TMI loading: (a) Whole spectra between 0 and 8 ppm, (b) Enlarged image between 0 and 4 ppm.

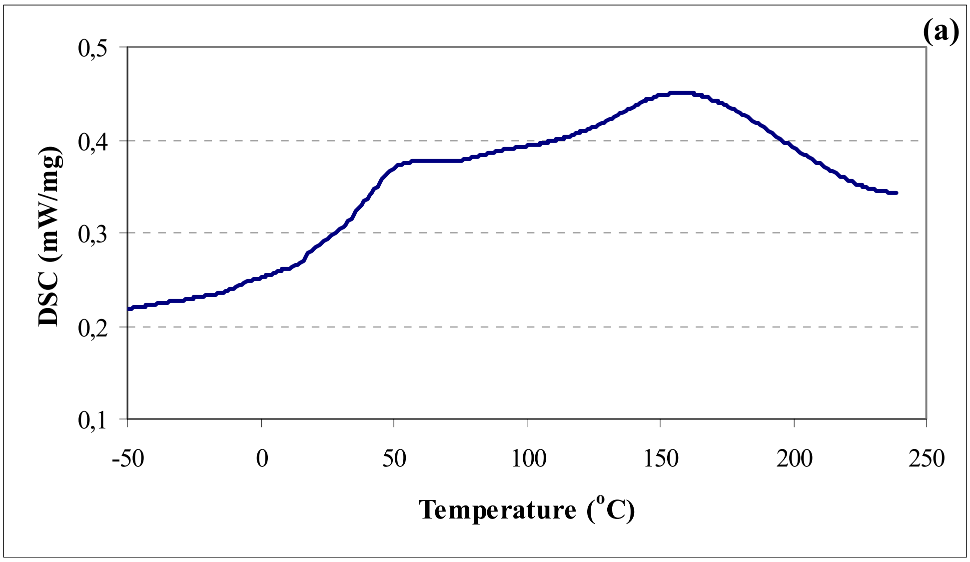

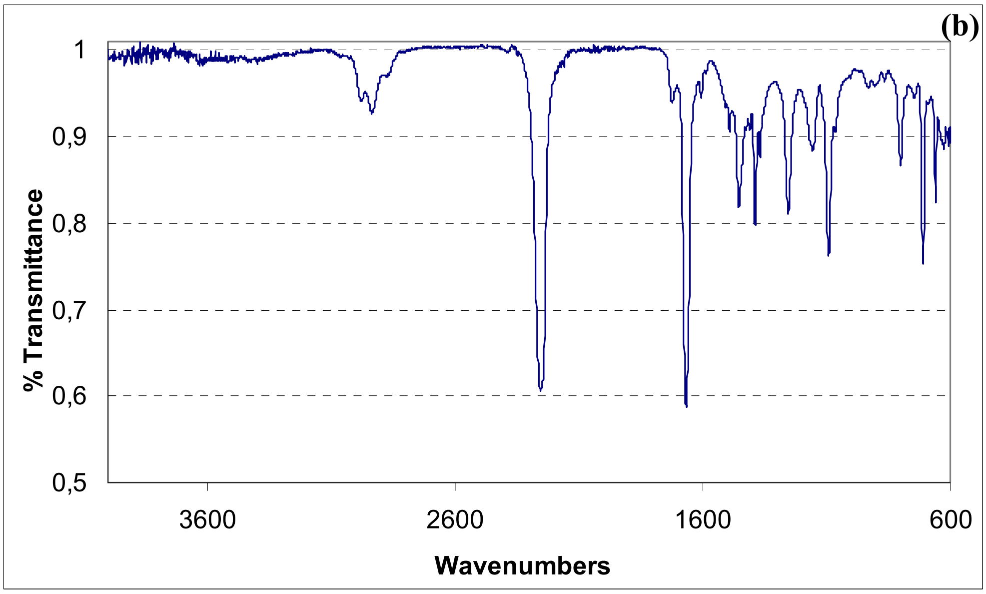

Figure 4.3 (a) DSC, and (b) FT-IR of poly-(AN-co-TMI) with 5 mole% TMI loading and in DMF.

In the NMR spectra (Figure 4.2), copolymer which was precipitated in methanol was used. The peaks at 8.02 (singlet) and two "five peaks" at 2.74 and 2.91 ppm are the peaks belonging to deuterated-DMF used during NMR analysis, and 3.48 (singlet) belongs to water as impurity. The broad peak marked as "a" in Figure 4.2 belongs to the four protons in the aromatic ring of TMI. The peaks at "b" and "c" represents the –CH– and $–CH_2–$ on the main chain of the copolymer. And three $–CH_3$'s of TMI resulted the peak at around 1.8 ppm. The peaks of protons attached to nitrogen and oxygen were not identified exactly. However, by using the integral data, the TMI amount of the product copolymer can be calculated. It was found 2.5, 5 and 10 mole% TMI loaded (initially) and presented in Figure 4.4. A linear relationship was obtained with a good regression value of 0.98. The results showed that the reactivity of TMI with AN is high, and the TMI molecules incorporated to the copolymer main chain is more than twice of the initial loading percentage.

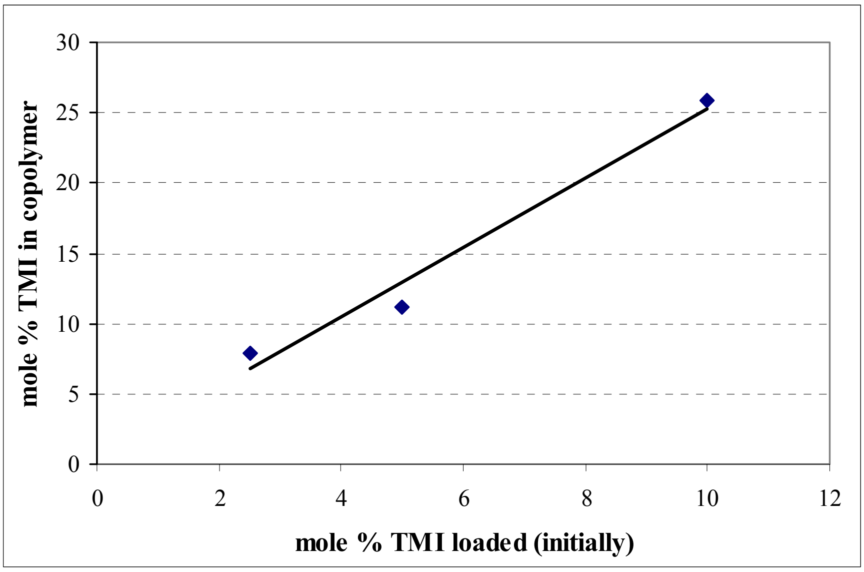

Figure 4.4 Calculated TMI percentages in HMW copolymers relative to TMI loading to the reactor.

In addition to the above mentioned copolymers, another copolymer with a lower molecular weight (LMW) was also synthesized with 5 mole% TMI loading. In this reaction, only the reaction solvent, DMF, was replaced with THF, while using the same reactant ratio, temperature and time. At the end of the reaction, an emulsion like liquid was obtained in the glass reactor. The molecular weight of the resultant polymer was measured as ~3500 gr/mol by Ubbelohde viscometer.

For the electrospinning of copolymers, required amount of crosslinker (Fluorolink-D or hydrocarbon) and two droplets of T2EH were added over the copolymer solution and mixed with vortex mixer. After the mixing, mixture was poured into a syringe and electrospun at 16 kV voltage, 10 cm tip-to-ground distance, and 12.5 μl/min flow rate for 45 minutes. After electrospinning, the aluminum foil was removed and cut into two. One half was annealed at least 8 hrs at 70°C for reorientation of perfluorinated groups to air-solid interface, whereas the other half was placed into desiccator at room temperature. By this way, the effect of annealing to the electrospun films was studied. The remaining of the mixture was subsequently cast onto microscope slides to study the effect of film morphology independent of the chemistry parameter. Like the electrospun films, one was placed to 70°C oven, and the other to the desiccator.

One question may arise as; during the electrospinning, due to the crosslinking reaction, is not there any viscosity increase? In this respect, the time dependence of the viscosity of the copolymer-Fluorolink-D mixture was studied with viscometer (Figure 4.5). The results showed that the viscosity does not considerably increase during the forty-five minutes. After that significant increase in viscosity, which may substantially affect the morphology of the film, was seen. Because our total electrospinning time, including mixing and pouring of the mixture to the syringe, was 45 minutes, the effect of viscosity change was neglected.

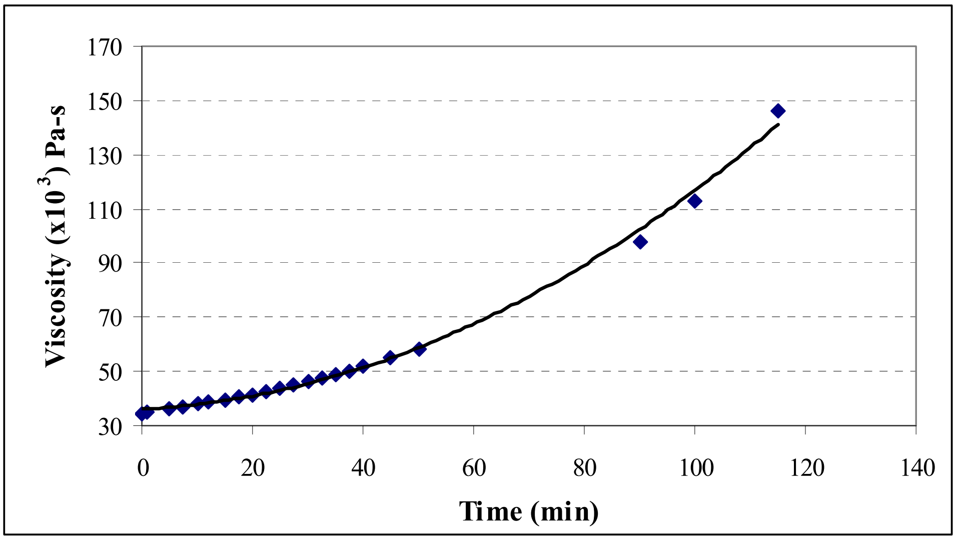

Figure 4.5 Time dependence of the viscosity of the electrospinning solution.

As we mentioned above, we planed to synthesis a crosslinked superhydrophobic surface that withstand whole type of chemicals without dissolving. From this point of view, testing of the solvent resistance was carried out by using a wide range of solvents covering ten different polarities, polar to apolar. No weight loss of the electrospun film was observed before and after two weeks soaking into these solvents. This proved the insoluble nature of our electrospun films.

4.2 Effect of Viscosity of Polymer Solution to the WCA of Electrospun Films

As we previously mentioned, viscosity of electrospinning solution is a key parameter that is affecting the morphology of the electrospun films. In this respect, we synthesized films with varying surface morphology, by mixing HMW poly-(AN-co-TMI) with 50 wt% Fluorolink-D (relative to polymer amount) in various quantities of DMF to create a range of viscosities. The viscosity was ranged between 31x10^{-3} Pa-s and 350x10^{-3} Pa-s.[67]

The SEM images of the electrospun films at various viscosities showed a change of morphology from predominantly bead to only fibers as the viscosity was increased (Figure 4.6). At low viscosity solution electrospinning mostly 1-3 μm in diameter spheres and 100-200 nm in diameter thin fibers were obtained. It is hard to see the fibers connecting the beads in Figure 4.6(a). The density of the beads was much more than the fiber. However, as the viscosity was increased the bead density decreased, and the fibers were become thicker, as 400-600 nm in diameter (Figure 4.6(c)). So, electrospinning of higher viscosity solution favors totally fiber containing electrospun films which is consistent with the literature.[67]

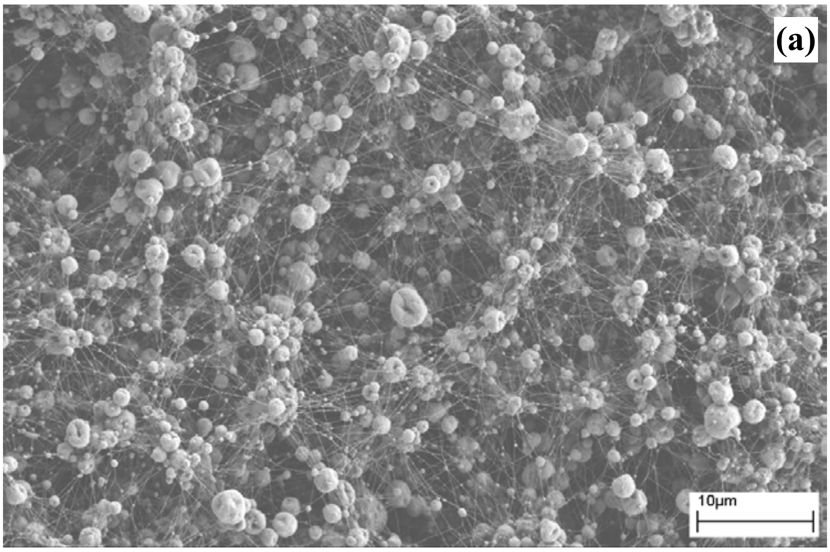

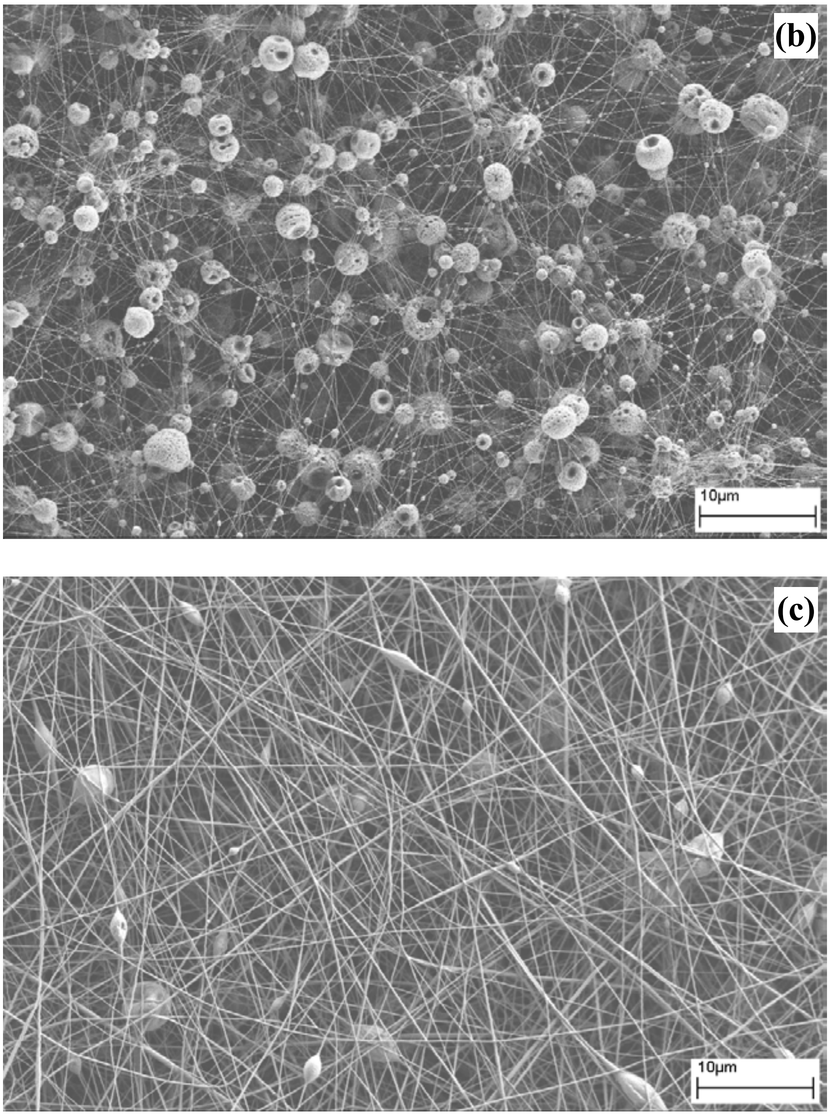

Figure 4.6 SEM images of electrospun films with viscosities: (a) 31x10-3 Pa-s, (b) 102x10-3 Pa-s, and (c) 348x10-3 Pa-s. The measurements were performed using a 1 keV beam and x5000 magnification.[46]

The WCA results and standard deviations of the electrospun films shown in Figure 4.6 were presented in Figure 4.7. Both annealed and normal electrospun films were given. In the graph, the filled squares and thick line represent the values and trend line of WCA of annealed electrospun films, whereas unfilled squares and thin line represent the normal samples. The WCA of the electrospun films were in the range of 150-155^{o}, which was at the WCA region of superhydrophobicity, like famous lotus plant. When the WCA of cast films were measured, the values were found as ranging at 96-99^{o} interval. The obvious result of the WCA study is: ~60^{o} WCA improvement was obtained by simply electrospinning the polymeric solution (Figure 4.8). The reason of the improvement was the discontinuities created by fibers and beads. Due to the presence of fibers and beads the contact area of the water droplet with the solid was reduced when compared with the cast film case. Thus, total attractive force exerted by the solid to the liquid was decreased. This weak attraction results the increase of WCA for electrospun films.

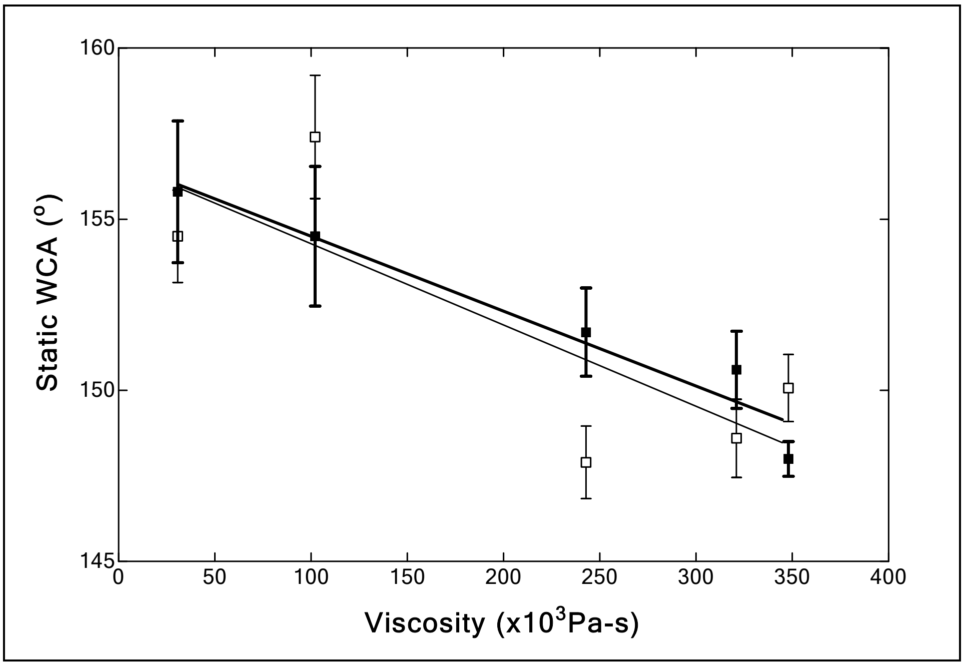

Figure 4.7 The effect of viscosity to WCA of normal and annealed electrospun films. ■ and thick trend line represent annealed electrospun samples, whereas □ and thin trend line represent normal electrospun samples.

The decrease of trend line both for WCA of annealed and normal electrospun films as the viscosity of the solution increased is distinct in the Figure 4.7. About 10^o of WCA loss was measured as the viscosity increased from $31x10^{-3}$ to $348x10^{-3}$ Pa-s. The cause of this trend can be explained by the density of beads and fibers in the films. The fibers lying on a surface create a tortuous surface in x-y plane. However, they are smooth in amplitude (z-axis). When the beads, bigger than fibers, is introduced into the micro-texture, they increase the roughness in amplitude. So, roughness in three dimensions is obtained. This results a longer and discontinuous three-phase interface at the bottom of the water droplet. As a result, the presence of beads increases the variation in roughness amplitude, so higher WCA is attained.

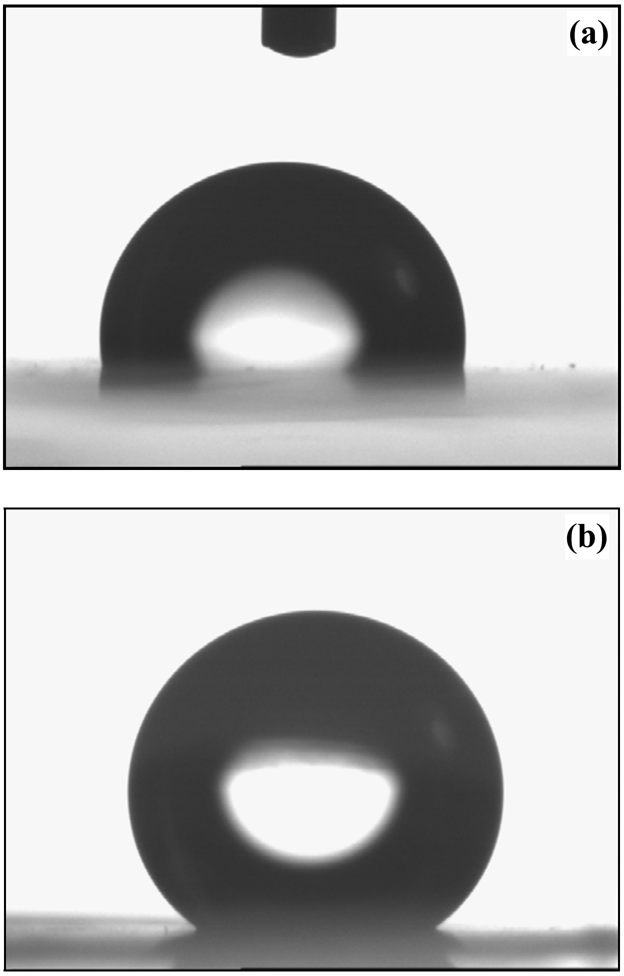

Figure 4.8 The photographs of water droplet on (a) cast film, and (b) electrospun film of the same viscosity and fluorine content solution.[46,67]

The comparison of trend lines of annealed and normal electrospun films in Figure 4.7 is important due to molecular orientation debate. Even several WCA values of normal samples were higher than the annealed ones; the trend line for normal samples was slightly below the trend line for annealed samples. This may be interpreted as an evidence of orientation of fluorinated moieties to the air-solid interface by annealing. However, for cast film case no WCA enhancement by annealing was observed. So, the orientation due to annealing cannot be claimed according to these results, and a study by X-Ray Photoelectron Spectroscopy (XPS) is required.

In the introduction section, the random nature of the electrospun films was mentioned. An evidence of this random nature can be seen during WCA measurements. We observed that when several samples were cut from the same sample and goniometrically measured, they rarely gave the same WCA average and standard deviation. For WCA average of different regions of the same sample, 2-3^{o} of shift was normal for electrospun films. This is caused by the random and uncontrollable nature of electrospinning process. Another, noteworthy happening is the height of the standard deviations bars in Figure 4.7. One can see the decrease of the height of the standard deviation bars in annealed samples as the fiber amount in the films was increased. The reason is as the fiber percentage increase the surface becomes more uniform (like a bed of fibers). So, the variation of the WCA at different regions reduces. The beads introduce a kind of discrepancy to the films, and increase the standard deviation of WCA measurements on the micro-textured surfaces.

In addition to WCA measurements, effect of electrospinning solution viscosity to tilt (sliding) angle of water droplet on electrospun films was also studied. Because the tilt angle of a superhydrophobic surface indicates the water-solid interfacial energy pinning a water droplet, the sliding angle threshold can effectively characterize the self-cleaning ability of a surface. As the fiber content (so the viscosity) increased on the micro-textured surfaces, a concurrent increase in sliding angle was observed, as $20.7^{o}\pm7.5^{o}$ for Fig 4.6(a), $52.6^{o}\pm5.6^{o}$ for Fig 4.6(b) and more than 90^{o} (no rolling) for other electrospun films. The explanation of this increase in sliding angle with the increase of fiber density is the same with the previous reasoning of WCA decrease with fiber density increase: longer and discontinuous three-phase interface results depinning of water droplet.

4.3 Effect of Fluorine Content and Hydrocarbon Addition to the WCA

By altering the viscosity of electrospinning solution, the water-repellency had been taken over the 150^{o} limit of superhydrophobicity. However, other parameters those are effective on the WCA of films is also present.

One candidate is variation of type and concentration of the crosslinking agent added to the solution. In this respect, electrospinning of different fluorine contents but at the same viscosity solutions ($51\text{x}10^{-3}$ Pa-s) were performed. The effect of fluorine concentration to WCA of annealed samples was presented in Figure 4.9. It was found that the WCA of the samples were differ 4-5^o even the concentration of fluorine were increased ten folds. Thus, the effect of fluorine is small when compared with viscosity effect. However, it should be noted that the combined outcome of concentration and viscosity had increased the WCA to ~160^o, which was higher than the WCAs of the viscosity effect study. The cast films of this study had resulted inconsistent results. Due to excess solvent, before drying, the phase separation between fluorine and copolymer phases took place, which resulted heterogeneous cast films with different WCA values on a single sample.

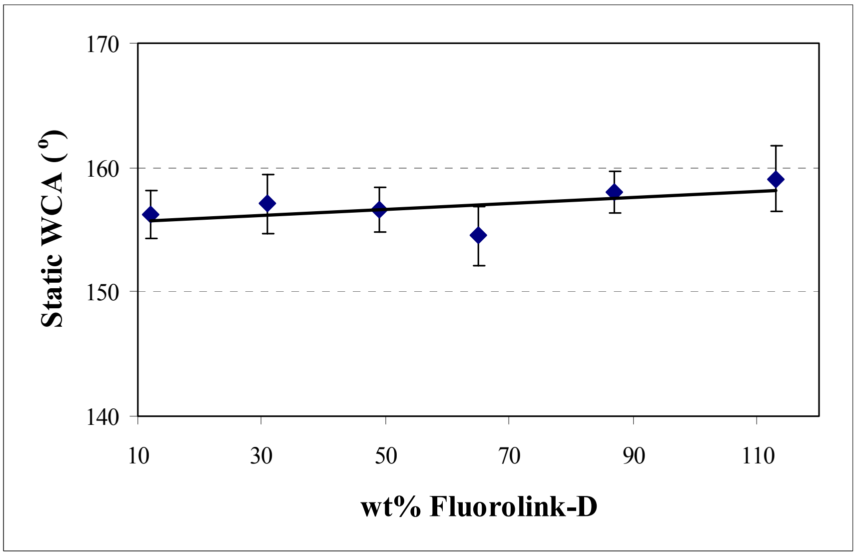

Figure 4.9 Effect of fluorine concentration (relative to copolymer weight) to WCA of annealed electrospun films.

In addition to Fluorolink-D, Ethylene Glycol, PEG 200 and PEG 1500 were also tested as hydrocarbon crosslinking agent. Both crosslinking agents were electrospun at two viscosities (35 and 150x10^{-3} Pa-s), and at two different agent concentration. In ethylene glycol case, the normal cast films were yielded 70-80^o WCA, whereas annealed cast films were yielded very low WCAs of 20-30^o. Thus, by annealing hydrocarbon parts, which can do hydrogen bonding with the water molecules reoriented to the solid-air interface. Because of this, the annealed samples yielded lower WCAs. Same WCA phenomenon had seen for electrospun films. In all cases, the annealed electrospun films of ethylene glycol added solutions were wetted by water, whereas the normal films were yielded WCA in 130-140^o range. For PEG 200 and PEG 1500 containing electrospun films, independent of annealing, viscosity and concentration, the films were easily absorbed the water. The reason is long hydrocarbon chains which do not hinder the entrance of water into the galleries between fibers and beads. The cast films of PEG 200 containing mixtures were measured ~60° WCA. In PEG 1500 case, it was also observed that annealing of the electrospun film resulted the melting of PEG regions, so the film roughness were permanently lost. As a conclusion, we can say that by electrospinning, we improved the hydrophobicity of hydrophobic polymers, but for hydrophilic materials, just the opposite reveals and wetting was enhanced.

4.4 Effect of Copolymer Molecular Weight to the WCA

The studies in Section 4.2 had demonstrated that as the percentage of beads in electrospun films had increased, the WCA was increased and water sliding angle was decreased. So, if a film containing solely beads is generated, the WCA and sliding angle will be further enhanced. However, the bead containing fibers can be obtained by viscosity manipulation up to a certain level. For example, when the solutions below 31×10^{-3} Pa-s viscosity tried to electrospin, a surface with low roughness was obtained due to the reach of non-evaporated solution to the grounded plate. For that reason, the synthesis and electrospinning of lower molecular weight (LMW) poly-(AN-co-TMI) was trialled[46]. The electrospinning of LMW polymer was carried at similar parameters as in the effect of viscosity study: 51×10^{-3} Pa-s and 50 wt% Fluorolink-D. This resulted a film consisted of only clustered polymeric beads ranging 0.5-3 μm in diameter (Figure 4.10). No fiber was observed in the film. When the WCA of this film was measured, the highest average static WCA for electrospun films in this study was achieved, 166.7°±2.2° (Figure 4.11). In addition to this, it should be noted that, as high as 174° static WCA was measured during goniometric studies. During the WCA measurements, because we could not leave the water droplet on the surface, we had used heavier water droplets than our previous studies.

Sliding angle studies of electrospun film of LMW gave 4.3°±0.8°, which was a really low sliding angle. High WCA and low sliding angle of this film indicates that this film is more suitable for self-cleaning applications when compared with the fiber-containing electrospun films.

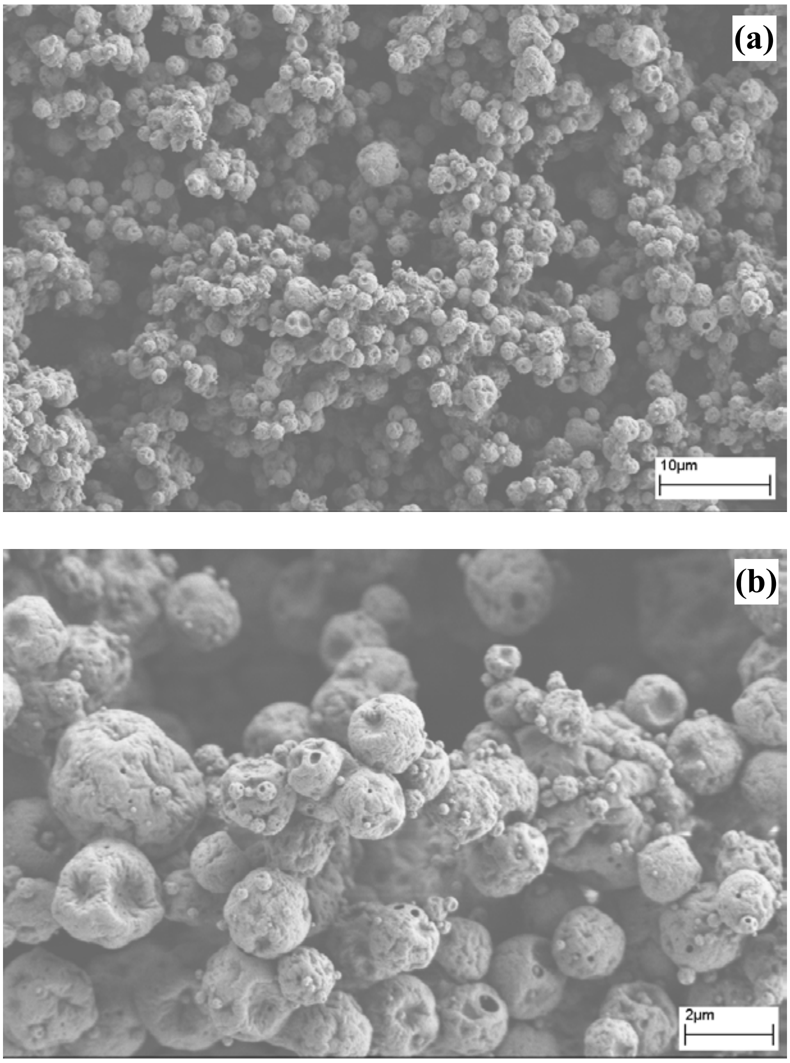

Figure 4.10 SEM images of electrospun film of LMW at (a) x5000 magnification, and (b) x20000 magnification.[46]

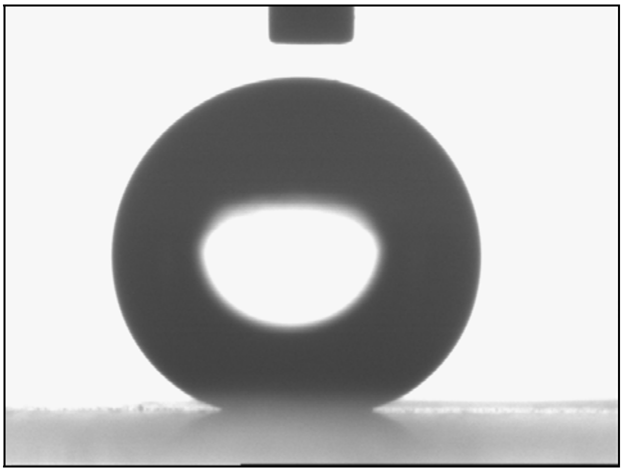

Figure 4.11 Photograph of a water droplet standing on totally bead containing surface.

4.5 WCA of Mechanically Pressed Electrospun Films

In the previous sections, we have mentioned the roughness on x-y plane and x-y-z, and stated that three dimensional roughness generated by the electrospinning of LMW polymer is enhanced the WCA value. However, not only the WCA value, but also the mechanical properties of a film are crucial for the determination of its application area. In this respect, the resistance of the films to mechanical load and their ultimate WCA under loading was measured via uniaxial pressing of a fiber rich and a totally bead electrospun film. The mechanical pressing results were presented in Figure 4.12. SEM and AFM images of mechanically pressed films were presented at Figure 4.13 and Figure 4.14, respectively.

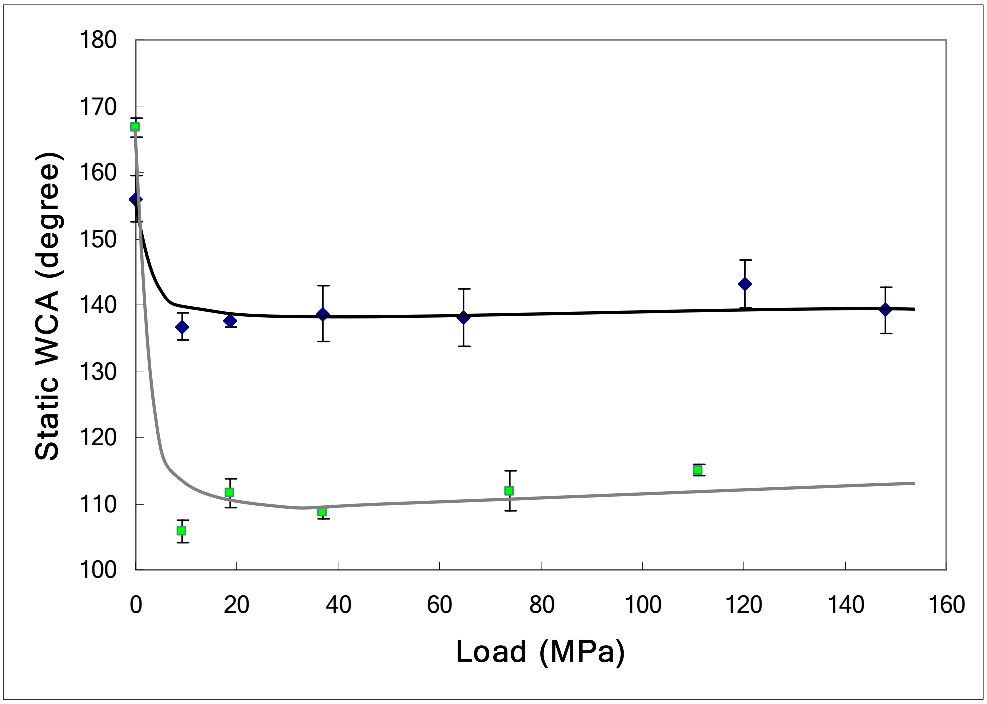

Figure 4.12 Mechanical pressing of electrospun films with various loads. The dark line is the film of $348x10^{-3}$ Pa-s viscosity HMW polymer, light one is the film of LMW polymer.

WCA of fiber rich electrospun film was decreased from 154° to 140° after 150 MPa pressing. However, WCA of totally bead morphology film was decreased to about

110° from 166°. Probably, the difference was resulted due to the fibers. The fibers were supported the structure like a skeleton and restricted their movement to flatten the surface. However, in solely bead films, the beads changed their places under the load and resulted closer packing. On the other hand, none of the samples were decreased to WCA values of cast film, which was 96-99°.

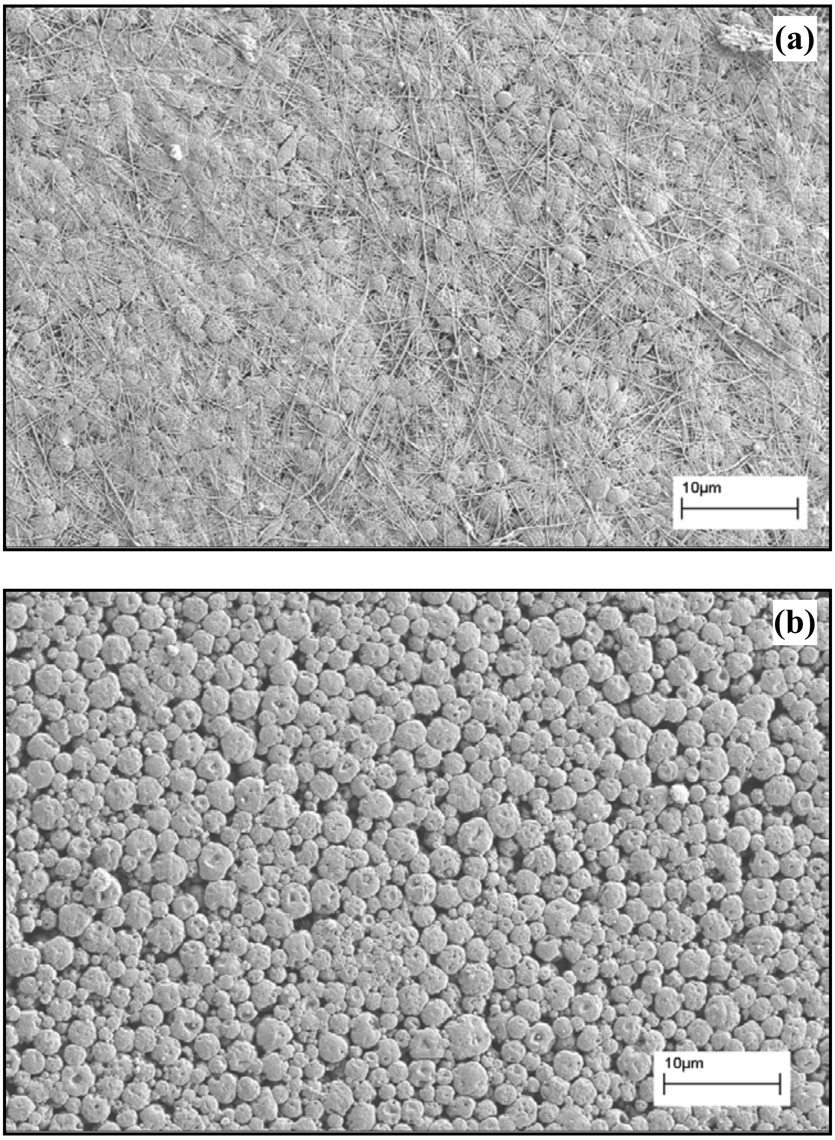

Figure 4.13 SEM images of 37 MPa mechanically pressed (a) fiber rich, (b) totally bead electrospun films.

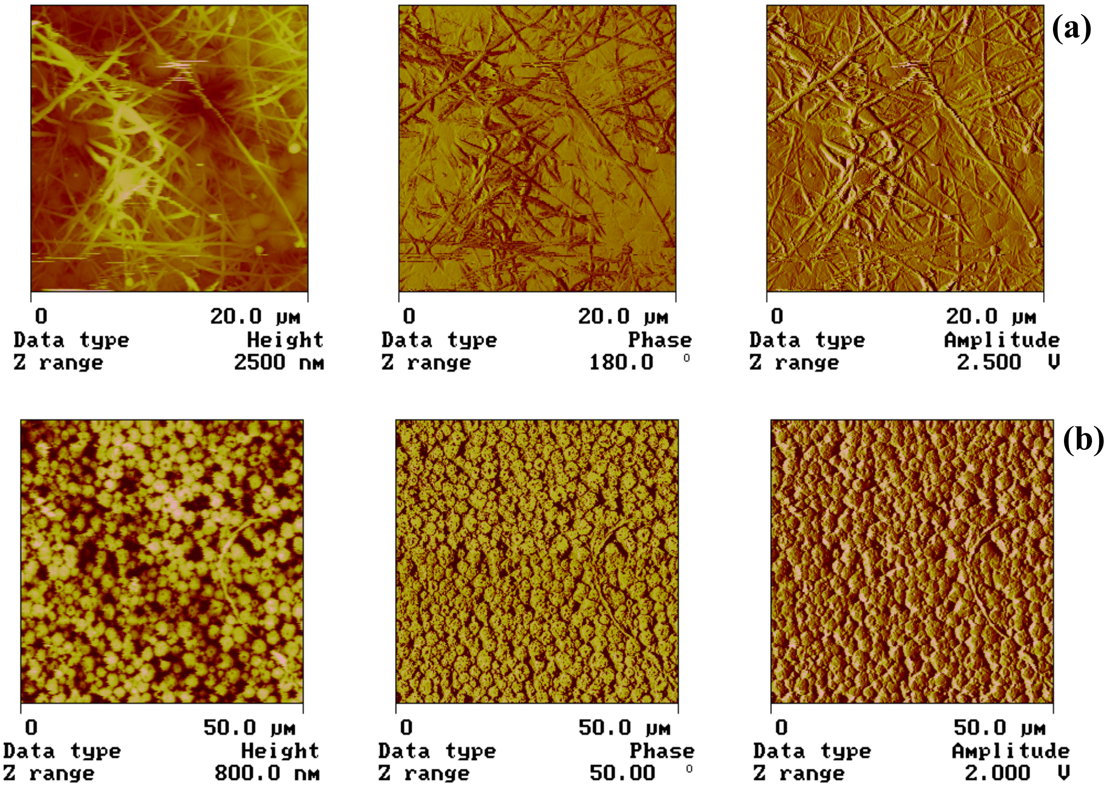

Figure 4.14 AFM images of pressed samples shown in Figure 4.13: (a) fiber rich, (b) totally bead electrospun films.

4.6 Water Droplet Pressing (Stability of Superhydrophobicity)

By using electrospinning surface, we generated superhydrophobic surfaces. However, the stability of this superhydrophobic state is vital, especially for the determination of application fields. Superhydrophobic surfaces which can maintain its Cassie regime (so, stable superhydrophobicity) originated superhydrophobicity may find exceptional application areas in marine, microfluidic and biotechnology applications.

Figure 4.14 reviews the stability tests that were performed on our samples. The pressure exerted onto the water droplet was calculated by measuring the gap between two plates and substituting it into Laplace Equation. The electrospun films that were shown in Figure 4.6 had variable densities of fibers in their morphology. The mostly fiber containing film (Figure 4.6(a)) had shown an excellent stability which is a good representative of stable Cassie regime.[46] Even under 400 Pa pressure very little decrease was measured, which can be considered as experimental error (Figure 4.15(a)). However, it was also observed that as the percentage of fiber in the film was increased, post-pressing WCA of water droplet was decreased. This means that as the fiber content increases, pinning of the water droplet arises. So, Cassie regime was turned to Wenzel regime after pressing the water droplet between two identical plates. This may be due to capillary action, and if once the water was inserted into the narrow space between fibers, it was impossible to contract it back. For the completely fiber morphology, only at 100 Pa, the droplet was divided into two after pressing, and one half was left at the top plate other at the bottom (Figure 4.15(b)).

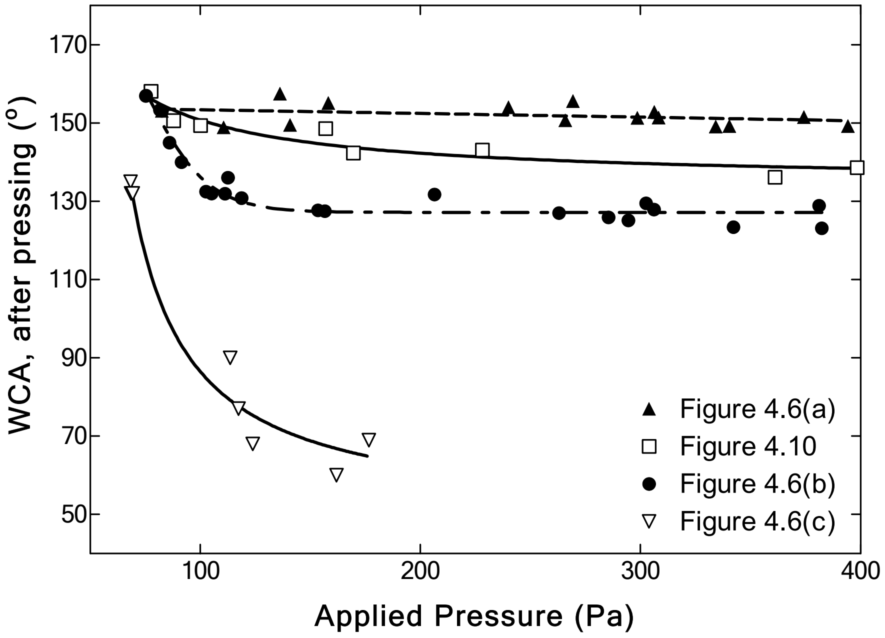

Figure 4.15 Pressing of water droplets between two identical superhydrophobic surfaces.

Hence, one may expect that totally bead morphology should exhibit a stable superhydrophobicity, too. However, when the film in Figure 4.10 was subjected to stability test, about 25° of WCA loss was measured. The reason of this loss is not clear. One probable reason may be related with the insufficient integrity of the film. Because the beads are not interconnected, but stacked, in each measurement the morphology was deteriorated.

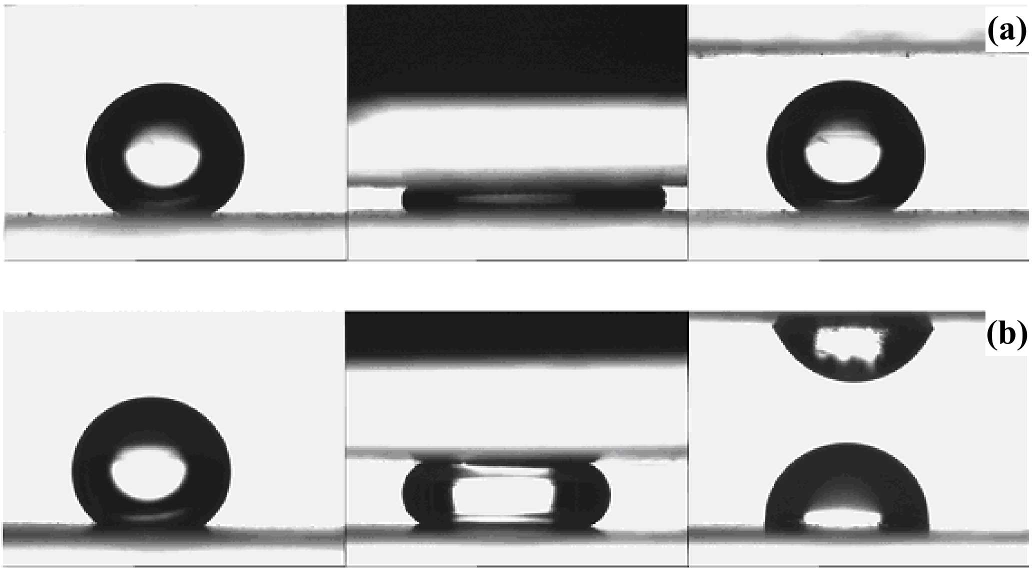

Figure 4.16 Water droplet pressing between two identical films covered surface. (a) The surface which contains mostly bead (like in Figure 4.6 (a)), and (b) the surface having a morphology of totally fiber (like in Figure 4.6 (c)).[46]

CHAPTER 5

ADDITIONAL EXPERIMENTS: RESULTS ON ELECTROSPINNING OF VARIOUS POLYMERS

The electrospun films, which were synthesized through out the Section 4 of this thesis, were chemically crosslinked, thus solvent resistant surfaces. However, for certain purposes, the synthesis of different property bearing polymers and electrospun surfaces may be needed. In this respect, current section will briefly review several other synthesis and electrospinning trials, which were performed during the study for Section 4, to open a gate to different ideas and future studies. First one is about the synthesis of superhydrophobic surface by using a perfluorinated linear polymer[68], second is the synthesis of an antibacterial and low-surface tension polymer and than electrospinning of it[69], and the final one is about electrospinning of very small amount of fluorine containing (only both ends of linear polymers were contained perfluorinated groups), which were previously synthesized by Nalan Bilgin.[70]

5.1 Superhydrophobic Surfaces via Fluorinated Linear Polymers

To synthesis the perfluorinated linear polymer AN and perfluoroalkyl ethylacrylate (PFAEA, Fluowet AC812) of Clariant was reacted in THF solution with the aid of AIBN initiator (Figure 5.1).[68] During the loading, PFAEA/AN mole ratio was 1/8, and AIBN amount was 0.05 mole % relative to AN. The reaction temperature was 65°C for 72 hours. The conversion to polymer was measured as ~ 60 %. The proton NMR of product linear polymer by using deuterated-DMF was given in Figure 5.2.

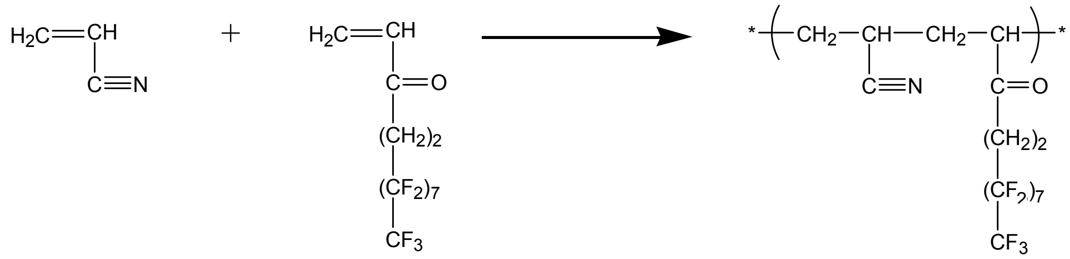

Figure 5.1 Reaction scheme of fluorinated linear polymer synthesis.

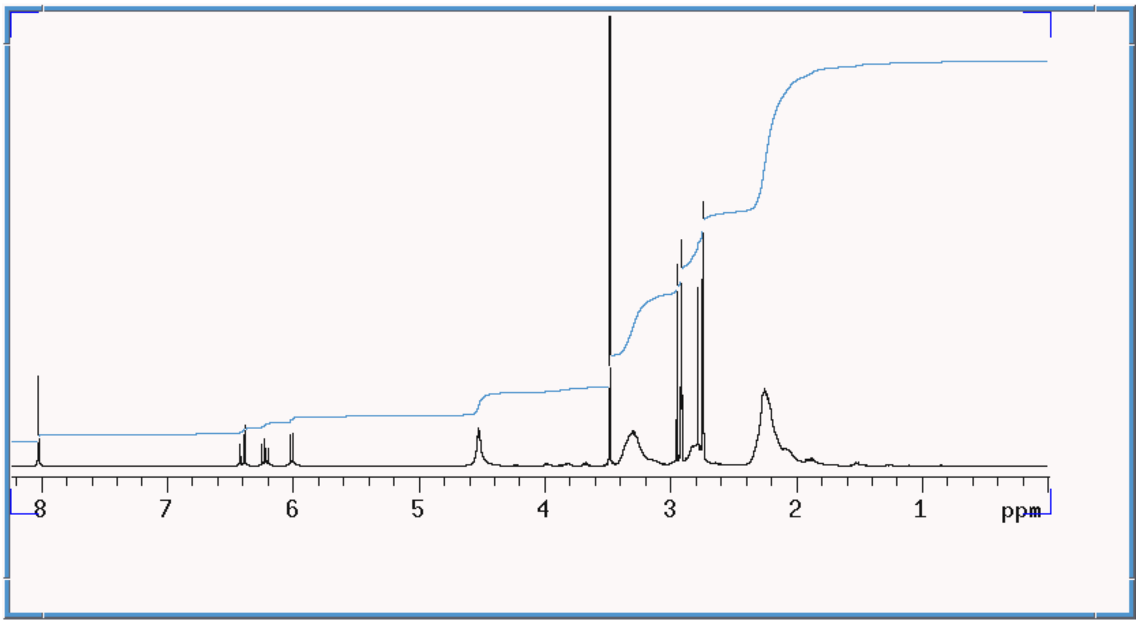

Figure 5.2 Proton NMR of perfluorinated linear polymer with deutearted-DMF solvent.

Electrospinning of this linear polymer was carried at 10 kV voltage, 10 cm tip-to-ground distance and 4 µl/min solution flowrate, where the solution had a 39.9 cP viscosity. The SEM images of the electrospun film indicated a totally bead morphology, however this time the beads have irregular shapes (Figure 5.3). The measurement of contact angle was carried with difficulty because it was hard to leave the water droplet onto the surface. The resultant WCA was averaged as 172.0±2.4^{o}. This value is higher than our crosslinked structures exhibited. Our studies are in progress on the parameters effecting to the WCA of linear perfluorinated electrospun films.

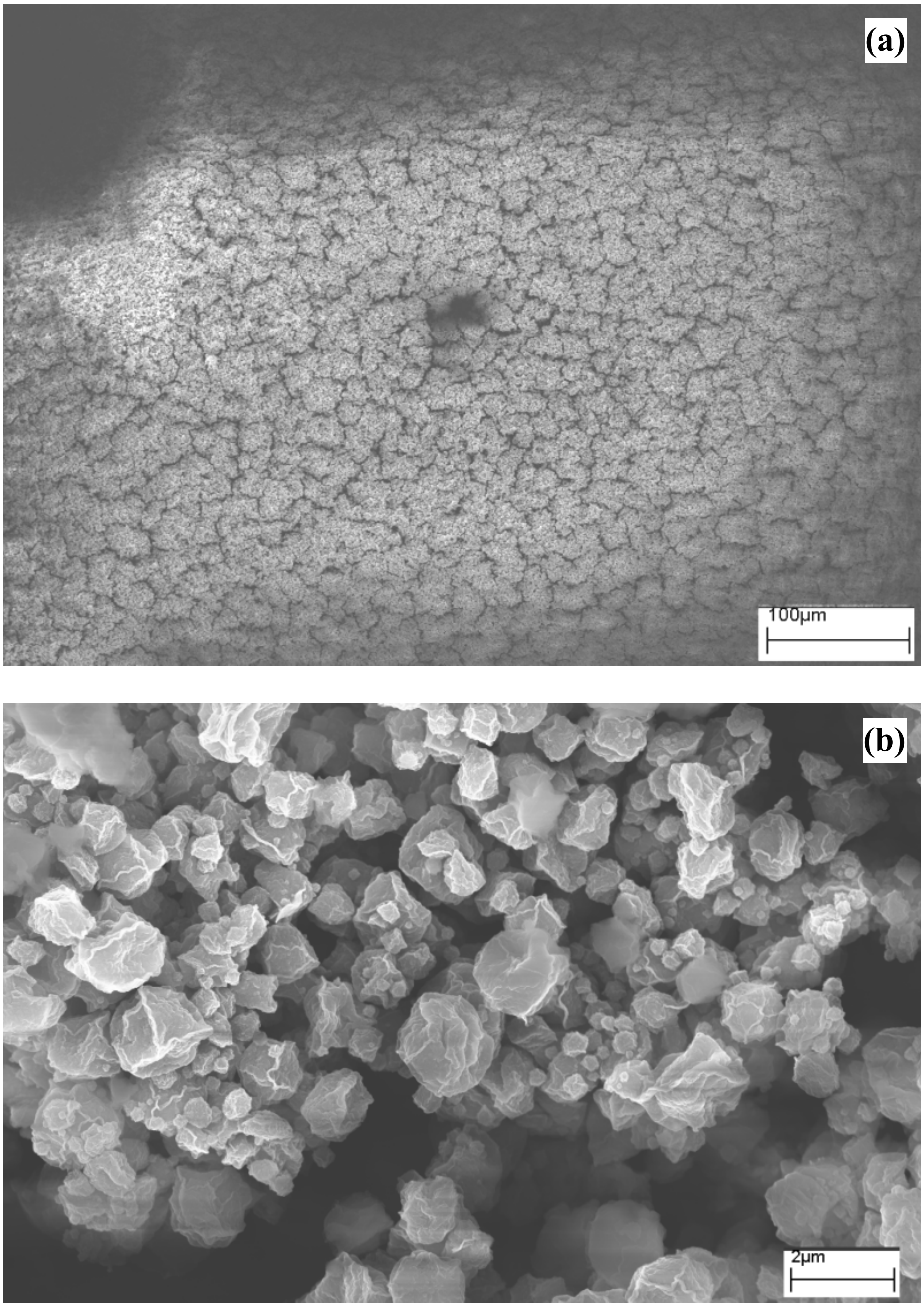

Figure 5.3 SEM images of electrospun films of perfluorinated linear polymer.

5.2 Generation of Antibacterial and Low Surface Energy Surface by Electrospinning

In this section, an attempt to combine both antibacterial and superhydrophobic ability on single polymer was reviewed. Antibacterial ability was introduced by inserting quaternary ammonium compound (QAC) into the main chain of the polymer. QACs have a large variety of usage areas from cosmetics to clothes softeners, but especially they are known to be good disinfectants. They have the general formula of $R_4N^+X^-$, cationic nitrogen structure. In a quaternary structure, nitrogen atom is covalently bonded to four groups and the positive charge is balanced by a negative counter ion. QACs are effective on both gram negative and gram positive bacteria. They are not effected from the protein concentration of the environment and don't loose their affectivity on bacteria over the course of time. The effectiveness of the agent against microorganisms is directly related to its area of contact with the microorganism's medium. Thus, enhancement of surface area by electrospinning is a good practice.[69]

In this respect, terpolymers containing various amounts of QAC were synthesized. The terpolymers were consisted of PFAEA (fluorinated moiety), vinylbenzyl-dimethylcocoammonium chloride monomer (VBDCC, antibacterial moiety) and polymethylmethacrylate (PMMA), which was used to enhance film forming property and to lower the cost (Figure 5.4). The bacterial affectivity of VBDCC monomer were compared with commercial biocides (Nipaguard and Bronopol), and our antibacterial monomer were displayed a significant performance against *Escherichia Coli* (XL1 blue) bacteria (Figure 5.5). PFAEA was used 10 mol%, and VBDCC was varied from 0 to 25 mol %. Terpolymerization reaction was carried at 70°C for 24 hours.

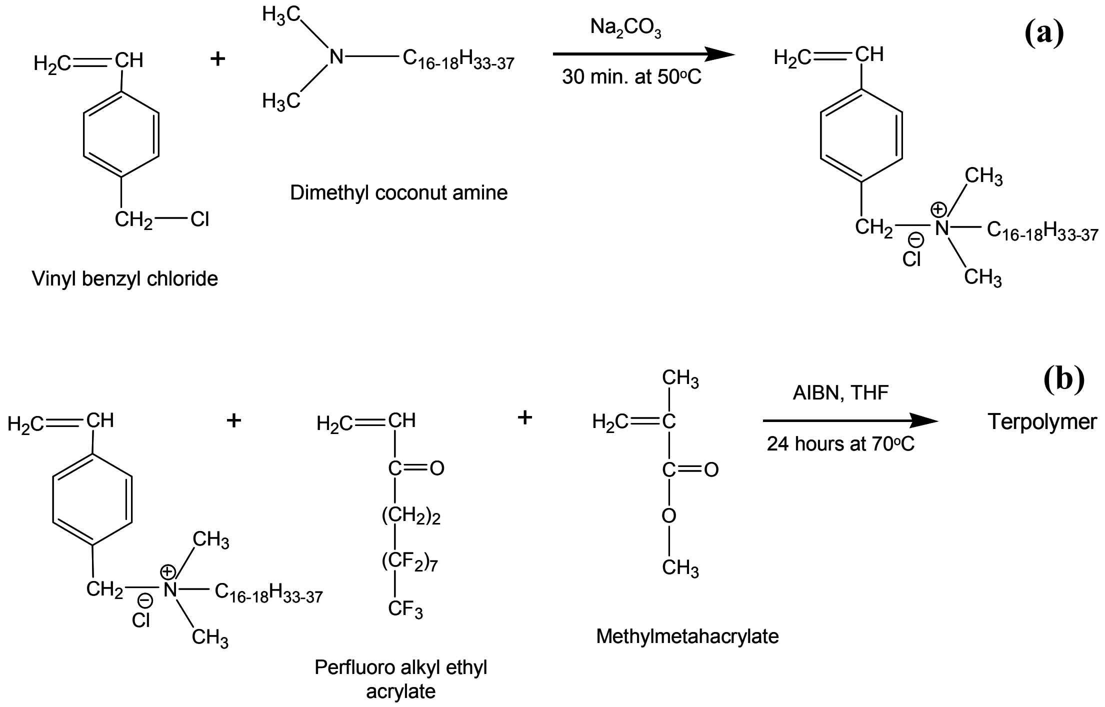

Figure 5.4 Scheme of the synthesis of: (a) Vinylbenzyl-dimethylcocoammonium chloride, (b) the terpolymer.

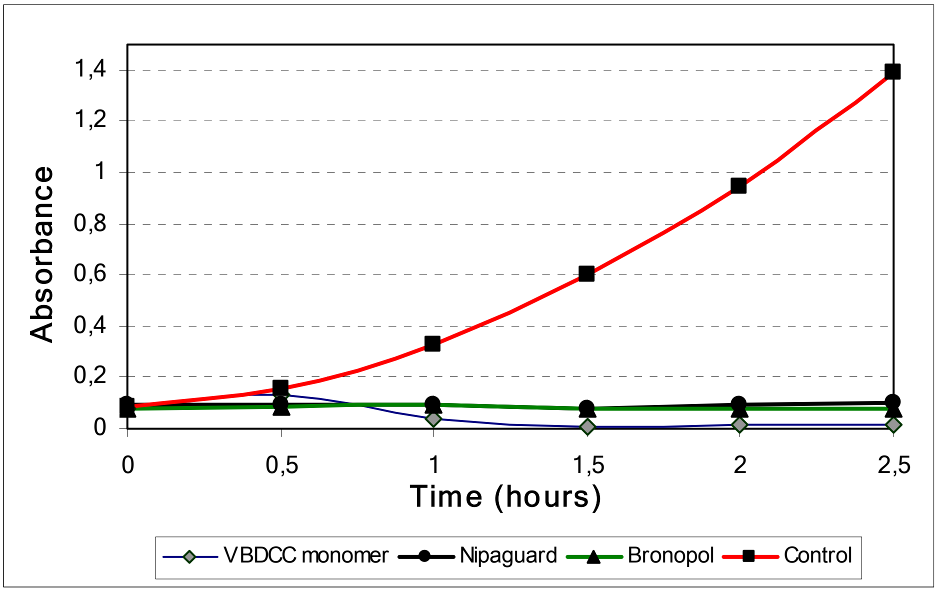

Figure 5.5 Comparison of the bacterial activity of our VBDCC monomer and commercial biocides.

The resultant terpolymer was electrospun after dissolving in THF-DMF (50/50 wt %) at 12 kV voltage, 10 cm tip-to-ground distance and 5 µl/min solution flowrate. Electrospinning of 0 mol % (quat-free) terpolymer resulted a flat film, whereas QAC containing, especially 25 mol %, terpolymers yielded a fluffy structure shown in Figure 5.6. Also, SEM images of quat-free and fluffy structure showed a fiber diameter difference between these two structures. Electrospinning of the quat-free polymer resulted a narrow fiber diameter distribution in the range of 150-250 nm. However, fluffy structures showed a diameter distribution between 40-800 nm, where one group was between 400-800 nm and a second group was 40-120 nm thickness. Due to fiber diameter decrease, average fiber diameter significantly decreases. Thus, effective surface area has increased per volume.

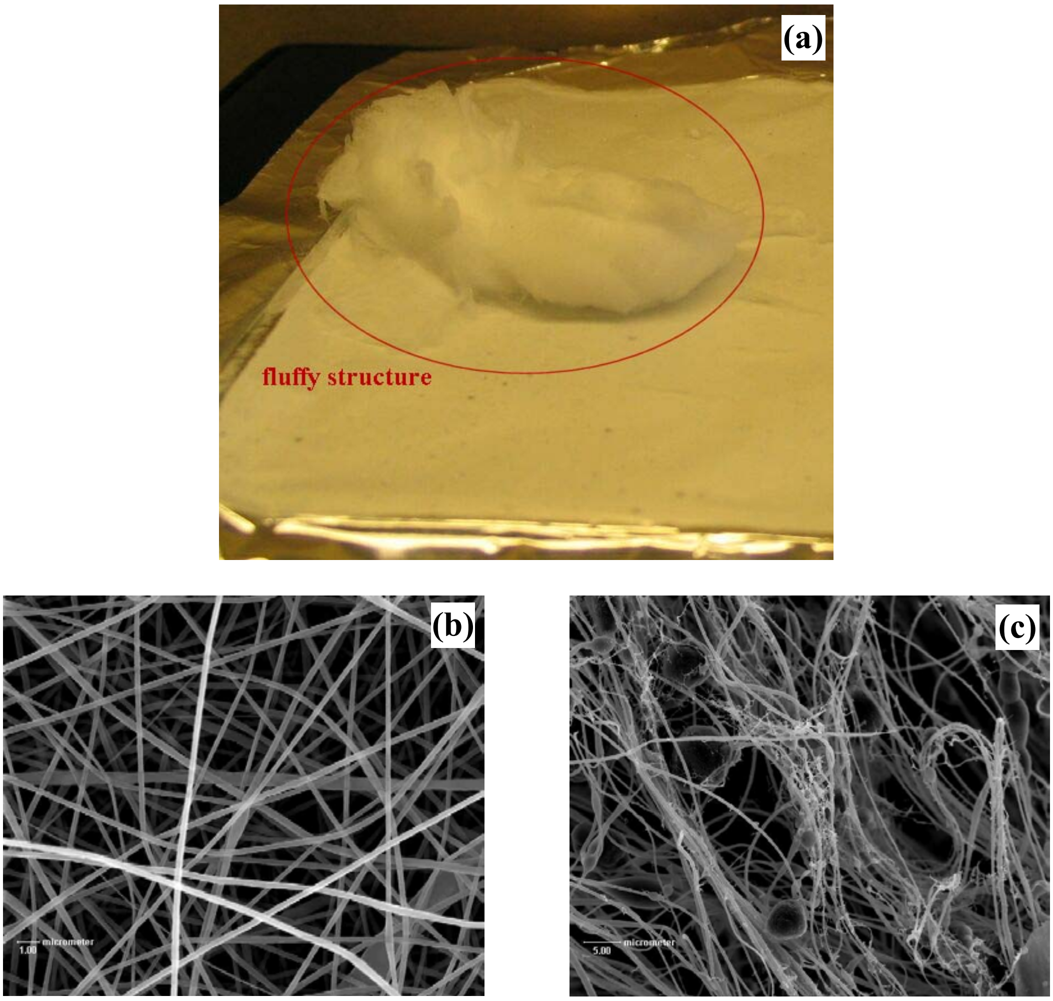

Figure 5.6 Images of fluffy structure and quat-free: (a) Photograph of fluffy structure, (b) SEM of quat-free electrospun film, and (c) SEM of 25 mol % QAC containing terpolymer.[69]

When the bacterial activity of 25 % quaternary group containing electrospun films was tested, it yielded poor results (Figure 5.7). However, when the normal film (cast film) of the same composition was grinded and its bacterial test was carried, superior results were obtained. To explain the reason of this occurrence, the non-fluorinated (only QAC and PMMA containing) copolymers were synthesized. When the cast and electrospun films of non-fluorinated copolymer were run, the activity of cast and electrospun samples were found the same and superior (Figure 5.8). Thus, we concluded that in the electrospun film of fluorine containing terpolymer, the fluorinated moieties restricted the penetration of bacteria containing media into the fluffy structure, and the effective surface area was decreased. When the fluorinated moiety was eliminated, the surface tension of the fibers had been raised, thus the media could penetrate and contact with the whole polymeric nanofibers. So, the antibacterial affectivity had been boosted.

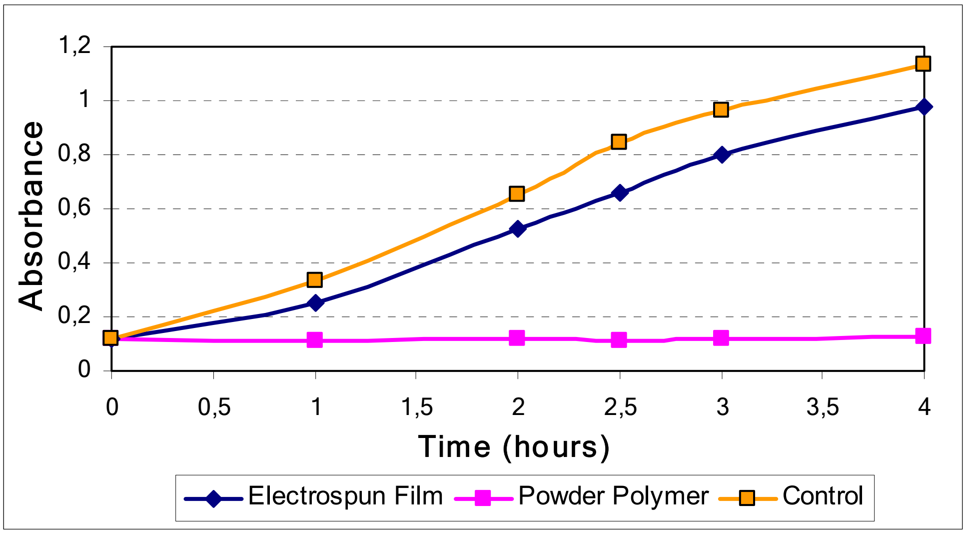

Figure 5.7 Bacterial activity test of fluorinated terpolymers. They had 25 mol % antibacterial moieties.

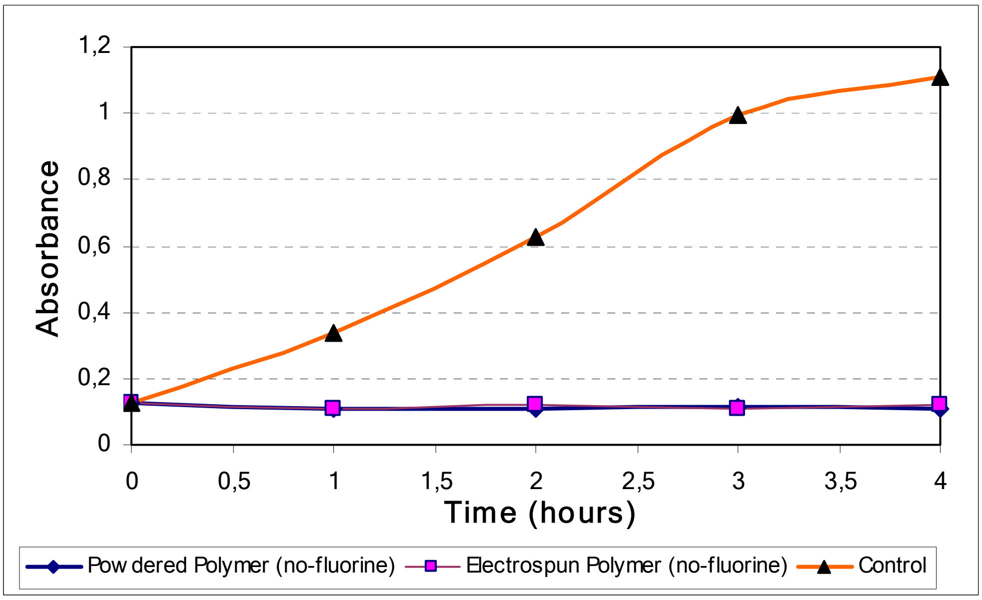

Figure 5.8 Bacterial activity test of non-fluorinated polymers (copolymer). They had 25 mol % antibacterial moieties.

At the beginning, we aimed to use the terpolymer for filtration of liquid and gas media, however we concluded that the usage of terpolymeric film is not possible for liquid media filtration, but for gas phase filtration it may find wide application due to its dual effect.

5.3 Electrospinning and WCA measurements of Fluorine End-capped Copolymers

In this study, electrospinning and WCA study on electrospun films were carried on previously synthesized fluorine end-capped (R_f, perflurohexyl ethanol) oligomers in the form of R_f–PAN–R_f and R_f–PMMA–R_f. The procedure for synthesis of fluorinated oligomers can be found in the MS thesis of Nalan Bilgin of Sabancı University.[70]

The electrospinning of R_f–PAN–R_f oligomers were carried at 10 kV and 7 µl/min solution flowrate at two different tip-to-ground distances of 10 and 13 cm. The solution viscosity was kept at ~$14x10^{-3}$ Pa-s. The resultant electrospun films were presented in Figure 5.9 for 10 cm and 5.10 for 13 cm. It should be noted that only increasing the distance, was enormously changed the morphology from totally fiber to high bead density morphology. The reason is the decreased value of voltage per cm, thus the mechanism of the attraction from tip to ground has been changed.[60] Due to the morphology change, the WCA of the films were measured as 146.1 ± 0.54^o for 10 cm distance and 165.9 ± 0.39^o for 13 cm distance. In the case of 13 cm the morphology was very similar to the film at Figure 4.6(a), in addition to extra nanosized bumps around the beads, which probably enhanced the WCA.

In the electrospinning of R_f–PMMA–R_f oligomers, the electrospun film (at 10 kV, 10 cm and 3µl/min) had uniform bead morphology (Figure 5.11). However, contrary to the case at Figure 4.10, this time the beads (less than 1 µm in diameter) were laid next to each other and formed a smoother surface. This resulted a lower WCA value of 145.3 ± 0.59^o.

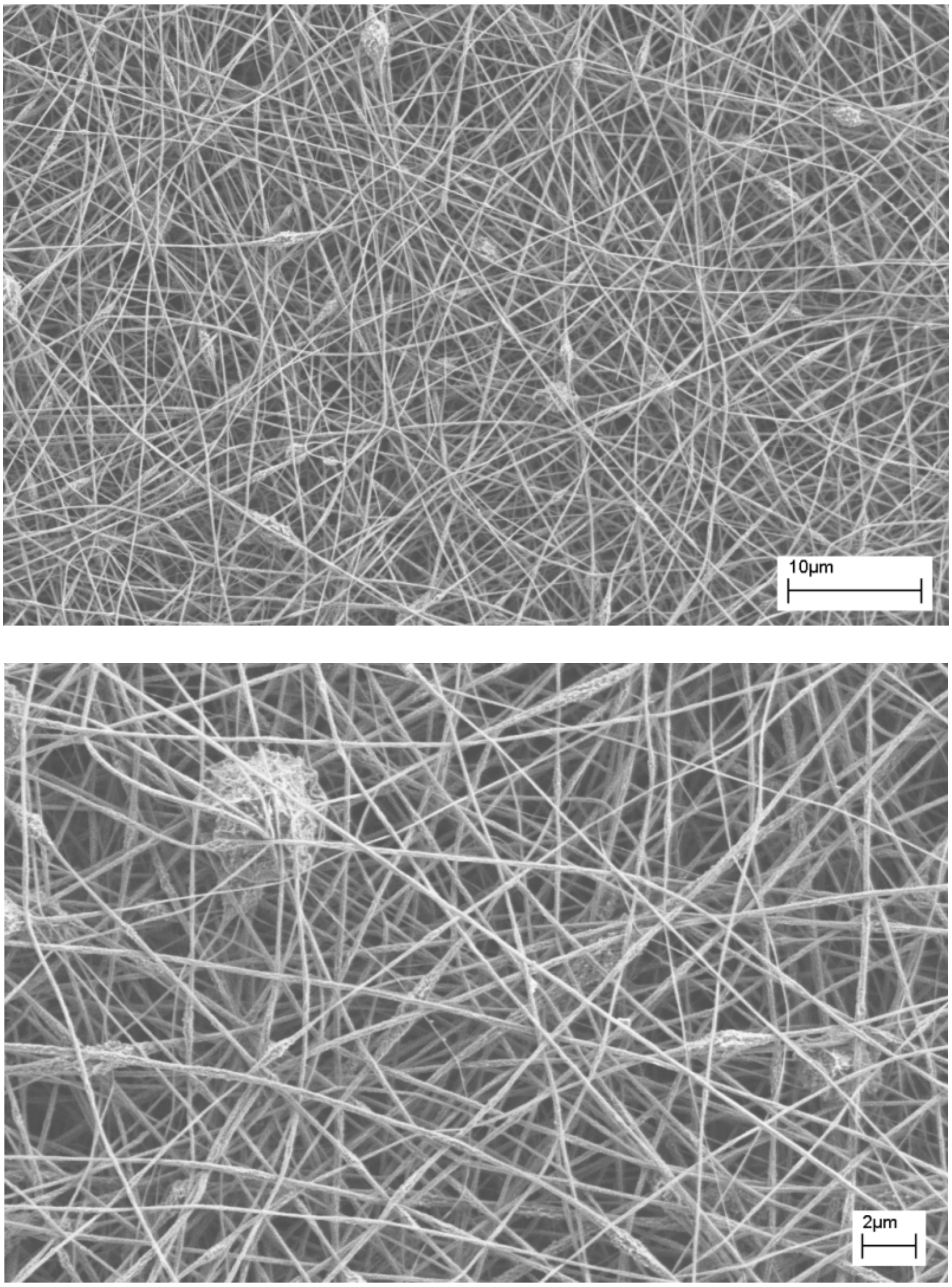

Figure 5.9 The electrospun films of R_f–PAN–R_f at10 cm tip-to-ground distance.

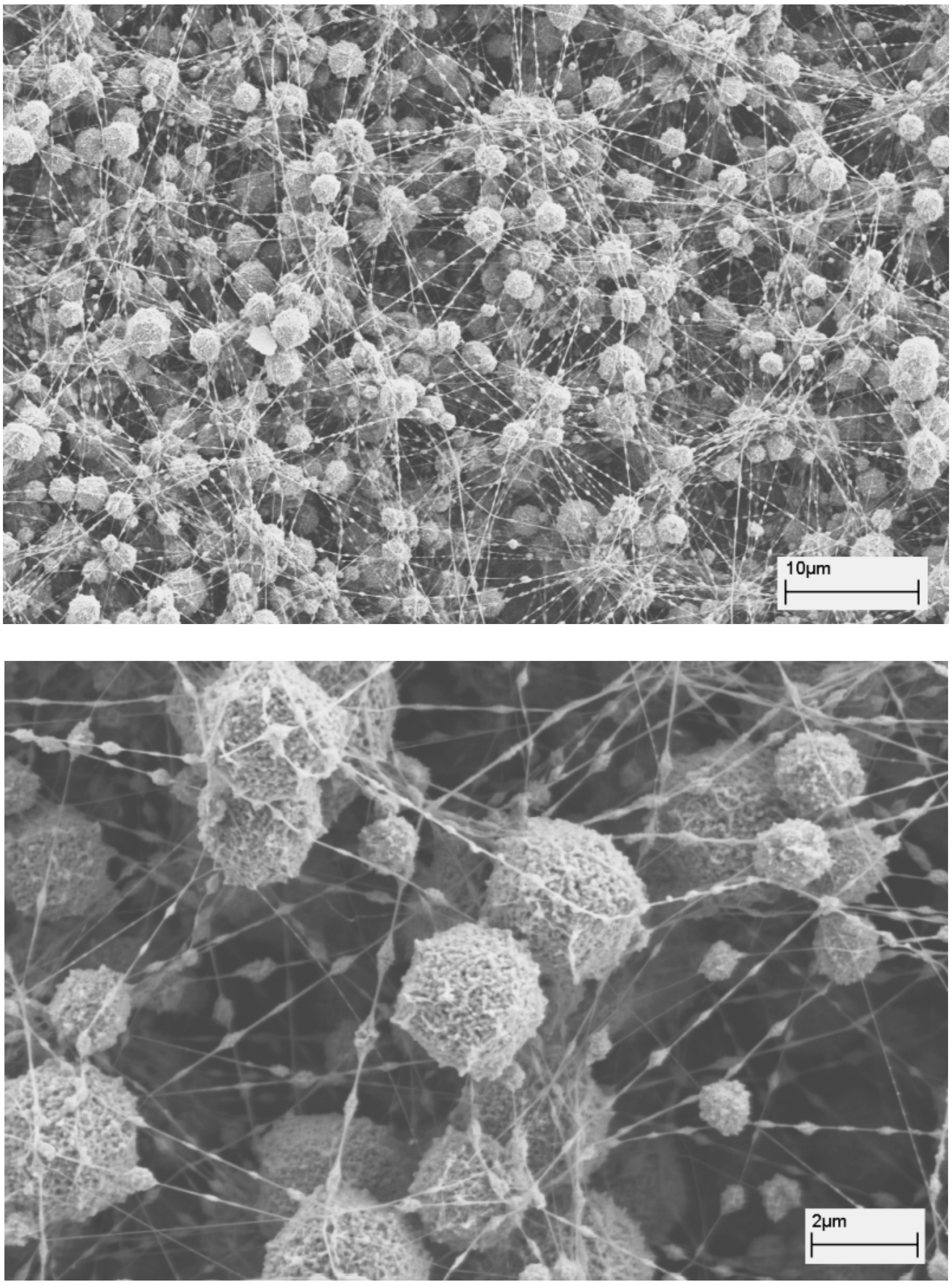

Figure 5.10 The electrospun films of R_f–PAN–R_f at 13 cm tip-to-ground distance.

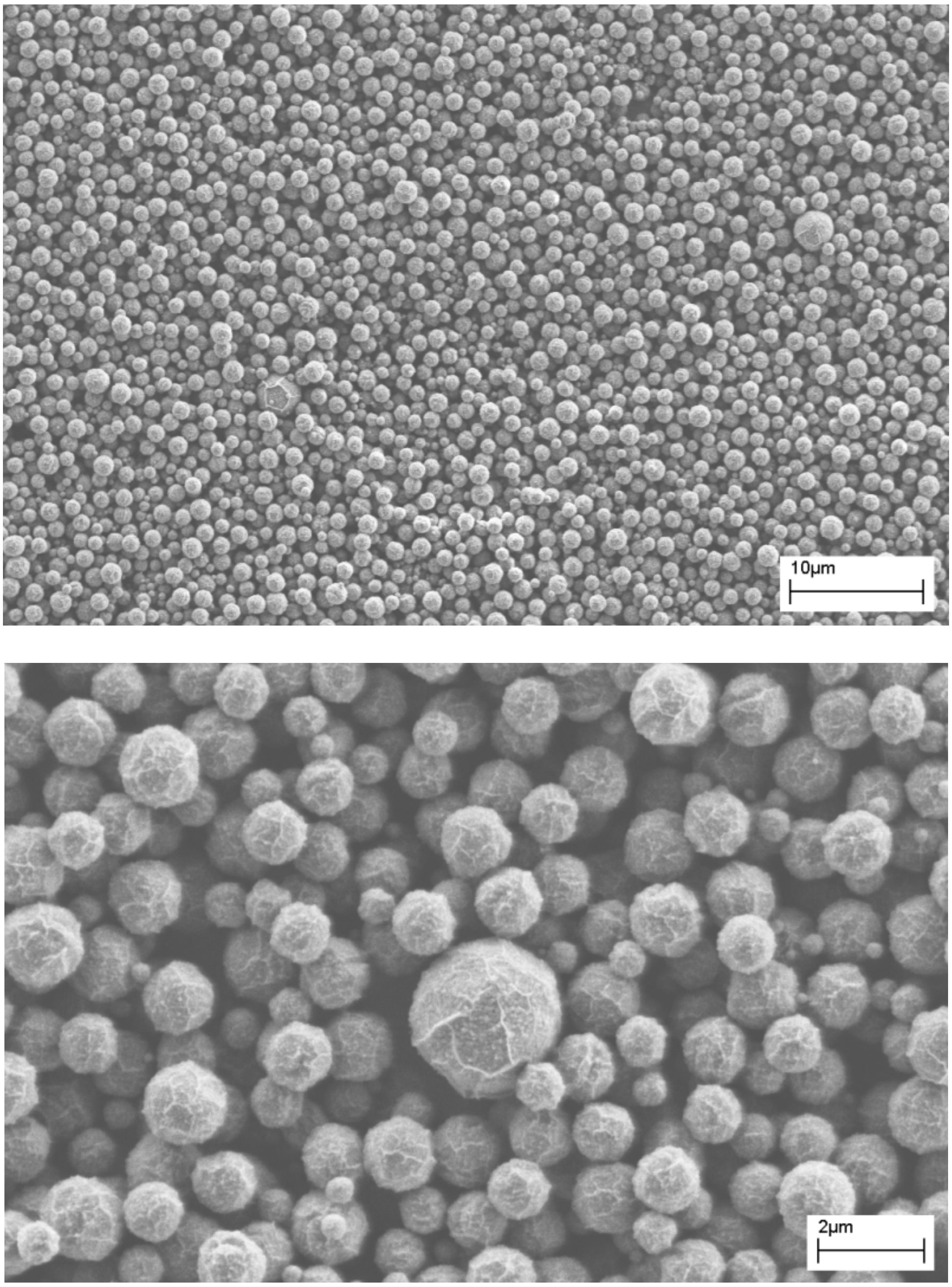

Figure 5.11 The electrospun films of R_f–PMMA–R_f.

Thus, electrospinning of very low percentage of fluorine containing copolymers were successfully carried, and the effect of distance from tip to ground was demonstrated. For certain cases, only variation of the distance may be sufficient to boost the WCA, and bring the value to superhydrophobic region.

CHAPTER 6

CONCLUSIONS AND SUGGESTED FUTURE WORK

In this study, solvent resistant polymeric superhydrophobic surfaces were generated via electrospinning. Poly-(AN-co-TMI) copolymer was synthesized, and electrospun after mixing with the hydroxyl-ended fluorinated oligomers. Several parameters during electrospinning were varied to understand their effect to morphology, WCA and sliding angle.

First, the effect of the viscosity of the electrospinning solution to the morphology and WCA of the electrospun film was studied. SEM images of the resultant films showed that as the viscosity of the polymeric solution was decreased, the amount of beads (bead density) in the films was increased. This is a consequence of electrospinning with a low solution viscosity. Below a certain viscosity limit, electrospinning of polymeric solutions generates beads in addition to nanofibers. During the goniometric studies of these microtextured films, it was observed that as the bead density of the films was increased, static WCA of the films was also increased. This is a result of the increased roughness by incorporation of 1-3μm beads into 100-600 nm fibers. When the film has a totally fiber structure, like a bed of fibers, it only has a roughness in x-y plane. However, if the beads larger than the fibers are incorporated into the film, a roughness in the third dimension (z-axis) is introduced. Higher density of beads results longer and less stable three-phase (air-liquid-solid) contact line, thus, lowered the interfacial energy between solid and liquid which results higher WCA.

Second, the ratio of fluorinated material in the electrospinning solution was varied while keeping the solution viscosity constant. Due to the cost point of view, the effect of fluorine ratio was found to be small (4-5^o improvement even increasing the fluorine content 10 folds). However, the combined effect of high bead density with high fluorine content resulted in 159° WCA, which was higher than the maximum value achieved in the viscosity effect study.

Additional efforts made to obtain higher WCA and lower sliding angle resulted in the desired achievement by lowering the molecular weight of copolymer. Electrospinning of low molecular weight copolymer resulted in a film consist of only clustered polymeric beads, attributed to Raleigh instability in the fluid flow during the electrospinning. The WCA of this film was measured as $166.7^o \pm 2.2^o$, and its water sliding angle was measured as $4.3^o \pm 0.8^o$. The explanation of such a high WCA, in addition to low sliding angle, was the same as in the previous case: Long and less stable water contact line causes less attraction of liquid by solid, thus higher WCA and lower sliding angle were obtained. The absence of fibers interconnecting the beads increased the level of amplitude variation over the films. So, the contact area between the solid-liquid was lowered this resulted in higher WCA and a lower sliding angle. However, because there are no fibers interconnecting the beads, the mechanical stability of this film is worse than the fiber containing morphologies.

Reorientation of fluorinated groups to air-solid interface by annealing of the films did not provide certain results like distinct increase in WCA of annealed samples. This may be due to the small diameter of the beads and fibers. Because the diameters are so small, the fluorine content in interface is high. So, annealing did not result in a beneficial increase in surface fluorine content, thus WCA. However, definite results can be obtained by X-ray photoelectron spectroscopy (XPS) studies on both the electrospuns and the cast films of annealed and not annealed samples.

Besides the fluorinated oligomers, hydrocarbon molecules (ethylene glycol and PEG 200) were also added to electrospinning solution. However, replacements of fluorine oligomers increased the overall surface energy of the films, resulting lower WCA values. In the ethylene glycol case, the WCA was significantly lowered, and in PEG 200 the electrospun films were absorbed the water droplet. Hence, increase of the length of hydrocarbon molecule resulted lower WCA.

The electrospun films were also mechanically pressed to investigate the influence of mechanical loading. The post-pressing WCA of the fiber and bead containing films were measured around 140^o, whereas solely bead containing films were around 110^o. The difference was credited due to the fibers which were supporting the structure like a skeleton and restricting the movement of beads to flatten the surface. In the solely bead films, probably, the beads changed their places under the load and resulted a closer packing and smooth surface which gave lower WCA. However, even under extreme loads, the WCA of the cast films (96-99^o) were not achieved.

In addition to previous studies, the stability of superhydrophobicity of our films was checked by pressing a water droplet between two identical superhydrophobic surfaces. Here, 31x10^{-3} Pa-s viscosity electrospun showed the maximum stability. This film has an extensive amount of beads which are interconnected with very thin fibers. The reason of this situation is not clear. On this subject, further investigations on the basis of surface roughness values may be useful. AFM and SEM studies did not provide reliable results in our studies for the determination of surface roughness. Hence, confocal microscope or near-field scanning optical microscope studies are required.

By this study, a new application field for the practical and inexpensive electrospinning process was presented. The level of superhydrophobicity can easily be tuned only by varying a parameter, like viscosity or molecular weight of the polymer. This ease increases the merit of the process. However, more study on the subject is needed. Especially, 2-3^o WCA change on different regions of the films may result unexpected consequences at critical applications. Thus, the parameters like electrospinning voltage, tip-to-ground distance and solution flowrate (they were kept constant through out the study) should be optimized to get consistent films. The self-cleaning ability of the films should be studied as well. One method may be: Placing the electrospun films into a cabinet and blowing dust on them, and washing the films for various periods of time and intensities of water, and then measure their WCA after drying. Also, studies on the pilot-plant scale electrospinning should be initiated in our university. This is crucial for the commercialization of the electrospinning process not only for superhydrophobicity applications, but also for larger scale production of electrospun films for catalyst, composite, fuel cell and biological applications.

REFERENCES

1. Baeyer, H. C. V. The Lotus Effect. *The Sciences* **40**, 12-15 (2000).
2. Barthlott, W. & Neinhuis, C. Purity of the sacred lotus, or escape from contamination in biological surfaces. *Planta* **202**, 1-8 (1997).
3. Neinhus, C. & Barthlott, W. Characterization and Distribution of Water-repellent, Self-cleaning Plant Surfaces. *Annals of Botany* **79**, 667-677 (1997).
4. Gould, P. Smart clean surfaces. *Materials Today* **6**, 44-48 (2003).
5. Nishino, T., Meguro, M., Nakamae, K., Matsushita, M. & Ueda, Y. The lowest surface free energy based on -CF3 Alignment. *Langmuir* **15**, 4321-4323 (1999).
6. Wenzel, R. N. Surface roughness and contact angle. *Industrial Engineering Chemistry* **28**, 988-994 (1936).
7. Cassie, A. B. D. & Baxter, S. Wettability of porous surfaces. *Transactions of Faraday Society* **40**, 546-551 (1944).
8. Erbil, H. Y., Demirel, A. L., Avci, Y. & Mert, O. Transformation of a Simple Plastic into a Superhydrophobic Surface. *Science* **299**, 1377-1380 (2003).
9. Nakajima, A., Hashimoto, K. & Watanabe, T. Recent Studies on Super-Hydrophobic Films. *Monatshefte für Chemie* **132**, 31-41 (2001).
10. Blossey, R. Self-cleaning surfaces-virtual realities. *Nature Materials* **2**, 301-306 (2003).
11. de Gennes, P. G. Wetting: statics and dynamics. *Reviews of Modern Physics* **57**, 827-863 (1985).

12. Bonn, D. Wetting transitions. *Current Opinion in Colloid and Interface Science* **6**, 22-27 (2001).

13. Quéré, D. Rough ideas on wetting. *Physica A* **313**, 32-46 (2002).

14. Coninck, J. D., de Ruijter, M. J. & Voué, M. Dynamics of wetting. *Current Opinion in Colloid and Interface Science* **6**, 49-53 (2001).

15. Chen, W. et al. Ultrahydrophobic and Ultralyophobic Surfaces: Some Comments and Examples. *Langmuir* **15**, 3395-3399 (1999).

16. Öner, D. & McCarthy, T. J. Ultrahydrophobic Surfaces. Effects of Topography Length Scale on Wettability. *Langmuir* **16**, 7777-7782 (2000).

17. *DSA 1.70 User Manual* (Krüss GmbH, Hamburg, 2001).

18. Miwa, M., Nakajima, A., Fujishima, A., Hashimoto, K. & Watanabe, T. Effects of the surface roughness on sliding angles of water droplets on superhydrophobic surfaces. *Langmuir* **16**, 5754-5760 (2000).

19. Yoshimitsu, Z., Nakajima, A., Watanabe, T. & Hashimoto, K. Effects of surface structure on the hydrophobicity and sliding behavior of water droplets. *Langmuir* **18**, 5818-5822 (2002).

20. Hare, E. F., Shafrin, E. G. & Zisman, W. A. Properties of Films of Adsorbed Fluorinated Acids. *Journal of Physical Chemistry* **58**, 236-239 (1954).

21. Tsibouklis, J. & Nevell, T. G. Ultra-Low Surface Energy Polymers: The Molecular Design Requirements. *Advanced Materials* **15**, 647-650 (2003).

22. Graham, P., Stone, M., Thorpe, A. A., Nevell, T. G. & Tsibouklis, J. Fluoropolymers with very low surface energy characteristics. *Journal of Fluorine Chemistry* **104**, 29-36 (2000).

23. Pullin, R. A., Nevell, T. G. & Tsibouklis, J. Surface energy characteristics and marine antifouling performance of poly(1H,1H,2H,2H-perfluorodecanoyl diitaconate) film structures. *Materials Letter* **39**, 142-148 (1999).

24. Tsibouklis, J. et al. Inhibiting bacterial adhesion onto surfaces: the non-stick coating approach. *International Journal of Adhesion and Adhesives* **20**, 91-96 (2000).

25. Wenzel, R. N. Surface roughness and contact angle. 1466-1467.

26. Cassie, A. B. D. Contact Angles. 11-15 (1948).

27. Johnson, R. E. J. & Dettre, R. H. in *Contact Angle, Wettability, and Adhesion* (ed. Gould, R. F.) 112-135 (American Chemical Society, Washington, D.C., 1963).

28. Otten, A. & Herminghaus, S. How Plants Keep Dry: A Physicist's Point of View. *Langmuir* **20**, 2405-2408 (2004).

29. Gu, Z.-Z. et al. Structural Color and the Lotus Effect. *Angewandte Chemie Int. Ed.* **42**, 894-897 (2003).

30. Lau, K. K. S. et al. Superhydrophobic Carbon Nanotube Forests. *Nanoletters* **3**, 1701-1705 (2003).

31. Shiu, J.-Y., Kuo, C.-W., Chen, P. & Mou, C.-Y. Fabrication of Tunable Superhydrophobic Surfaces by Nanosphere Lithography. *Chemistry of Materials* **16** (2004).

32. Feng, L. et al. A Super-Hydrophobic and Super-Olephilic Coating Mesh Film for the Separation of Oil and Water. *Angewandte Chemie Int. Ed.* **43**, 2012-2014 (2004).

33. Feng, L. et al. Creation of a Superhydrophobic Surface from an Amphiphilic Polymer. *Angewandte Chemie Int. Ed.* **42**, 800-802 (2003).

34. Zhao, B., Moore, J. S. & Beebe, D. J. Surface-Directed Liquid Flo Inside Microchannels. *Science* **291**, 1023-1026 (2001).

35. Koga, K., Gao, G. T., Tanaka, H. & Zeng, X. C. Formation of Ordered Ice Nanotubes Inside Carbon Nanotubes. *Nature* **412**, 802 (2001).

36. Hummer, G., Rasaiah, J. G. & Noworyta, J. P. Water Conduction Through the Hydrophobic Channel of a Carbon Nanotube. *Nature* **414**, 188 (2001).

37. Zhang, X.-T., Sato, O. & Fujishima, A. Water Ultrarepellency Induced by Nanocolumnar ZnO Surface. *Langmuir* **20**, 6065-6067 (2004).

38. Liu, H., Feng, L., Zhai, J., Jiang, L. & Zhu, D. reversible Wettability of a Chemical Vapor Deposition Prepared ZnO Film between Superhydrophobicity and Superbydrophilicity. *Langmuir* **20**, 5659-5661 (2004).

39. Krupenkin, T. N., Taylor, J. A., Schneider, T. M. & Yang, S. From Rolling Ball to Complete Wetting: The Dynamic Tuning of Liquids on Nanostructured Surfaces. *Langmuir* **20**, 3824-3827 (2004).

40. Sun, T. et al. Control over the Wettability of an Aligned Carbon Nanotube Film. *Journal of American Chemical Society* **125**, 14996-14997 (2003).

41. Patankar, N. A. On the modeling of hydrophobic contact angle on rough surfaces. *Langmuir* **19**, 1249-1253 (2003).

42. Lafuma, A. & Quéré, D. Superhydrophobic states. *Nature Materials* **2**, 457-460 (2003).

43. He, B., Patankar, N. A. & Lee, J. Multiple equilibrium droplet shapes and design criterion for rough hydrophobic surfaces. *Langmuir* **19**, 4999-5003 (2003).

44. Marmur, A. The lotus effect: Superhydrophobicity and metastability. *Langmuir* **20**, 3517-3519 (2004).

45. Bico, J., Marzolin, C. & Quéré, D. Pearl drops. *Europhysics Letters* **47**, 220-226 (1999).

46. Acatay, K., Simsek, E., Ow-Yang, C. & Menceloglu, Y. Z. Achieving Tunable, Superhydrophobically Stable Polymeric Surfaces by Electrospinning. *Angewandte Chemie Int. Ed.* (in print).

47. Huang, Z.-M., Zhang, Y.-Z., Kotaki, M. & Ramakrishna, S. A review on polymer nanofibers by electrospinning and their application in nanocomposites. *Composite Science and Technology* **63**, 2223-2253 (2003).

48. Frenot, A. & Chronakis, I. S. Polymer nanofibers assembled by electrospinning. *Current Opinion in Colloid and Interface Science* **8**, 64-75 (2003).

49. Fong, H. & Reneker, H. R. in *Structure formation in polymeric fibers* (ed. Salem, D. R.) 225-246 (Hanser Publications, Germany, 2001).

50. Rangpukan, R. & Reneker, H. R. in *The Fiber Society Spring Meeting* (Raleigh NC, 2001).

51. Doshi, J. & Reneker, H. R. Electrospinning process and application of electrospun fibers. *Journal of Electrostatics* **35**, 151-160 (1995).

52. Deitzel, J. M., Kleinmeyer, J., Harris, D. & Tan, N. C. B. The effect of processing variables on the morphology of electrospun nanofibers and textiles. *Polymer* **42**, 261-272 (2001).

53. Bergshoef, R. H. & Vansco, G. J. Transparent nanofibers with ultrathin, electrospun nylon-4,6 fiber reinforcement. *Advanced Materials* **11**, 1362-1365 (1999).

54. Yarin, A. L., Koombhongse, S. & Reneker, H. R. Bending instability in electrospinning of nanofibers. *Journal of Applied Physics* **89**, 4836-4846 (2001).

55. Shin, Y. M., Hohman, M. M., Brenner, M. P. & Rutledge, G. C. Electrospinning: A whipping fluid jet generates submicron polymer fibers. *Applied Physics Letters* **78**, 1149-1151 (2001).

56. Demir, M. M., Yılgör, I., Yılgör, E. & Erman, B. Electrospinning of polyurethane fibers. *Polymer* **43**, 3303-3309 (2002).

57. Demir, M. M. in *Faculty of Engineering and Natural Sciences* 59 (Sabancı University, İstanbul, 2001).

58. Theron, S. A., Zussman, E. & Yarin, A. L. Experimental investigation of the governing parameters in the electrospinning of polymer solutions. *Polymer* **45**, 2017-2030 (2004).

59. Zong, X. et al. Structure and process relationship of electrospun bioadsorbable nanofiber membranes. *Polymer* **43**, 4403-4412 (2002).

60. Fong, H., Chun, I. & Reneker, H. R. Beaded nanofibers formed during electrospinning. *Polymer* **40**, 4585-4592 (1999).

61. Fong, H. & Reneker, H. R. Elastomeric nanofibers of styrene-butadiene-styrene triblock copolymer. *Journal of Polymer Science Part B-Polymer Physics* **37**, 3488-3493 (1999).

62. Koski, A., Yim, K. & Shivkumar, S. Effect of molecular weight on fibrous PVA produced by electrospinning. *Materials Letter* **58**, 493-497 (2004).

63. Grafe, T., Gogins, M., Barris, M., Schaefer, J. & Canepa, R. in *Filtration 2001 International Conference of the INDA* (Donaldson Company Inc., Chicago, 2001).

64. Graham, K. et al. in *15th Annual Technical Conference of the American Filtration and Seperations Society* (Donaldson Company Inc., Texas, 2002).

65. Perrin, D. D., Armarego, W. L. F. & Perrin, D. R. *Purification of Laboratory Chemicals* (Pergamon Press Ltd., Great Britain, 1980).

66. Brandup, E. H., Immergut, E. A. & Grulke. *Polymer Handbook* (John Wiley and Sons, USA, 1999).

67. Acatay, K., Gulgun, M. A. & Menceloglu, Y. Z. Process for Preparing Superhydrophobic Surface Compositions, Surfaces Obtained by Said Process and Use of Them (2003, Turkey, PCT/TR03/00067)

68. Acatay, K. et al. in *Fluoropolymers 2004* (Savannah, Georgia, USA, 2004).

69. Acatay, K., Simsek, E., Akel, M. & Menceloglu, Y. Z. in *Nanoengineered Nanofibrous Materials* (eds. Guceri, S., Gogotsi, Y. & Kuznetsov, V.) (Kluwer Academic Publications, Antalya, Turkey, 2003).

70. Bilgin, N. in *Faculty of Engineering and Natural Sciences* pp. 71 (Sabanci University, Istanbul, 2003).

APPENDIX A

Table A.1 Constants for commonly used solvents. Unless otherwise indicated the values are valid for 20oC and 760 torr.

Chemical Name	**Polarity Index (P)**	**Boiling Point (°C)**	**Density (g/ml)**	**Dielectric Constant**	**Viscosity (cP)**	**Surface Tension (dyn/cm)**
1,1,2-Trichlorofluoroethane	0,0	47,57	1,564 (25°C)	2,41 (25°C)	0,71	NA
1,2,4-Trichlorobenzene	NA	213,50	1,4540	2,24 (25°C)	NA	NA
1,4-Dioxane	4,8	101,32	1,0336	2,25	1,37	34,45 (15°C)
2-Methoxyethanol	5,5	124,60	0,9646	16,93	1,72	31,80 (15°C)
Acetone	5,1	56,29	0,7900	20,07 (25°C)	0,36	23,32
Acetonitrile	5,8	81,60	0,7822	37,50	0,38 (15°C)	19,10
Chlorobenzene	2,7	131,69	1,1058	5,62 (25°C)	0,80	33,28
Chloroform	4,1	61,15	1,4892	4,81	0,57	27,16
Cyclohexane	0,1	80,72	0,7785	2,02	1,00	24,98
Cyclopentane	0,1	49,26	0,7454	1,97	0,44	22,42
Dichloromethane	3,1	39,75	1,3260	8,93 (25°C)	0,44	28,12
Dimethyl Acetamide	6,5	166,10	0,9415	37,78 (25°C)	2,14	32,43 (30°C)
Dimethyl Sulphoxide	7,2	189,00	1,1004	46,68	2,24	NA
Ethyl Acetate	4,4	77,11	0,9006	6,02 (25°C)	0,45	23,75
Ethyl Alcohol	NA	78,32	0,7892	24,55 (25°C)	1,1 (25°C)	22,32
Ethyl Ether	2,8	34,55	0,7133	4,33	0,24	17,06
Ethylene Dichloride	3,5	83,48	1,2530	10,36 (25°C)	0,79	32,23
Heptane	0,1	98,43	0,6837	1,92	0,42	20,30
Hexane	0,1	68,70	0,6594	1,88 (25°C)	0,31	17,91
Isobutyl Alcohol	4,0	107,70	0,8016	16,68	NA	22,98
Iso-Octane	0,1	99,24	0,6919	1,94	0,50	18,77
Isopropyl Alcohol	3,9	82,26	0,7854	19,92 (25°C)	2,40	21,79 (15°C)
Methanol	5,1	64,70	0,7913	32,70 (25°C)	0,59	22,55

Methyl Ethyl Ketone	4,7	79,64	0,8049	18,51	0,43	24.00 (25ºC)
Methyl Isobutyl Ketone	4,2	117,40	0,8008	13,11 (25ºC)	0,58	23,64
Methyl n-Propyl Ketone	4,5	102,40	0,8082	15,45	0,51	25,09
Methyl t-Butyl Ether	2,5	55,20	0,7405	NA	0,27	19,4 (24ºC)
N,N-Dimethylformamide	6,4	153,00	0,9487	36,71 (25ºC)	0,92	36,76
n-Butyl Acetate	4,0	126,11	0,8796	5,01	0,74	25,09
n-Butyl Alcohol	3,9	117,50	0,8097	17,51 (25ºC)	2,98	24,57
n-Butyl Chloride	1,0	78,44	0,8862	7,39	0,45	23,75
N-Methylpyrrolidone	6,7	202,00	1,0304	32,2 (25ºC)	1,67 (25ºC)	NA
n-Propyl Alcohol	4,0	97,20	0,8037	20,33 (25ºC)	2,30	23,70
o-Dichlorobenzene	2,7	180,48	1,3058	9,93 (25ºC)	1,32 (25ºC)	26,84
o-Xylene	2,5	144,41	0,8802	2,57	0,81	30,03
Pentane	0,0	36,07	0,6262	1,84	0,23	15,48 (25ºC)
Propylene Carbonate	6,1	241,70	1,2006	64,90	NA	41,93
Pyridine	5,3	115,25	0,9832	12,40	0,95	36,88
Tetrahydrofuran	4,0	66,00	0,8880	7,58 (25ºC)	0,55	26,40 (25ºC)
Toluene	2,4	110,62	0,8669	2,38 (25ºC)	0,59	28,53
Trietyhl amine	NA	89,50	0,7276	2,42 (25ºC)	0,36 (25ºC)	20,66
Trifluoro acetic acid	NA	71,80	1,4890	8,55	0,93	13,63 (24ºC)
Water	10,2	100,00	0,9982	80,10	1,00	72,80

APPENDIX B

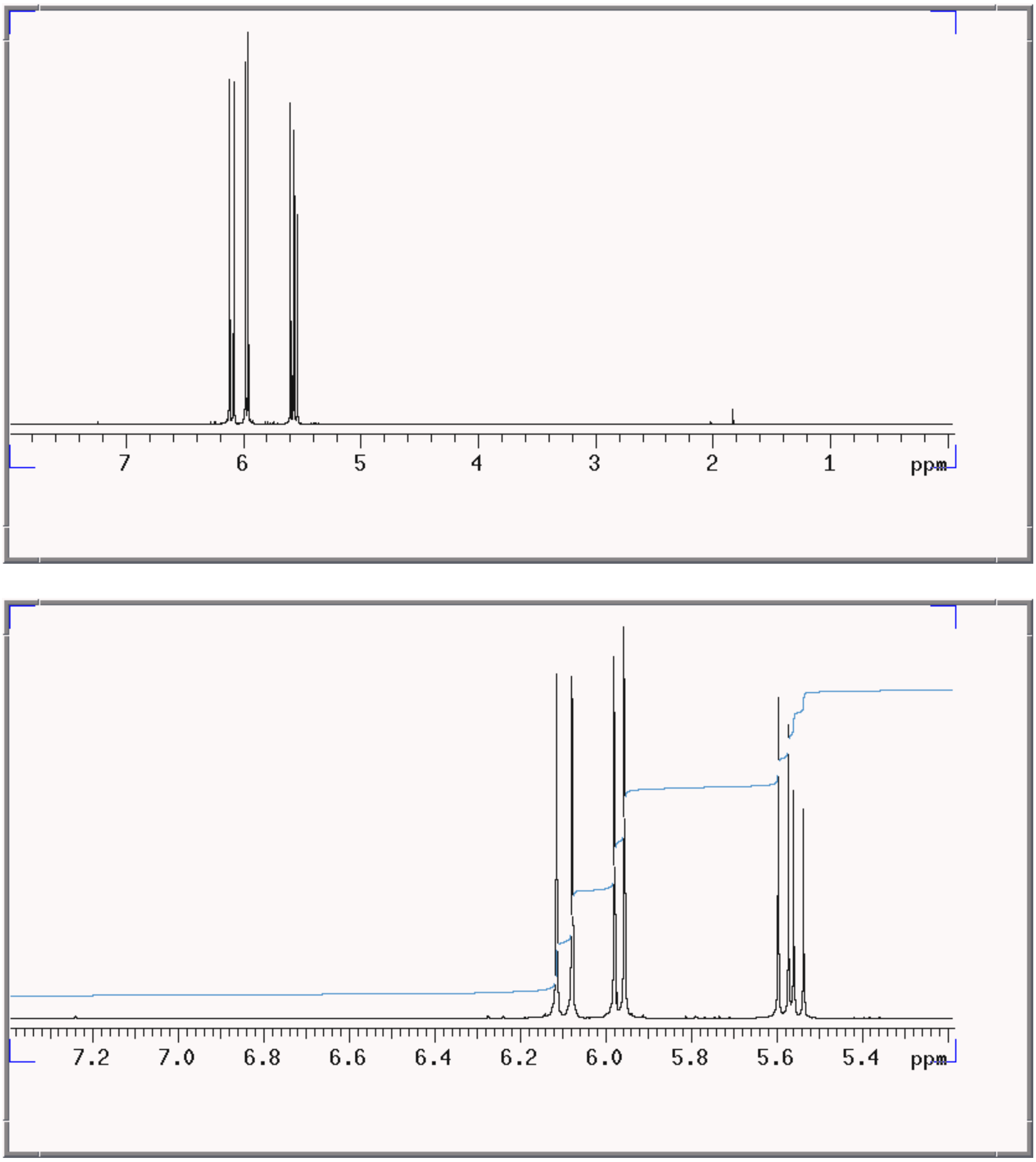

Figure B.1 Proton NMR results of AN used through out the dissertation.

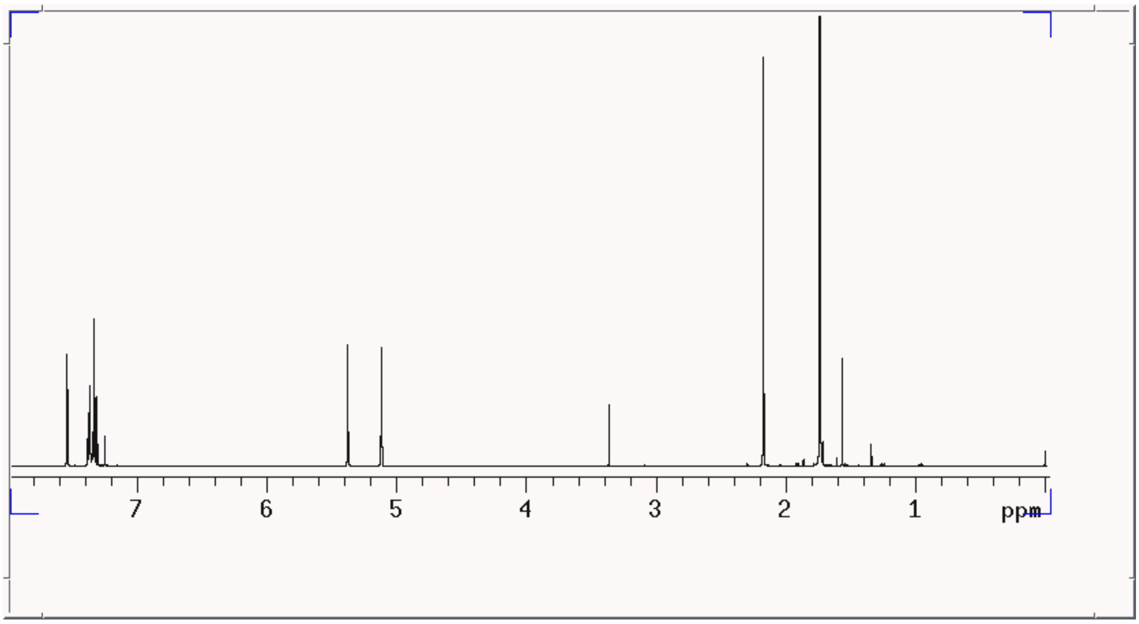

Figure B.2 Proton NMR of TMI used throughout the dissertation.

REFERENCES

1. Baeyer, H. C. V. The Lotus Effect. *The Sciences* **40**, 12-15 (2000).
2. Barthlott, W. & Neinhuis, C. Purity of the sacred lotus, or escape from contamination in biological surfaces. *Planta* **202**, 1-8 (1997).
3. Neinhus, C. & Barthlott, W. Characterization and Distribution of Water-repellent, Self-cleaning Plant Surfaces. *Annals of Botany* **79**, 667-677 (1997).
4. Gould, P. Smart clean surfaces. *Materials Today* **6**, 44-48 (2003).
5. Nishino, T., Meguro, M., Nakamae, K., Matsushita, M. & Ueda, Y. The lowest surface free energy based on -CF3 Alignment. *Langmuir* **15**, 4321-4323 (1999).
6. Wenzel, R. N. Surface roughness and contact angle. *Industrial Engineering Chemistry* **28**, 988-994 (1936).
7. Cassie, A. B. D. & Baxter, S. Wettability of porous surfaces. *Transactions of Faraday Society* **40**, 546-551 (1944).
8. Erbil, H. Y., Demirel, A. L., Avci, Y. & Mert, O. Transformation of a Simple Plastic into a Superhydrophobic Surface. *Science* **299**, 1377-1380 (2003).
9. Nakajima, A., Hashimoto, K. & Watanabe, T. Recent Studies on Super-Hydrophobic Films. *Monatshefte für Chemie* **132**, 31-41 (2001).
10. Blossey, R. Self-cleaning surfaces-virtual realities. *Nature Materials* **2**, 301-306 (2003).
11. de Gennes, P. G. Wetting: statics and dynamics. *Reviews of Modern Physics* **57**, 827-863 (1985).

12. Bonn, D. Wetting transitions. *Current Opinion in Colloid and Interface Science* **6**, 22-27 (2001).

13. Quéré, D. Rough ideas on wetting. *Physica A* **313**, 32-46 (2002).

14. Coninck, J. D., de Ruijter, M. J. & Voué, M. Dynamics of wetting. *Current Opinion in Colloid and Interface Science* **6**, 49-53 (2001).

15. Chen, W. et al. Ultrahydrophobic and Ultralyophobic Surfaces: Some Comments and Examples. *Langmuir* **15**, 3395-3399 (1999).

16. Öner, D. & McCarthy, T. J. Ultrahydrophobic Surfaces. Effects of Topography Length Scale on Wettability. *Langmuir* **16**, 7777-7782 (2000).

17. *DSA 1.70 User Manual* (Krüss GmbH, Hamburg, 2001).

18. Miwa, M., Nakajima, A., Fujishima, A., Hashimoto, K. & Watanabe, T. Effects of the surface roughness on sliding angles of water droplets on superhydrophobic surfaces. *Langmuir* **16**, 5754-5760 (2000).

19. Yoshimitsu, Z., Nakajima, A., Watanabe, T. & Hashimoto, K. Effects of surface structure on the hydrophobicity and sliding behavior of water droplets. *Langmuir* **18**, 5818-5822 (2002).

20. Hare, E. F., Shafrin, E. G. & Zisman, W. A. Properties of Films of Adsorbed Fluorinated Acids. *Journal of Physical Chemistry* **58**, 236-239 (1954).

21. Tsibouklis, J. & Nevell, T. G. Ultra-Low Surface Energy Polymers: The Molecular Design Requirements. *Advanced Materials* **15**, 647-650 (2003).

22. Graham, P., Stone, M., Thorpe, A. A., Nevell, T. G. & Tsibouklis, J. Fluoropolymers with very low surface energy characteristics. *Journal of Fluorine Chemistry* **104**, 29-36 (2000).

23. Pullin, R. A., Nevell, T. G. & Tsibouklis, J. Surface energy characteristics and marine antifouling performance of poly(1H,1H,2H,2H-perfluorodecanoyl diitaconate) film structures. *Materials Letter* **39**, 142-148 (1999).

24. Tsibouklis, J. et al. Inhibiting bacterial adhesion onto surfaces: the non-stick coating approach. *International Journal of Adhesion and Adhesives* **20**, 91-96 (2000).

25. Wenzel, R. N. Surface roughness and contact angle. 1466-1467.

26. Cassie, A. B. D. Contact Angles. 11-15 (1948).

27. Johnson, R. E. J. & Dettre, R. H. in *Contact Angle, Wettability, and Adhesion* (ed. Gould, R. F.) 112-135 (American Chemical Society, Washington, D.C., 1963).

28. Otten, A. & Herminghaus, S. How Plants Keep Dry: A Physicist's Point of View. *Langmuir* **20**, 2405-2408 (2004).

29. Gu, Z.-Z. et al. Structural Color and the Lotus Effect. *Angewandte Chemie Int. Ed.* **42**, 894-897 (2003).

30. Lau, K. K. S. et al. Superhydrophobic Carbon Nanotube Forests. *Nanoletters* **3**, 1701-1705 (2003).

31. Shiu, J.-Y., Kuo, C.-W., Chen, P. & Mou, C.-Y. Fabrication of Tunable Superhydrophobic Surfaces by Nanosphere Lithography. *Chemistry of Materials* **16** (2004).

32. Feng, L. et al. A Super-Hydrophobic and Super-Olephilic Coating Mesh Film for the Separation of Oil and Water. *Angewandte Chemie Int. Ed.* **43**, 2012-2014 (2004).

33. Feng, L. et al. Creation of a Superhydrophobic Surface from an Amphiphilic Polymer. *Angewandte Chemie Int. Ed.* **42**, 800-802 (2003).

34. Zhao, B., Moore, J. S. & Beebe, D. J. Surface-Directed Liquid Flo Inside Microchannels. *Science* **291**, 1023-1026 (2001).

35. Koga, K., Gao, G. T., Tanaka, H. & Zeng, X. C. Formation of Ordered Ice Nanotubes Inside Carbon Nanotubes. *Nature* **412**, 802 (2001).

36. Hummer, G., Rasaiah, J. G. & Noworyta, J. P. Water Conduction Through the Hydrophobic Channel of a Carbon Nanotube. *Nature* **414**, 188 (2001).

37. Zhang, X.-T., Sato, O. & Fujishima, A. Water Ultrarepellency Induced by Nanocolumnar ZnO Surface. *Langmuir* **20**, 6065-6067 (2004).

38. Liu, H., Feng, L., Zhai, J., Jiang, L. & Zhu, D. reversible Wettability of a Chemical Vapor Deposition Prepared ZnO Film between Superhydrophobicity and Superbydrophilicity. *Langmuir* **20**, 5659-5661 (2004).

39. Krupenkin, T. N., Taylor, J. A., Schneider, T. M. & Yang, S. From Rolling Ball to Complete Wetting: The Dynamic Tuning of Liquids on Nanostructured Surfaces. *Langmuir* **20**, 3824-3827 (2004).

40. Sun, T. et al. Control over the Wettability of an Aligned Carbon Nanotube Film. *Journal of American Chemical Society* **125**, 14996-14997 (2003).

41. Patankar, N. A. On the modeling of hydrophobic contact angle on rough surfaces. *Langmuir* **19**, 1249-1253 (2003).

42. Lafuma, A. & Quéré, D. Superhydrophobic states. *Nature Materials* **2**, 457-460 (2003).

43. He, B., Patankar, N. A. & Lee, J. Multiple equilibrium droplet shapes and design criterion for rough hydrophobic surfaces. *Langmuir* **19**, 4999-5003 (2003).

44. Marmur, A. The lotus effect: Superhydrophobicity and metastability. *Langmuir* **20**, 3517-3519 (2004).

45. Bico, J., Marzolin, C. & Quéré, D. Pearl drops. *Europhysics Letters* **47**, 220-226 (1999).

46. Acatay, K., Simsek, E., Ow-Yang, C. & Menceloglu, Y. Z. Achieving Tunable, Superhydrophobically Stable Polymeric Surfaces by Electrospinning. *Angewandte Chemie Int. Ed.* (in print).

47. Huang, Z.-M., Zhang, Y.-Z., Kotaki, M. & Ramakrishna, S. A review on polymer nanofibers by electrospinning and their application in nanocomposites. *Composite Science and Technology* **63**, 2223-2253 (2003).

48. Frenot, A. & Chronakis, I. S. Polymer nanofibers assembled by electrospinning. *Current Opinion in Colloid and Interface Science* **8**, 64-75 (2003).

49. Fong, H. & Reneker, H. R. in *Structure formation in polymeric fibers* (ed. Salem, D. R.) 225-246 (Hanser Publications, Germany, 2001).

50. Rangpukan, R. & Reneker, H. R. in *The Fiber Society Spring Meeting* (Raleigh NC, 2001).

51. Doshi, J. & Reneker, H. R. Electrospinning process and application of electrospun fibers. *Journal of Electrostatics* **35**, 151-160 (1995).

52. Deitzel, J. M., Kleinmeyer, J., Harris, D. & Tan, N. C. B. The effect of processing variables on the morphology of electrospun nanofibers and textiles. *Polymer* **42**, 261-272 (2001).

53. Bergshoef, R. H. & Vansco, G. J. Transparent nanofibers with ultrathin, electrospun nylon-4,6 fiber reinforcement. *Advanced Materials* **11**, 1362-1365 (1999).

54. Yarin, A. L., Koombhongse, S. & Reneker, H. R. Bending instability in electrospinning of nanofibers. *Journal of Applied Physics* **89**, 4836-4846 (2001).

55. Shin, Y. M., Hohman, M. M., Brenner, M. P. & Rutledge, G. C. Electrospinning: A whipping fluid jet generates submicron polymer fibers. *Applied Physics Letters* **78**, 1149-1151 (2001).

56. Demir, M. M., Yılgör, I., Yılgör, E. & Erman, B. Electrospinning of polyurethane fibers. *Polymer* **43**, 3303-3309 (2002).

57. Demir, M. M. in *Faculty of Engineering and Natural Sciences* 59 (Sabancı University, İstanbul, 2001).

58. Theron, S. A., Zussman, E. & Yarin, A. L. Experimental investigation of the governing parameters in the electrospinning of polymer solutions. *Polymer* **45**, 2017-2030 (2004).

59. Zong, X. et al. Structure and process relationship of electrospun bioadsorbable nanofiber membranes. *Polymer* **43**, 4403-4412 (2002).

60. Fong, H., Chun, I. & Reneker, H. R. Beaded nanofibers formed during electrospinning. *Polymer* **40**, 4585-4592 (1999).

61. Fong, H. & Reneker, H. R. Elastomeric nanofibers of styrene-butadiene-styrene triblock copolymer. *Journal of Polymer Science Part B-Polymer Physics* **37**, 3488-3493 (1999).

62. Koski, A., Yim, K. & Shivkumar, S. Effect of molecular weight on fibrous PVA produced by electrospinning. *Materials Letter* **58**, 493-497 (2004).

63. Grafe, T., Gogins, M., Barris, M., Schaefer, J. & Canepa, R. in *Filtration 2001 International Conference of the INDA* (Donaldson Company Inc., Chicago, 2001).

64. Graham, K. et al. in *15th Annual Technical Conference of the American Filtration and Seperations Society* (Donaldson Company Inc., Texas, 2002).

65. Perrin, D. D., Armarego, W. L. F. & Perrin, D. R. *Purification of Laboratory Chemicals* (Pergamon Press Ltd., Great Britain, 1980).

66. Brandup, E. H., Immergut, E. A. & Grulke. *Polymer Handbook* (John Wiley and Sons, USA, 1999).

67. Acatay, K., Gulgun, M. A. & Menceloglu, Y. Z. Process for Preparing Superhydrophobic Surface Compositions, Surfaces Obtained by Said Process and Use of Them (2003, Turkey, PCT/TR03/00067)

68. Acatay, K. et al. in *Fluoropolymers 2004* (Savannah, Georgia, USA, 2004).

69. Acatay, K., Simsek, E., Akel, M. & Menceloglu, Y. Z. in *Nanoengineered Nanofibrous Materials* (eds. Guceri, S., Gogotsi, Y. & Kuznetsov, V.) (Kluwer Academic Publications, Antalya, Turkey, 2003).

70. Bilgin, N. in *Faculty of Engineering and Natural Sciences* pp. 71 (Sabanci University, Istanbul, 2003).